**E-ISSN:** 2148-6247

# Turkish Journal of PHARMACEUTICAL SCIENCES

An Official Journal of the Turkish Pharmacists' Association, Academy of Pharmacy

Volume: 23 Issue: 3 June 2026



www.turkjps.org

EMERGING SOURCES CITATION INDEX

PubMed Central PubMed Scopus TRDİZİN

galenos Publishing House

Turkish Journal of
# PHARMACEUTICAL SCIENCES



## OWNER

Mehmet İrfan DEMİRCİ on behalf of the Turkish Pharmacists' Association

## Editor-in-Chief

**Prof. S. Kutay DEMİRKAN, Pharm.D.**

Hacettepe University Faculty of Pharmacy, Department of Clinical Pharmacy, Ankara, Türkiye
E-mail: ktydmrkn@gmail.com

## Associate Editors

**Prof. Betül OKUYAN, Ph.D.**
Marmara University Faculty of Pharmacy, Department of Clinical Pharmacy, İstanbul, Türkiye
E-mail: betulokuyan@gmail.com

**Prof. İ. İrem TATLI ÇANKAYA, Ph.D.**
Hacettepe University Faculty of Pharmacy, Department of Pharmaceutical Botany, Ankara, Türkiye
E-mail: itatli@hacettepe.edu.tr

**Prof. Hande SİPAHİ, Ph.D.**
University of Health Sciences Faculty of Pharmacy, Department of Pharmaceutical Toxicology, İstanbul, Türkiye
E-mail: handesipahi@hotmail.com

**Prof. Canan OĞAN HASÇİÇEK, Ph.D.**
Ankara University Faculty of Pharmacy, Department of Pharmaceutical Technology, Ankara, Türkiye
E-mail: cogan@pharmacy.ankara.edu.tr

**Assoc. Prof. Esra EROĞLU, Ph.D.**
İstanbul University Faculty of Pharmacy, Department of Pharmacognosy, İstanbul, Türkiye
E-mail: eseroglu@istanbul.edu.tr

## Editorial Board

**Prof. Afonso Miguel CAVACO, Ph.D.**
Lisbon University Faculty of Pharmacy, Department of Pharmacy, Pharmacology and Health Technologies, Lisboa, Portugal
E-mail: acavaco@campus.ul.pt

**Prof. Bambang KUSWANDI, Ph.D.**
Chemo and Biosensors Group, Faculty of Pharmacy University of Jember, East Java, Indonesia
E-mail: b_kuswandi.farmasi@unej.ac.id

**Prof. Bezhan CHANKVETADZE, Ph.D.**
Ivane Javakhishvili Tbilisi State University, Institute of Physical and Analytical Chemistry, Tbilisi, Georgia
E-mail: jpba_bezhan@yahoo.com

**Prof. Blanca LAFFON, P.D.**
DICOMOSA group, Advanced Scientific Research Center (CICA), University of A Coruña, Department of Psychology, Area Psychobiology, Central Services of Research Building (ESCI), Campus Elviña s/n, A Coruña, Spain
E-mail: blanca.laffon@udc.es

**Prof. Christine LAFFORGUE, Ph.D.**
Paris Saclay University Faculty of Pharmacy, Department of Dermopharmacology and Cosmetology, Paris, France
E-mail: christine.lafforgue@universite-paris-saclay.fr

**Prof. Dietmar FUCHS, Ph.D.**
Innsbruck Medical University, Center for Chemistry and Biomedicine, Institute of Biological Chemistry, Biocenter, Innsbruck, Austria
E-mail: dietmar.fuchs@i-med.ac.at

**Prof. Fernanda BORGES, Ph.D.**
Porto University Faculty of Sciences, Department of Chemistry and Biochemistry, Porto, Portugal
E-mail: fborges@fc.up.pt

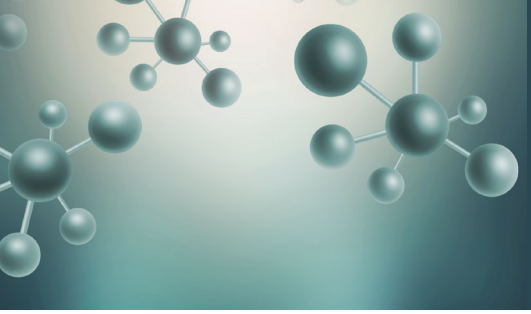
**Prof. Francesco EPIFANO, Ph.D.**
Università degli Studi G. d'Annunzio Chieti e Pescara, Chieti CH, Italy
E-mail: francesco.epifano@unich.it

**Prof. Göksel ŞENER, Ph.D.**
Fenerbahçe University Faculty of Pharmacy, Department of Pharmacology, İstanbul, Türkiye
E-mail: gsener@marmara.edu.tr

**Prof. Gülbin ÖZÇELİKAY, Ph.D.**
Ankara University Faculty of Pharmacy, Department of Pharmacy Management, Ankara, Türkiye
E-mail: gozcelikay@ankara.edu.tr

**Prof. Hermann BOLT, Ph.D.**
Dortmund University, Leibniz Research Centre, Institute of Occupational Physiology, Dortmund, Germany
E-mail: bolt@ifado.de

**Prof. Hildebert WAGNER, Ph.D.**
Ludwig-Maximilians University, Center for Pharmaceutical Research, Institute of Pharmacy, Munich, Germany
E-mail: h.wagner@cup.uni-muenchen.de



Turkish Journal of
# PHARMACEUTICAL SCIENCES

## Editorial Board

**Prof. K. Arzum ERDEM GÜRSAN, Ph.D.**
Ege University Faculty of Pharmacy, Department of Analytical Chemistry, İzmir, Türkiye
E-mail: arzum.erdem@ege.edu.tr

**Prof. Luciano SASO, Ph.D.**
Sapienza University Faculty of Pharmacy and Medicine, Department of Physiology and Pharmacology "Vittorio Erspamer", Rome, Italy
E-mail: luciano.saso@uniroma1.it

**Prof. Maarten J. POSTMA, Ph.D.**
University of Groningen (Netherlands), Department of Pharmacy, Unit of Pharmacoepidemiology and Pharmacoeconomics, Groningen, Holland
E-mail: m.j.postma@rug.nl

**Prof. Meriç Köksal AKKOÇ, Ph.D.**
Yeditepe University Faculty of Pharmacy, Department of Pharmaceutical Chemistry, İstanbul, Türkiye
E-mail: merickoksal@yeditepe.edu.tr

**Prof. Robert RAPOPORT, Ph.D.**
Cincinati University Faculty of Pharmacy, Department of Pharmacology and Cell Biophysics, Cincinati, USA
E-mail: robertrapoport@gmail.com

**Prof. Rob VERPOORTE, Ph.D.**
Leiden University, Natural Products Laboratory, Leiden, Netherlands
E-mail: verpoort@chem.leidenuniv.nl

**Prof. Tayfun UZBAY, Ph.D.**
Üsküdar University Faculty of Medicine, Department of Medical Pharmacology, İstanbul, Türkiye
E-mail: tayfun.uzbay@uskudar.edu.tr

**Prof. Wolfgang SADEE, Ph.D.**
Ohio State University, Center for Pharmacogenomics, Ohio, USA
E-mail: wolfgang.sadee@osumc.edu

**Assoc. Prof. Nadja Cristhina DE SOUZA PINTO, Ph.D.**
University of São Paulo, Institute of Chemistry, São Paulo, Brazil
E-mail: nadja@iq.usp.br

**Assoc. Prof. Neslihan Aygün KOCABAŞ, Ph.D. E.R.T**
Total Research and Technology Feluy Zone Industrielle Feluy, Refining and Chemicals, Strategy-Development-Research, Toxicology Manager, Seneffe, Belgium
E-mail: neslihan.aygun.kocabas@total.com

Turkish Journal of
PHARMACEUTICAL SCIENCES



## Advisory Board

**Prof. Yusuf ÖZTÜRK, Ph.D.**
Anadolu University Faculty of Pharmacy, Department of Pharmacology, Eskişehir, Türkiye

**Prof. Tayfun UZBAY, Ph.D.**
Üsküdar University Faculty of Medicine, Department of Medical Pharmacology, İstanbul, Türkiye
ORCID: orcid.org/0000-0002-9784-5637

**Prof. K. Hüsnü Can BAŞER, Ph.D.**
Anadolu University Faculty of Pharmacy, Department of Pharmacognosy, Eskişehir, Türkiye

**Prof. Yılmaz ÇAPAN, Ph.D.**
Hacettepe University Faculty of Pharmacy, Department of Pharmaceutical Technology, Ankara, Türkiye

**Prof. Sibel A. ÖZKAN, Ph.D.**
Ankara University Faculty of Pharmacy, Department of Analytical Chemistry, Ankara, Türkiye

**Prof. Ekrem SEZİK, Ph.D.**
İstanbul Health and Technology University Faculty of Pharmacy, Department of Pharmacognosy, İstanbul, Türkiye

**Prof. Gönül ŞAHİN, Ph.D.**
Eastern Mediterranean University Faculty of Pharmacy, Department of Pharmaceutical Toxicology, Famagusta, Cyprus

**Prof. Sevda ŞENEL, Ph.D.**
Hacettepe University Faculty of Pharmacy, Department of Pharmaceutical Technology, Ankara, Türkiye

**Prof. Sevim ROLLAS, Ph.D.**
Marmara University Faculty of Pharmacy, Department of Pharmaceutical Chemistry, İstanbul, Türkiye

**Prof. Göksel ŞENER, Ph.D.**
Fenerbahçe University Faculty of Pharmacy, Department of Pharmacology, İstanbul, Türkiye
ORCID: 0000-0001-7444-6193

**Prof. Erdal BEDİR, Ph.D.**
İzmir Institute of Technology, Department of Bioengineering, İzmir, Türkiye

**Prof. Nurşen BAŞARAN, Ph.D.**
Hacettepe University Faculty of Pharmacy, Department of Pharmaceutical Toxicology, Ankara, Türkiye

**Prof. Bensu KARAHALİL, Ph.D.**
Gazi University Faculty of Pharmacy, Department of Pharmaceutical Toxicology, Ankara, Türkiye

**Prof. Betül DEMİRCİ, Ph.D.**
Anadolu University Faculty of Pharmacy, Department of Pharmacognosy, Eskişehir, Türkiye

**Prof. Bengi USLU, Ph.D.**
Ankara University Faculty of Pharmacy, Department of Analytical Chemistry, Ankara, Türkiye

**Prof. Ahmet AYDIN, Ph.D.**
Yeditepe University Faculty of Pharmacy, Department of Pharmaceutical Toxicology, İstanbul, Türkiye

**Prof. İlkay ERDOĞAN ORHAN, Ph.D.**
Gazi University Faculty of Pharmacy, Department of Pharmacognosy, Ankara, Türkiye

**Prof. Ş. Güniz KÜÇÜKGÜZEL, Ph.D.**
Fenerbahçe University Faculty of Pharmacy, Department of Pharmaceutical Chemistry, İstanbul, Türkiye

**Prof. Engin Umut AKKAYA, Ph.D.**
Dalian University of Technology, Department of Chemistry, Dalian, CHINA

**Prof. Esra AKKOL, Ph.D.**
Gazi University Faculty of Pharmacy, Department of Pharmacognosy, Ankara, Türkiye

**Prof. Erem BİLENSOY, Ph.D.**
Hacettepe University Faculty of Pharmacy, Department of Pharmaceutical Technology, Ankara, Türkiye

**Prof. Uğur TAMER, Ph.D.**
Gazi University Faculty of Pharmacy, Department of Analytical Chemistry, Ankara, Türkiye

**Prof. Gülaçtı TOPÇU, Ph.D.**
Bezmialem Vakıf University Faculty of Pharmacy, Department of Pharmacognosy, İstanbul, Türkiye

**Prof. Hasan KIRMIZIBEKMEZ, Ph.D.**
Yeditepe University Faculty of Pharmacy, Department of Pharmacognosy, İstanbul, Türkiye

**Douglas Siqueira DE ALMEIDA CHAVES, Ph.D.**
Federal Rural University of Rio de Janeiro, Department of Pharmaceutical Sciences, Rio de Janeiro, Brazil

***Members of the Advisory Board consist of the scientists who received Science Award presented by TEB Academy of Pharmacy in chronological order.***

Turkish Journal of
# PHARMACEUTICAL SCIENCES

**Please refer to the journal's webpage (https://www.turkjps.org/) for "Editorial Policy" and "Instructions to Authors".**

The editorial and publication process of the **Turkish Journal of Pharmaceutical Sciences** are shaped in accordance with the guidelines of ICMJE, WAME, CSE, COPE, EASE, and NISO. The Turkish Journal of Pharmaceutical Sciences is indexed in **PubMed, PubMed Central, Thomson Reuters / Emerging Sources Citation Index, Scopus, ULAKBİM, Türkiye Citation Index, Embase, EBSCO Host, Türk Medline, Cabi, CNKI.**

The journal is published online.

**Owner:** Turkish Pharmacists' Association, Academy of Pharmacy

**Responsible Manager:** Kutay DEMİRKAN

galenos yayınevi

**Publisher Contact**
**Address:** Molla Gürani Mah. Kaçamak Sk. No: 21/1
34093 İstanbul, Türkiye
**Phone:** +90 (530) 177 30 97
**E-mail:** info@galenos.com.tr/yayin@galenos.com.tr
**Web:** www.galenos.com.tr | **Publisher Certificate Number:** 14521

**Publication Date:** October 2026
**E-ISSN:** 2148-6247
International scientific journal published bimonthly.

Turkish Journal of
PHARMACEUTICAL SCIENCES

## CONTENTS

### ORIGINAL ARTICLES

122 *Development, Validation, and Application of a Highly Sensitive RP-HPLC Method for the Determination and Release Profile Comparison of Levonorgestrel from Silicone-Based Contraceptive Implants*
Abul Kalam Lutful KABIR, Sitesh Chandra BACHAR, Md. MONIRUZZAMAN, Emdad HOSSAIN

130 *Investigation of the Effect of Calcitriol on Radiofrequency Radiation-Exposed Breast Cancer Cell Lines*
Ece MİSER SALİHOĞLU, Mualla Pınar ELÇİ, Tuğba FATSA, Sema ÖREN, Meriç EŞMEKAYA, Sevgi YARDIM

140 *Polypharmacy and Glycemic Status in Individuals with Diabetes and Pre-Diabetes: Iranian Multi-Center Osteoporosis Study 2021*
Sarmad SALEHI, Azin RASHIDI, Mohanna KHOJASTE, Pardis ZAREPOUR, Neda CHERAGHLOO, Safoora GHARIBZADEH, Ozra Tabatabaei MALAZY, Afshin OSTOVAR

150 *Nadifloxacin-Loaded Thermosensitive In Situ Gel Formulations with a Quality by Design Approach*
Ece ÖZCAN BÜLBÜL, Burçin İZBUDAK, Ayça BAL ÖZTÜRK, Neslihan ÜSTÜNDAĞ OKUR

165 *Furanocoumarins from the Roots of Cachrys cristata DC.: Isolation, Anticholinesterase Activity, and Molecular Docking Studies*
Fadıl Kaan KURAN, Ceren KUŞ, Zehra Ezel DOLAP, Şule Nur KARAVUŞ, Kübra Şeyma ÖZTÜRK, Gülsüm ALTIPARMAK ÜLBEGİ, Mahmut MİSKİ

174 *Synthesis, Characterization, and In Vitro Anticancer Activity of $Fe_3O_4$-PEG-Quercetin Nanoparticles in a Non-Small Cell Lung Cancer (NSCLC) Model*
Yeşim SİS, Mükerrem Betül YERER

Turk J Pharm Sci 2026;23(3):122-129
**DOI:** 10.4274/tjps.galenos.2026.56783

ORIGINAL ARTICLE

# Development, Validation, and Application of a Highly Sensitive RP-HPLC Method for the Determination and Release Profile Comparison of Levonorgestrel from Silicone-Based Contraceptive Implants

**Abul Kalam Lutful KABIR[1,2]*, Sitesh Chandra BACHAR[1], Md. MONIRUZZAMAN[3], Emdad HOSSAIN[2]***

[1]University of Dhaka, Department of Pharmaceutical Technology, Dhaka, Bangladesh
[2]Jadavpur University, Department of Pharmaceutical Technology, Kolkata, India
[3]Techno Drugs Ltd., Dhaka, Bangladesh

## ABSTRACT

**Objectives:** Levonorgestrel (LNG), a synthetic progestin containing implants, has emerged as one of the most reliable, effective, and long-acting reversible contraceptive (LARC) methods for preventing unintended pregnancies. The current study aimed to develop and validate a simple, rapid, and highly sensitive reverse-phase high-performance liquid chromatography (HPLC) technique for the quantification and release profile comparison of LNG from different silicone-based LARC implants.

**Materials and Methods:** All the analysis was performed using HPLC equipped with UV/UV-VIS detector with the help of Waters C18 column of 250 × 4.6 mm dimension, 5 µm sized particle with mobile phase consisting of water and acetonitrile in the ratio of 30:70 (v/v%) at room temperature and 1 mL/minute flow rate, injection volume of 50 µl with the detection wavelength of 240 nm. The developed method was then validated as per International Council for Harmonisation of Technical Requirements for Pharmaceuticals for Human Use (ICH) guidelines and then the validated method was used successfully to quantify LNG and for a comparative release profile study of two marketed implants, Femiplant and Sino-implant (II). The obtained release data were assessed and compared using fit factors ($f_1$ & $f_2$) to compare one formulation with another.

**Results:** All parameters met the limits according to ICH guidelines. The total time needed for analysis was 12 minutes, having LNG eluting with a retention time of 5.8 min (± 0.2). The average LNG content was obtained to be 98.52 to 101.32% (± 0.05%). From the release kinetic study, $f_1$ and $f_2$ values of Femiplant against Sino-implant (II) determined was 10 and 62, respectively, both of which meet the acceptable limits.

**Conclusion:** The devolved method was straightforward and quick for any sample preparation, which could be used for routine analysis, in-process quality control analysis, and stability study analysis, among others. Moreover, Femiplant presented similar release kinetics compared to the World Health Organization prequalified implant Sino-implant (II), thereby having similar bioavailability and ensuring the consistent therapeutic effect of both implants.

**Keywords:** RP-HPLC, method development and validation, LNG, contraceptive implant, release profile comparison

***Correspondence:** lutful@du.ac.bd, emdad@rediffmail.com **ORCID-ID:** orcid.org/0000-0001-9911-1648; emdad@rediffmail.com. **ORCID-ID:** orcid.org/0000-0001-9110-6449

**Received:** 12.08.2025 **Accepted:** 09.09.2026 **Publication Date:** 27.10.2026

**Cite this article as:** Kabir AKL, Bachar SC, Moniruzzaman M, Hossain E. Development, validation, and application of a highly sensitive RP-HPLC method for the determination and release profile comparison of levonorgestrel from silicone-based contraceptive implants. Turk J Pharm Sci. 2026;23(3):122-129

Copyright© 2026 The Author(s). Published by Galenos Publishing House on behalf of Turkish Pharmacists' Association.
This is an open access article under the Creative Commons Attribution-NonCommercial-NoDerivatives 4.0 (CC BY-NC-ND) International License.

## INTRODUCTION

Hormonal contraceptive subdermal implants are small, flexible rods about the size of a matchstick that provide a continuous release of the low-dose synthetic progestin levonorgestrel (LNG), an effective hormonal treatment intended to control menstrual complaints and endometriosis.[1,2] LNG, similar to the natural progesterone hormone, is a potent medication used in various birth control systems, e.g., emergency oral contraceptive pills, daily combined oral contraceptives with ethinylestradiol, three-month injectable contraceptives, silicone-based long-acting reversible contraceptive (LARC) implants, and intrauterine devices for birth spacing.[3-5]

Various types of LNG-releasing LARC implants are available worldwide including Jadelle of Bayer Oy, Finland, and Levoplant/Sino-implant (II) of Shanghai Dahua Pharmaceuticals Company Limited, China, Jadena and Duplant of Indonesia containing LNG which is effective for up to 3-5 years of effective contraception.[6-9] Implanon NXT, also known as Nexplanon, now replaces Implanon with a one-rod system containing etonorgestrel and is considered effective for 3 years of contraceptive action, although a new study describes its effectiveness for contraception for up to 5 years.[10,11] Norplant, consisting of six capsules, provides 5-7 years of effectiveness, but it became obsolete in 2008 and is not valid for use now. All LNG-containing subdermal implants, consisting of two flexible rods, are placed in a V-shaped configuration, with the rods positioned at a 30-degree angle and 8 to 10 cm above the elbow in a woman's upper arm. Higher doses of LNG are released during the first 6 to 12 months after insertion, with the daily dose declining to a steady 30 to 35 μg per day throughout the shelf life of the system.[12] LNG is a synthetic progesterone hormone available as a naturally occurring female sex hormone, and its chemical formula is $C_{21}H_{28}O_2$ (d-Norgestrel)-13β-ethyl-17α-hydroxy-18,19-dinorpregn-4-en-20-yn-3-one (molecular weight is 312.47 g/mol) shown in Figure 1. LNG Implants primarily act by stopping ovulation (the release of eggs from the ovaries), thickening the cervical mucus, and blocking sperm from reaching the eggs.[13-15]

Several analytical techniques, such as UV spectrophotometry, mass spectrometry, reverse-phase high-performance liquid chromatography (HPLC), and LC-MS/MS, can be used for the quantification of LNG, alone or in combination with ethinylestradiol in various dosage forms. Among them, HPLC is one of the important techniques because of its linearity, accuracy, specificity, precision, robustness, and suitability for sample stability analysis.[16-23] Five years ago, Femiplant, like Jadelle and Levoplant/Sino-Implant II, a long-acting reversible sub-dermal contraceptive implant containing 150 mg of LNG, approved by the Directorate General of Drug Administration, was introduced into the national family planning program of the government of Bangladesh to provide three years of contraception; it is manufactured by a leading local pharmaceutical manufacturer, Techno Drugs Ltd.

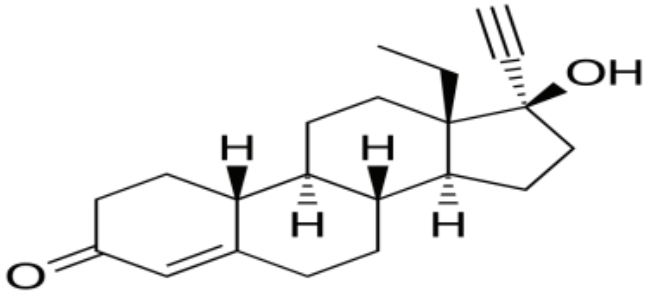



**Figure 1.** Chemical structure of LNG.
LNG, levonorgestrel.

In this study, we had an attempt for developing and validating a very simple, rapid, reliable and sensitive as well as constant RP-HPLC method as per International Council for Harmonisation of Technical Requirements for Pharmaceuticals for Human Use (ICH) guidelines[24] to determine and quantify LNG from LARCs subdermal hormonal implants and this newly developed technique has been validated as per ICH guidelines and utilized to quantify and evaluate the comparative release characteristics and kinetic profiles of LNG from two marketed implant formulations like Femiplant of Techno Drugs Ltd, Bangladesh and Levoplant (Sino- Implant II) of Shanghai Dahua Pharmaceuticals Co., Ltd. China which is also a World Health Organization (WHO) prequalified product, both of them are effective for contraception up to 3 years that are available worldwide.

## MATERIALS AND METHODS

*Chemicals and apparatus with instrumentation*

LNG (the active pharmaceutical ingredient) was obtained as a gift sample. Two marketed subdermal implant products, Femiplant and Sino-implant (II), which consist of two flexible, matchstick-like plastic rods, each rod containing 75 mg of LNG, were procured from the market. HPLC-grade solvents such as acetonitrile (Fischer-Scientific, UK) and chloroform (Merck, Germany), HPLC-ready water from Ultra-Pure System, 0.45 μm membrane disc filters, and 0.22 μm syringe filters were used. Moreover, for sample preparation, an electronic microbalance, a sonicator, and a planetary centrifugal mixer were utilized. The Waters RP-HPLC system, equipped with a degasser, autosampler, quaternary solvent delivery pump, column oven, and UV/UV-VIS detector, was used for the development and validation of the method. Data acquisition, processing, and evaluation were performed using LabSolutions software (version 6.40 SP1, Shimadzu).

*Wavelength detection*

A 0.1 mg/mL LNG stock solution was prepared using 60% acetonitrile, and serial dilution was performed to obtain a 10 μg/mL LNG concentration. This solution was then scanned between 200 nm and 400 nm using a UV spectrophotometer. The wavelength was fixed at 240 nm, and the spectra were recorded.

*Chromatographic condition*

All analyses were performed using a Waters RP-HPLC system equipped with a UV/UV-VIS detector. The separation of LNG

had been completed with the help of $C_{18}$ column of 250 × 4.6 mm dimensions, 5 μm sized particle in an isocratic mode of mobile phase composed of water and acetonitrile in the ratio of 30:70 (v/v). Drug elution was conducted at room temperature with a flow rate of one mL/minute, an injection volume of 50 μL, and a total run time of 12 minutes at a detection wavelength of 240 nm. Before injecting the blank and drug solutions, the HPLC system was equilibrated for approximately one hour by degassing with the mobile phase. Then the blank solution was passed through the syringe filter (0.22 μm) and finally injected to ensure that there was no interference from the solvent.

*Preparation of blank solution*

The blank solution was prepared using 60% acetonitrile.

*Preparation of LNG stock solution*

25 mg of LNG working standard in powder form was weighed accurately and transferred to an amber-colored 100 mL volumetric flask. Then 60 mL of acetonitrile, and the mixture was sonicated for 10 minutes to dissolve completely, and the volume was made up to the mark by thorough mixing. This solution is termed the standard stock solution.

*Preparation of LNG standard solution*

3.0 mL of the standard stock solution was diluted with acetonitrile to prepare an LNG standard solution of 3.0 μg/mL. The prepared solution was then filtered with a 0.45-micron filter.

*Preparation of calibration curve of standard solutions*

A stock solution of the LNG standard was used to prepare a calibration curve with concentrations ranging from 40% to 120% of the standard concentration in 60% acetonitrile. The solutions were filtered through a 0.45-micron filter, transferred to HPLC vials, and each concentration was injected in triplicate and analyzed using the proposed method.

*Preparation of sample solution*

LNG implants having ≈44 ± 0.5 mm of length containing total 150 mg of LNG were collected from the supplier. Average weight was determined (≈228 ± 2 mg) and three implant rods (of each type) were taken and cut into small fragments (~1 mm length). The cut-piece samples equivalent to two rods were transferred to a 100 mL dried volumetric flask; 60 mL of reagent-grade chloroform was added, the mixture was sonicated for 20 minutes, allowed to stand for at least one hour, and then diluted with chloroform to a final volume of 100 mL. Then it was filtered through Whatman filter paper, and 0.5 mL of the solution was transferred into a 100 mL dried volumetric flask and evaporated to dryness. Sixty mL of acetonitrile was poured, sonicated for 10 minutes, and the final volume was obtained. Finally, this solution was filtered for analysis through a 0.2 μm syringe filter. The obtained concentration was 7.5 μg/mL. Assays of all the samples were carried out by injecting them into the HPLC after system suitability testing and under the above conditions.

*RP-HPLC method validation*

According to ICH guidelines Q2 (R1), the method has been validated for the following parameters: specificity, linearity, accuracy (recovery), precision, robustness, and sample solution stability.

*System suitability*

The suitability of the system has been evaluated by injecting a blank solution and a standard solution of LNG and measuring parameters such as tailing factor, theoretical plates, and relative standard deviation (%RSD). The acceptance limits for system suitability and the method were: RSD of peak area for LNG no more than 2%, United States Pharmacopeia (USP) tailing factor no more than 2, and theoretical plates no less than 2000 for the column.

*Specificity*

The method specificity was demonstrated using an HPLC system by injecting a blank solution, a placebo, and an LNG standard solution. Analysis of the obtained chromatograms showed that the blank and placebo solutions exhibited the retention time of the active pharmaceutical ingredient without interference.

*Linearity*

Linearity was assessed using a series of solutions prepared by quantitative dilution of the LNG stock solution over the range of 40% to 120% of the working concentration. A calibration curve has been plotted using the average peak area from triplicate injections against solution concentration. The slope, intercept, and correlation coefficient were measured from the curve to confirm the linearity of the proposed method.

*Accuracy*

By spiking the solution, the accuracy of the analytical technique was measured at three concentrations of LNG: 80%, 100%, and 120%. For each concentration, triplicates were prepared and evaluated for percent recovery and percent RSD.

*Precision*

Intra-day precision (repeatability) of the placebo solution was assessed on the same day by spiking it with six different standard solutions of LNG (3.0 μg/mL), with short intervals between measurements under similar operating conditions. The percent recovery and %RSD were determined to assess the repeatability, and inter-day precision was evaluated by comparing values obtained on two different days for separate HPLC analyses.

*Robustness*

The robustness of method has been carried out by changing a small and slow variation in the flow rate of ± 0.2 mL/min and mobile phase composition of ± 5%. The standard LNG solution was measured under those changed conditions, and the percentage RSD for LNG peak area, no. of theoretical plates, and the USP tailing factor for the column were then determined.

*Stability of the sample solution*

The stability of LNG-based implant systems was tested at regular intervals for up to 72 hours at normal temperature. During each interval, the values for LNG peak area, theoretical plates, and tailing factor were evaluated.

*Application of the method*

The applicability of the method for assaying LNG and evaluating its release profile from two marketed formulations of LARC implants was assessed.

*Analysis of LNG implant*

*Assay or content determination*

In this study, the developed HPLC assay was performed on the commercially available subdermal implant products Femiplant and Levoplant/Sino-Implant II, which contain 150 mg of LNG in two rods, and LNG was quantified for each implant. The quantity of drug released for each sample was measured by peak-area measurement at 240 nm, and the LNG assay per device was then performed using the following formula.

Assay (%);

$$= \frac{A_{Sample} \times C_{Std} \times P_{Std}}{A_{Std} \times C_{Sample}}$$

**Where,**

$A_{Sample}$ = Area of sample solution,

$A_{Std}$ = Area of standard solution,

$P_{Std}$ = Potency of standard LNG in percentage,

$C_{Std}$ = Concentration of standard solution,

$C_{Sample}$ = Concentration of sample solution.

*Release study of LNG*

Six sets of LNG implants (both Femiplant and Levoplant) were taken and divided into pairs. Both ends were tied up with fine threads, respectively and were suspended in a 100 mL stoppered transparent iodine bottle. The distance to the bottom of the bottle was approximately 1 cm. Then, 100 mL of purified water was added, and the iodine bottles were placed in a 37 °C constant-temperature oscillator. The round-trip speed was 60 round trips per minute. The amplitude was 3 cm. After 24 hours of constant temperature oscillation, the solution was discarded. Then, 100 mL of purified water was added, and oscillation continued for 24 hours. The above operation was repeated for 7 days. The solutions from the 3rd, 5th, and 7th days were pooled to form the test solution and then filtered through a 0.45-micron filter. The samples collected on days 3 and 7 were selected for further quantitative analysis and comparison; the remaining samples were not further analyzed. Standard and sample solutions were injected after the system suitability test. The LNG release per day from each set of implants was calculated using the following formula.

Released amount of LNG in µg per set per day;

$$= \frac{A_{Sample} \times W_{Std} \times 1 \times 100 \times 1000}{A_{Std} \times 100 \times 100 \times 1} \times P_{Std}$$

Where,

$A_{Sample}$ = Area of sample solution,

$A_{Std}$ = Area of standard solution,

$P_{Std}$ = Potency of standard LNG in percentage,

$W_{Std}$ = Weight of standard LNG.

*Statistical analysis*

All the data were analyzed using IBM SPSS Statistics for Windows, Version 20.0.; New York, USA. The Paired Samples t-test was used for comparisons within two groups and data were expressed as mean ± standard deviation.

## RESULTS

*Method development and optimization by RP-HPLC*

Various ratios of water: acetonitrile, such as 20:80, 30:70, 40:60, and 50:50, have been used for method optimization. The optimum mobile phase was chosen based on retention time, resolution, number of theoretical plates, and tailing factor at the maximum detection wavelength of 240 nm by UV spectrophotometry in chloroform. An appropriate separation of LNG having better resolution and less tailing factor of water and acetonitrile in ratio of 30:70 at flow rate of 1 mL/min by $C_{18}$ (250 x 4.6 mm) column of an isocratic condition through 50 µL injection fixing as an optimized condition by HPLC.

*Method validation by RP-HPLC*

The system suitability results presented in the study indicate that all checked parameters met the acceptance limits for the LNG standard solution. The active drug had retained at 5.8 minutes (± 0.02) having percent RSD of 0.1 of the peak area. It indicates good repeatability in this system. There was no interference from diluents, impurities, or other excipients at the detection wavelength. The observed tailing factor was less than 1.05, indicating acceptable peak symmetry. Moreover, the no. of theoretical plates was at least 2000 in all runs on the chromatograph (Figure 2).

*Specificity of method*

The chromatograms found from blank, placebo and standard solution of LNG showed that no interference observed at the retention time of 5.8 (± 0.02) for LNG (Figure 2). Peaks were obtained for the blank solution at 2.6 minutes and for the placebo at 1.4 minutes, indicating that the peaks were pure for the analytes and confirming the specificity of the method with respect to retention time.

The close agreement among results obtained at three concentrations (80%, 100%, and 120% of the LNG solution) showed the accuracy of the proposed method. The overall percent recovery ranged from 99.75% to 100% based on 3 spiked samples. The mean percent recovery of LNG at three concentrations met the acceptance criteria shown in Table 1; hence, the method was accurate.

*Precision of method*

The average %RSD of LNG in the repeatability study of six replicate injections is shown in Table 2; values for intra-day and inter-day quantification were within the limits, confirming the high precision and repeatability of the developed method.

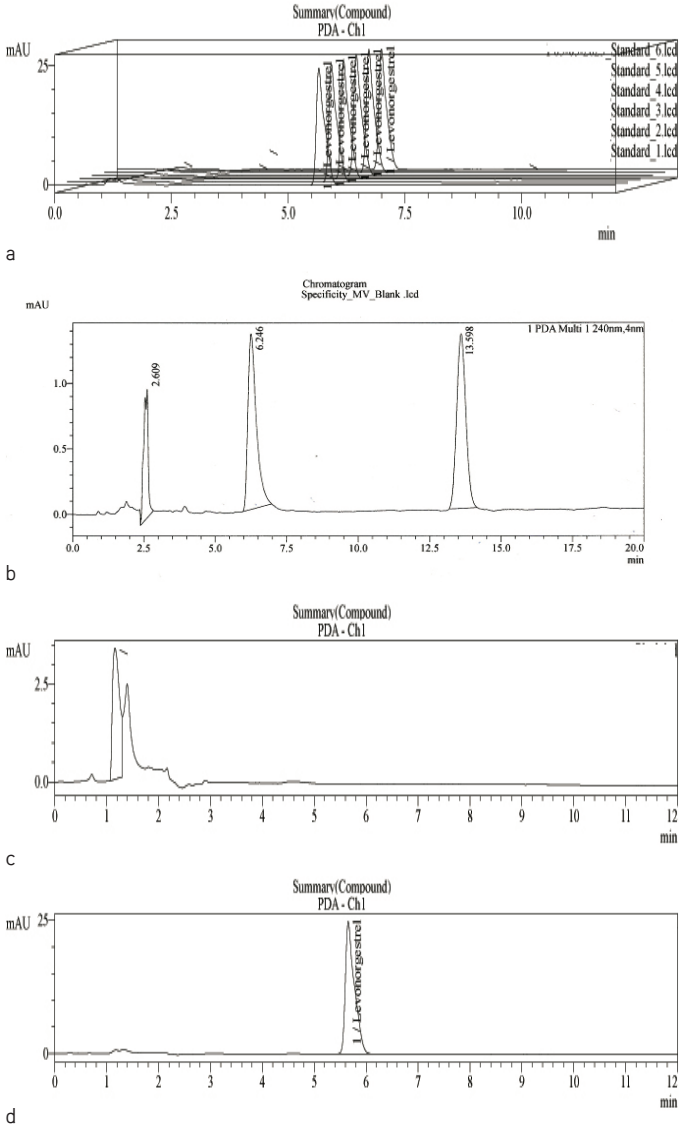



**Figure 2.** (a) HPLC chromatogram for method validation of LNG.
(b) HPLC chromatogram of blank solution.
(c) HPLC chromatogram of placebo.
(d) HPLC chromatogram of sample solution.
LNG, levonorgestrel; HPLC, high-performance liquid chromatography.

*Linearity of method*

The calibration curve obtained with the standard LNG solution was linear over various concentration ranges (shown in Figure 3), and the results indicate that the method met the limit of acceptance for linearity.

*Robustness of method*

Robustness was evaluated in three LNG sample solutions by introducing small variations in chromatographic parameters; the values obtained are shown in Table 3. The percent assay of three LNG standard solutions obtained met the limit of acceptance (tailing factor was less than 2 and the percent RSD was less than 2%) confirming that the method was robust with respect to small variations in flow rate of mobile phase (± 0.2 mL/min), wavelength (± 2 nm) and volume of mobile phase composition (± 5%).

*Stability of the analytical sample solution*

The stability of the analytes was evaluated by analyzing LNG standard and sample solutions stored at room temperature and sampled at various time intervals. The results indicated that the analytes were stable for 72 hours, and the parameters (peak area, tailing factor, and theoretical plates) shown in Table 4 met the acceptance limits; consequently, no significant decomposition of LNG was observed.

*Assay or content determination*

The validated method was utilized for the analysis of LNG-releasing implants in two marketed subdermal implant preparations, such as Femiplant and Levoplant/Sino-Implant, each containing 150 mg LNG (Figures 4 and 5). The average content of LNG was obtained to be 98.52% to 101.32% (± 0.05%). The time needed for sample preparation was less than half an hour and total run time was12 minute, enabling a quick determination of several samples in case of routine or quality control analysis of LNG from flexible silicone-based implants and the low RSD values indicating the suitability of proposed method for analysis of LNG releasing subdermal implant system available in the market.

*Release profile evaluation of LNG implants*

The graphs presented in Figures 6-8 show a release profile very similar to those of the two marketed LNG implant preparations, which report an extremely similar pattern of LNG release compared with the mean daily in vivo release of LNG: 100 μg daily in the first month, 40 μg daily at 24 months, and 30 μg daily after three years following subdermal insertion. This analysis did not show any indication of significant differences in behavior between the two LNG formulations and therefore

**Table 1. LNG study of accuracy and recovery (n=3).**

| % level | Spiked conc. (μg/mL) | Obtained conc. (μg/mL) | Recovery (%) | RSD (%) |
|---|---|---|---|---|
| 80 | 5.5 | 5.5 | 99.75 | 0.35 |
| 100 | 9.5 | 10.0 | 100 | 0.50 |
| 120 | 12.7 | 15.8 | 99.98 | 0.52 |

LNG, levonorgestrel; RSD (%), percent relative standard deviation.

**Table 2. Intra-day and inter-day results of precision (n=6).**

| Precision | Peak area | RSD (%) | %Recovery factor | RSD (%) recovery |
|---|---|---|---|---|
| Intra-day (repeatability) | 57750 | 0.560 | 1.525 | 0.55 |
| Inter-day precision | | | | |
| Day 1, system 1, analyst 1 | 55650 | 2.552 | 1.654 | 0.43 |
| Day 2, system 1, analyst 1 | 55765 | 2.342 | 1.697 | 1.32 |
| Day 2, system 2, analyst 2 | 66765 | 2.653 | 1.669 | 2.55 |

RSD (%), percent relative standard deviation.

**Table 3. Results of robustness under various parameters (n=6).**

| Parameters | Percent RSD | Average tailing factor | Theoretical plate |
|---|---|---|---|
| Flow rate at 1.2 mL/min | 0.11 | 1.525 | 32923 |
| Flow rate at 0.8 mL/min | 0.09 | 1.654 | 32883 |
| Water: acetonitrile, 40:60 | 0.07 | 1.697 | 35976 |
| Water: acetonitrile, 20:80 | 0.06 | 1,669 | 33645 |

RSD, relative standard deviation.

**Table 4. Results for stability study.**

| Time interval (hours) | Peak area | Tailing factor (acceptance limit, <2) | Theoretical plate (acceptance limit, NLT 2000) |
|---|---|---|---|
| 0 | 56750 | 1.725 | 33923 |
| 24 | 57650 | 1.674 | 34883 |
| 48 | 59765 | 1.637 | 34976 |
| 72 | 59915 | 1,662 | 35645 |

NLT, not less than.

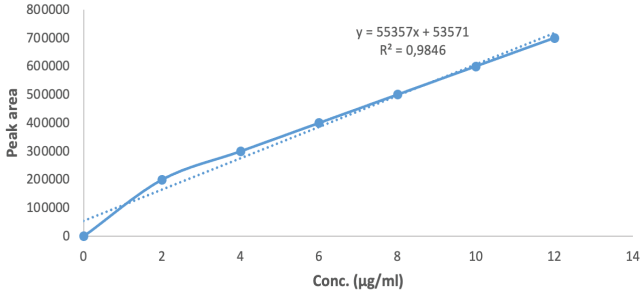



**Figure 3.** Linearity curve of LNG. Accuracy of method.
LNG, levonorgestrel.

failed to explain the unsuccessful results observed in vivo bioequivalence studies. Moreover, we determined the fit factors, such as $f_1$ (similarity factor) and $f_2$ (dissimilarity factor), by applying the following formulas to confirm whether the release profile of Femiplant is comparable to that of Levoplant/ Sino-Implant-II.

In this study, the comparison of $f_1$ and $f_2$ values thus offers an opportunity to easily compare and determine pairs of release profile and it is observed that $f_1$ (difference factor)

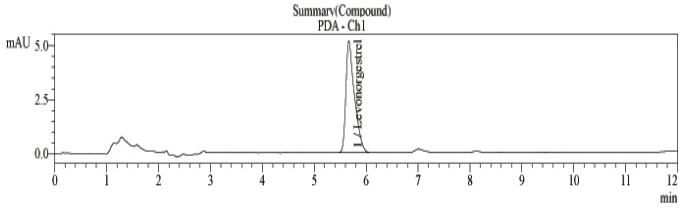



**Figure 4.** Representative HPLC chromatogram for the assay of LNG from femiplant.
LNG, levonorgestrel; HPLC, high-performance liquid chromatography.

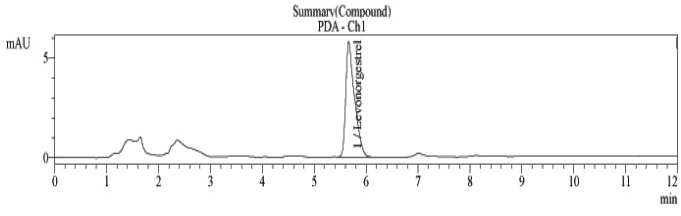



**Figure 5.** Representative HPLC chromatogram for the assay of LNG from Levoplant.
LNG, levonorgestrel; HPLC, high-performance liquid chromatography.

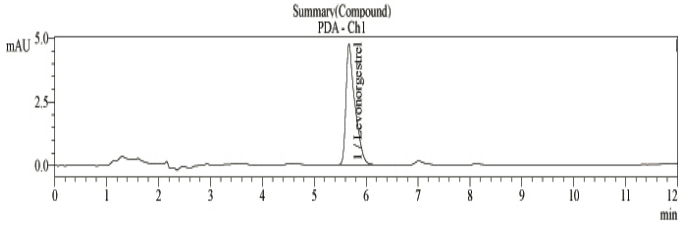



**Figure 6.** Representative chromatogram of release profile study of LNG from Femiplant at seventh day.

LNG, levonorgestrel; HPLC, high-performance liquid chromatography.

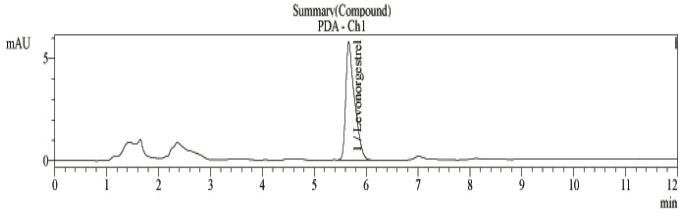



**Figure 7.** Representative chromatogram of release profile of LNG from Levoplant at seventh day.

LNG, levonorgestrel.

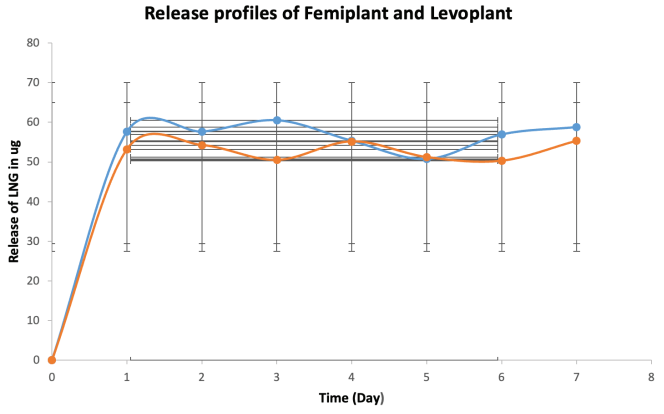



**Figure 8.** Release profile between Femiplant (green line) and Levoplant (pink line).

**Table 5. Release profile comparison of femiplant and sino-implant.**

| LNG-implants | Difference factor of Femiplant compared to Levoplant (f1) | Similarity factor of Femiplant compared to levoplant (f2) |
|---|---|---|
| Femiplant | 10 | 62 |
| Acceptance criteria | 0-15 | 50-100 |

LNG, levonorgestrel.

and $f_2$ (similarity factor) value between Femiplant against Sino-Implant (Levoplant) is 10 and 62 respectively, shown in Table 5, both of them met the acceptance criteria indicating a very similar release profile for both of the silicone-based implants thereby having similar bioavailability and ensuring the consistent therapeutic effect of these two products.

## DISCUSSION

In our study, a specific and robust HPLC method was developed and optimized for the quantification of LNG from contraceptive subdermal implants. Among several mobile phase compositions examined, a combination of water: acetonitrile (30:70 v/v) at a 1.0 mL/min flow rate utilizing a $C_{18}$ reverse phase column of 250 × 4.6 mm under isocratic conditions formed sharp and symmetric peaks with an acceptable retention time and resolution, detecting at 240 nm provided optimal sensitivity for LNG determination.

System suitability results established the suitability of the system, with a retention time of 5.8 ± 0.02 minute, tailing factor ‹1.05, and theoretical plates ›2000, demonstrating outstanding effectiveness and repeatability. The absence of interference from blank or placebo samples confirmed method specificity, and the method demonstrated excellent linearity over the concentration range, meeting ICH criteria. In addition, the method demonstrated high precision, with mean recovery values of 99.75% and 100%, and outstanding accuracy, with %RSD values ‹2% for both intra- and inter-day analyses. Minor variations in chromatographic factors did not significantly affect the results, confirming the robustness of the technique. LNG remained stable for up to 72 hours, demonstrating the system's suitability for routine analysis.

The validated method was used for LNG assay and for comparing release profiles of two marketed formulations, Femiplant and Levoplant/Sino-Implant, yielding values between 98.52% and 101.32% and meeting the content uniformity standard. The release profiles of both types of implants were comparable, with $f_1$ = 10 and $f_2$ = 62, meeting the similarity criteria and indicating equivalent release profiles and bioavailability performance.

Overall, the developed RP-HPLC method proved to be simple, precise, accurate, specific, and robust, making it appropriate for routine QC analysis and release-rate studies in subdermal contraceptive implant dosage forms.

### *Study limitations*

The current study may be limited by the number and variety of samples analysed, as well as the degree of method validation across the various implant dosage forms. Moreover, this comparative analysis between two types of silicone-based contraceptive implant formulations limited the generalizability of the results to other formulations, such as polymer-based implants. In addition, similar *in vitro* release profiles of Levonorgestrel do not necessarily ensure equivalence with in vivo findings under physiological conditions for contraceptive effectiveness and therefore require suitable pharmacokinetic or bioequivalence studies in a clinical setting.

## CONCLUSION

The developed HPLC method demonstrated simple, rapid, and efficient sample preparation, making it appropriate for routine analysis, in-process quality control, and stability studies of LNG in subdermal implants. Method validation confirmed that specificity, linearity, accuracy, precision, and robustness met the acceptance criteria as per ICH guidelines, ensuring that the method was consistent and reproducible. Importantly, this method was used effectively to assess the release-kinetic profiles of marketed formulations without interference. With a total run time of 12 minutes (less than 30 minutes), the method enables high-throughput analysis, allowing rapid quantification of a large number of samples for routine or quality-control laboratory analyses. Application of this method to commercially available implants showed that Femiplant had a release profile comparable to Sino-implant (II), a WHO-prequalified subdermal implant. Such similarity in release kinetics offers strong evidence of bioequivalence between the two types of implants.

*Ethics*

**Ethics Committee Approval:** Not required.

**Informed Consent:** Not required.

*Footnotes*

*Authorship Contributions*

Concept: A.K.L.K., E.H., M.M., Design: A.K.L.K., M.M., Data Collection or Processing: A.K.L.K., E.H., M.M., Analysis or Interpretation: A.K.L.K., E.H., Literature Search: A.K.L.K., E.H., Writing: A.K.L.K., E.H., S.C.B., M.M.

**Conflict of Interest:** The authors declare no conflicts of interest.

**Financial Disclosure:** The authors declared that this study received no financial support.

## REFERENCES

1. Rocca ML, Palumbo AR, Visconti F, Di Carlo C. Safety and benefits of contraceptives implants: a systematic review. Pharmaceuticals (Basel). 2021;14:548.
2. Manoukian OS, Arul MR, Sardashti N, Stedman T, James R, Rudraiah S, Kumbar SG. Biodegradable polymeric injectable implants for long-term delivery of contraceptive drugs. J Appl Polym Sci. 2018;135:46068.
3. Hassan Ilegbusi P. Contraceptive implants [Internet]. Studies in Family Planning. IntechOpen; 2022.
4. Al Dalaty A, Gualeni B, Coulman SA, Birchall JC. Models and methods to characterise levonorgestrel release from intradermally administered contraceptives. Drug Deliv Transl Res. 2022;12:335-349.
5. Sivin I, Nash H, Waldman S. Jadelle® LNG rod implants: a summary of scientific data and lessons learned from programmatic experience. Population Council. 2002.
6. Callahan RL, Taylor D, Jenkins DW, Owen DH, Cheng L, Cancel AM, Dorflinger LJ, Steiner MJ. In vivo release of levonorgestrel from Sino-implant (II) — an innovative comparison of explant data. Contraception. 2015;92:350-355.
7. Wathoni N, Alfauziah TQ, Rantika N. Evolution of contraceptive implants: a review. International Journal of Applied Pharmaceutics. 2018;10:16-22.
8. Fuchs R, Taylor D, Jenkins DW, Brache V, Luo D, Dorflinger LJ, Steiner MJ. Levonorgestrel release rates measured through analysis of two-rod contraceptive explants. Contracept X. 2020;2:100039.
9. Berzas JJ, Rodríguez J, Castañeda G. Simultaneous determination of ethinylestradiol and levonorgestrel in oral contraceptives by derivative spectrophotometry. Analyst. 1997;122:41-44.
10. Pal VK, Pal Y. Analytical method development and method validation for determination assay and content uniformity of levonorgestrel by reversed-phase high performance liquid chromatography. Asian J Pharm Clin Res. 2020;13:101-107.
11. Díaz-Cruz MS, López de Alda MJ, López R, Barceló D. Determination of estrogens and progestogens by mass spectrometric techniques (GC/MS, LC/MS and LC/MS/MS). J Mass Spectrom. 2003;38:917-923.
12. Veeran MG, C K, B B, Painuly D, Aprem AS. RP-HPLC method validation for fast extraction and quantification of Levonorgestrel drug from silicone based intrauterine device intended for in-process and finished formulation. Daru. 2021;29:185-193.
13. Kabir AKL, Hossain E. Comparison between Levonorgestrel and Etonogestrel implants, the two silicone-based long-acting reversible subdermal contraceptives. Med Pharmacol OA. 2025;4:01-05.
14. Kassaye L, Genete G. Evaluation and comparison of in-vitro dissolution profiles for different brands of amoxicillin capsules. Afr Health Sci. 2013;13:369-375.
15. Brache V, Alvarez F, Faundes A. Mechanism of action of levonorgestrel contraceptive implants. Gynecological Endocrinology. 2001;15:14-20.
16. Cirrincione LR, Penchala SD, Scarsi KK, Podany AT, Winchester LC, Back DJ, Khoo SH, Fletcher CV, Siccardi M, Else LJ. Development, validation and utilization of a highly sensitive LC-MS/MS method for quantification of levonorgestrel released from a subdermal implant in human plasma. J Chromatogr B Analyt Technol Biomed Life Sci. 2018;1084:106-112.
17. Kabir AKL, Moniruzzaman M, Bachar SC, Hossain E. RP-HPLC method development, validation and application for quantification assay and release kinetics of etonogestrel from contraceptive subdermal implant. Bangladesh Pharmaceutical Journal. 2026;29:246-253.
18. Kabir AKL, Uddin MN, Rony SR, Bachar SC, Hossain E. LC-MS/MS method development, validation, and application for levonorgestrel assay from contraceptive implants in Bangladeshi women. Sci Rep. 2026.
19. Rahman SM, Lutfulkabir A, Jahan MD, Momen AZ, Rouf AS. Validation and application of reversed phase high-performance liquid chromatographic method for quantification of pizotifen malate in pharmaceutical solid dosage formulations. Pak J Pharm Sci. 2010;23:435-441.
20. Patel PU, Patal BM. Development and validation of stability indicating reverse phase high performance liquid chromatographic method for estimation of levonorgestrel in bulk dosage form. IJPDA. 2014;2:311-318.
21. Chang HF, Wang JQ, Wang B, Deng AP. An immunochromatographic assay for rapid and simultaneous detection of levonorgestrel and methylprednisolone in water samples. Chin Chem Lett. 2013;24:937-940.
22. Lee IH, Park HN, Kim NS, Park HJ, Park S, Shin D, Kang H. Detection of illegal abortion-induced drugs using rapid and simultaneous method for the determination of abortion-induced compounds by LC-MS/MS. Chromatographia. 2019;82:1365-1371.
23. Fuchs R, Taylor D, Jenkins DW, Brache V, Luo D, Dorflinger LJ, Steiner MJ. Levonorgestrel release rates measured through analysis of two-rod contraceptive explants. Contracept X. 2020;2:100039.
24. International Conference on Harmonization of Technical Requirements for Registration of Pharmaceuticals for Human Use. ICH Harmonised Tripartite Guideline. Validation of Analytical Procedures: Text and Methodology, Q2(R1).2005; 4:1-13.

Turk J Pharm Sci 2026;23(3):130-139
**DOI:** 10.4274/tjps.galenos.2026.65179

ORIGINAL ARTICLE

# Investigation of the Effect of Calcitriol on Radiofrequency Radiation-Exposed Breast Cancer Cell Lines

Ece MİSER SALİHOĞLU[1], Mualla Pınar ELÇİ[2], Tuğba FATSA[3], Sema ÖREN[3], Meriç EŞMEKAYA[4], Sevgi YARDIM[1]*

[1]Gazi University Faculty of Pharmacy, Department of Biochemistry, Ankara, Türkiye
[2]University of Health Sciences Gülhane, Institute of Stem Cell Lab, Ankara, Türkiye
[3]University of Health Sciences Gülhane, Institute of Health Sciences, Molecular Laboratory, Ankara, Türkiye
[4]Gazi University Faculty of Medicine, Department of Biophysics, Ankara, Türkiye

## ABSTRACT

**Objectives:** Radiofrequency (RF) fields have been classified as probable human carcinogens and nonthermal. RF radiation can increase oxidative stress and inflammation in tissues. Vitamin D has been studied for many years for its anti-cancer properties and its ability to suppress cancer cell growth. In this study, we aimed to examine the effects of RF exposure on cell viability, free radical formation, and inflammation, as well as the therapeutic effect of vitamin D against such effects. MCF-7 and MDA-MB-231 cells were exposed to 2.1-GHz W-CDMA-modulated RF radiation.

**Materials and Methods:** The MTT was used for cell viability, and the FITC-conjugated annexin-V/PI was applied for apoptosis. The vitamin D receptor (VDR), NF-κB, cyclooxygenase-2 (COX-2), and *p53* gene expression levels were studied using real-time PCR. Reactive oxygen species (ROS) analysis was performed using flow cytometry.

**Results:** A statistically significant decrease in MCF-7 cell viability ($p < 0.001$) was observed with increasing doses of calcitriol compared to the control group; no significant difference in MDA-MB-231 cell viability was observed ($p > 0.05$). ROS analysis revealed that calcitriol caused significant decreases in cell viability in both cell types. Both cell lines showed a statistically significant increase in p53 expression with increasing calcitriol doses. An increase in the expression of VDR, NF-κB B, and COX-2 was also observed in MCF-7 cells.

**Conclusion:** We observed that while calcitriol administered after RF exposure did not cause statistically significant changes in ROS levels, we observed that it caused an increase in messenger RNA expression of apoptosis and inflammation markers, which could be evaluated in cancer treatment or prevention.

**Keywords:** Radiofrequency radiation, breast cancer, calcitriol, ROS, apoptosis

## INTRODUCTION

Mobile devices emit and receive low-intensity radiofrequency (RF) signals during operation. This RF radiation (RFR) can cause a series of changes and damage to biological tissues, which can be explained by thermal or non-thermal mechanisms.[1,2] Thermal effects occur when electromagnetic energy absorbed by the body raises the temperature of the body or of its tissues. This temperature increase persists until it is stabilized by blood circulation. Thermoregulatory mechanisms can counteract the elevated body temperature caused by RF sources such as mobile phones. The non–thermal effects of RF radiation are observed at energy levels that do not raise tissue or whole-

*Correspondence: sevgiy@gazi.edu.tr, ORCID-ID: orcid.org/0000-0002-0927-5188

Received: 05.12.2025 Accepted: 14.09.2026 Publication Date: 27.10.2026

Cite this article as: Salihoğlu EM, Elçi MP, Fatsa T, Ören S, Eşmekaya M, Yardım S. Investigation of the effect of calcitriol on radiofrequency radiation-exposed breast cancer cell lines. Turk J Pharm Sci. 2026;23(3):130-139

Copyright© 2026 The Author(s). Published by Galenos Publishing House on behalf of Turkish Pharmacists' Association.
This is an open access article under the Creative Commons Attribution-NonCommercial-NoDerivatives 4.0 (CC BY-NC-ND) International License.

body temperature to levels that damage tissue or the whole body. At these energy levels, free radical production has been reported to increase in tissues exposed to RFR.[3]

The effects of electromagnetic fields on biological tissues have become a topic of increasing research interest, especially as the use of communication systems such as cell phones, base stations, and wireless internet has increased rapidly. Previous studies have shown that non-thermal RF radiation can induce changes at the molecular or cellular levels.[4,5] As a result of epidemiological studies, RF fields have been classified as probable human carcinogens (Group 2B) by IARC.[6] Despite epidemiological studies indicating an increased risk of cancer, experimental investigations provide limited information on the effects and mechanisms of RF, and findings in this area remain controversial.

Another important phenomenon that should be emphasized in cancer studies is the role of free radicals. Reactive oxygen species (ROS) are continuously produced as by-products of cellular processes. The most important source of endogenous ROS is the mitochondrion.[7] Low- and moderate-intensity ROS are effective in protecting cells against infectious agents, regulating signal transduction pathways, and initiating responses to mitogenic stimuli. Due to overproduction of ROS, the oxidant/antioxidant balance in cells may shift toward oxidants, leading to oxidative stress.[8] Cancer cells exhibit high ROS production due to their rapid metabolism and impaired cellular signaling. Cancer cells exhibit greater growth and proliferation than normal cells. They activate growth factor pathways to achieve this. This triggers excessive production of ROS in organelles such as the mitochondria and endoplasmic reticulum of cancer cells, as well as increased activity of NADPH oxidases.[9,10] Another important metabolic process associated with cancer and ROS production is inflammation. Inflammation is an important immune defense mechanism in which the body recruits immune cells to defend against an irritant or pathogen. Inflammation can develop either acutely or chronically. When hemostasis is impaired in tissues for any reason, various bioactive stimuli are released from cells, which causes leukocyte mobilization towards the trauma site.[11] The long-term persistence of these responses can cause chronic inflammation and many diseases, especially cancer.[12]

Currently, cancer research has shifted its focus to the causes and treatment methods of the disease. One of the substances investigated in this context is vitamin D. It has been studied for many years for its anti-cancer and suppressive effects on cancer cell growth.[13] It has also been suggested that vitamin D has antioxidant properties, including inducing the expression of antioxidant defense system components, such as glutathione (GSH), GSH peroxidase, and superoxide dismutase, and suppressing the expression of NADPH oxidase. However, there are few studies on its antioxidant properties, and it is unclear whether it is an antioxidant or a pro-oxidant.[14,15] Cholecalciferol (vitamin D3) is formed in the skin by the interaction between 7-dehydrocholesterol and sunlight. Vitamin D3 and oral vitamin D are metabolized in the liver to 25-hydroxycholecalciferol [calcifediol; 25(OH)D3], and this compound is then hydroxylated at the 1α-position in the kidney to convert it into the active form, 1,25-dihydroxycholecalciferol [calcitriol; 1,25(OH)2D3]. The well-known function of 1,25(OH)2D3 is to help regulate serum calcium concentrations.[16] The biomarkers of vitamin D in humans are mostly 25(OH)D3 and, less frequently, 1,25(OH)2D3.[17] Studies are based on these indicators of serum vitamin D levels. Vitamin D deficiency is defined as a serum vitamin D level of less than 20 ng/mL (50 nmol/L). Epidemiologic studies on vitamin D levels in cancer patients show that these levels are lower than normal.[18] Active vitamin D interacts with the vitamin D receptor (VDR) on the target cell. This structure must be activated for vitamin D to exert its effects inside the cell. The lower-than-normal serum vitamin D levels in individuals who have not been exposed to sufficient sunlight may be attributed to VDR inactivation. Especially in individuals with cancer, it can be seen that vitamin D cannot fulfill its anti-cancer effects due to the disruption of the VDR structure as a result of the effects of cancerous cells.[19]

Breast cancer is one of the leading causes of cancer-related mortality among women worldwide. In addition to conventional anticancer therapies, calcitriol has been investigated in combination with various treatment modalities, including chemotherapy, radiotherapy, and supportive interventions, because of its antiproliferative and immunomodulatory properties. However, to the best of our knowledge, no previous study has evaluated the effects of calcitriol administered following RF exposure in breast cancer cell lines. Although breast cancer patients are continuously exposed to non-thermal RF radiation in daily life, it remains unclear whether calcitriol can modulate RF-induced cellular responses. Therefore, the present study aimed to evaluate the effects of calcitriol, administered after RF exposure, on cell viability, oxidative stress, apoptosis, and inflammation-related gene expression in MCF-7 and MDA-MB-231 breast cancer cells (Figure 1).

## MATERIALS AND METHODS

*Cell culture*

MCF-7 (ATCC® HTB22™) and MDA-MB-231 (ATCC® HTB-26™) cell lines were used in our study. Cell lines were incubated at 37 °C in a 5% $CO_2$ incubator and passaged when they reached 80% confluence. DMEM (Capricorn Scientific, Germany) supplemented with 10% fetal bovine serum (FBS) (Capricorn Scientific, FBS-HI11B, Germany), 100 IU/mL penicillin, and 100 µg/mL streptomycin (Capricorn Scientific, PS-B, Germany) was used as the culture medium.

*RF exposure*

The RF exposure system consisted of an RF exposure cabinet with a half-wave dipole antenna mounted at its center. The exposure cabinet had air holes in the upper and lower parts. A fan was placed under the exposure cabinet to ensure homogeneous temperature distribution within the exposure system (TR2016 12016B). Wideband code division multiple access (W-CDMA)-modulated RF radiation at 2.1 GHz was produced by a vector signal generator (Rohde & Schwarz, Model SMBV100A, Munich, Germany). The system was placed inside a 5% $CO_2$

incubator with a 95% humidified environment. The incubator temperature was maintained at 37 °C. An isotropic probe and an R&S®FSH handheld spectrum analyzer, manufactured by Rohde & Schwarz (Munich, Germany), were used to measure the electric field generated by the antenna. Two 12-well plates containing MCF-7 and MDA MB 231 cells were placed around the dipole antenna and simultaneously exposed to 2.1 GHz W-CDMA modulated RF radiation for 24 h. Sham-control samples were maintained under the same conditions as RF-exposed samples, except that the signal generator was off. Specific absorption rate (SAR) was determined according to the formula SAR = $\sigma/\rho \cdot |ERMS|^2$, where $\sigma$ is the electrical conductivity (S/m) of the medium, |ERMS| is the root mean square magnitude of the E-field strength (V/m), and $\rho$ is the mass density (kg/m$^3$) of the medium. The average SAR was calculated to be 0.632 W/kg.

*Experimental design*

Cells were divided into five experimental groups: (i) negative control (NC; without RF exposure), (ii) positive control (PC; RF exposure without calcitriol treatment), (iii) RF + 0.1 μM calcitriol, (iv) RF + 1 μM calcitriol, and (v) RF + 10 μM calcitriol. Cells in the RF-treated groups were first exposed to RF for 24 h and subsequently treated with calcitriol at the indicated concentrations. The negative control group was maintained under identical culture conditions without RF exposure. All experiments were performed in triplicate (n = 3 independent biological replicates).

The cells were placed in the *in vitro* RF field exposure system and exposed to a 2.1 GHz W-CDMA-modulated RF field with an average SAR of 0.632 W/kg for 24 h. At the end of exposure, cells were simultaneously harvested from the system to measure cell proliferation, gene expression, and apoptosis.

*Administration of calcitriol*

Calcitriol (1,25-dihydroxycholecalciferol; Cayman Chemical, USA) was dissolved in ethanol to prepare a 1 mg/mL (2.4 mM) stock solution. Working solutions were subsequently prepared by serial dilution in DMEM to obtain the desired final concentrations (0.1, 1, and 10 μM). Fresh working solutions were prepared immediately before each experiment and added directly to the culture medium.

*Cell viability assay*

The cells were seeded in a 96-well plate at 200 cells per mm$^3$ and incubated for 24 hours at 37 °C and 5% $CO_2$. Cells were then exposed to RF radiation and treated with calcitriol (0.1, 1, and 10 μM). After 24 hours of incubation, 20 μl of MTT (Sigma M2128 St. Louis, MO, USA) solution was added to each well, and the plates were incubated for 3–4 hours. At the end of the incubation, the supernatant was carefully aspirated without touching the cells. One hundred μL of isopropyl alcohol was added to each well, and the plate was incubated for 2 hours at room temperature in the dark. At the end of the procedure, the plate was gently shaken and read at 570 nm (BioTek Synergy HTX, USA).

*Annexin-V analysis*

$5 \times 10^5$ cells were used for apoptosis analysis. Cells treated with various doses of calcitriol for 24 hours were collected by trypsinization; the cell pellet was resuspended in 100 μL of binding buffer, containing $5 \times 10^5$ cells in 500 μL. Then, 5 μL of annexin and 20 μL of PI were added and mixed by pipetting. After incubation for 30 minutes at room temperature in the dark, 400 μL of 1X binding buffer was added, and the sample was analyzed using a flow cytometer (BD Accuri™ C6 Plus, USA).

*ROS analysis*

1 x $10^5$ cells were obtained in PBS, centrifuged at 1000 rpm for 5 minutes, and the supernatant was discarded. Cell pellets were resuspended in 200 μL of DCF-DA solution and incubated for 30 minutes at 37 °C in the dark. The cells were then centrifuged at 1000 rpm for 5 min, and the supernatant containing the DCF-DA solution was removed. Cells were resuspended in 100 μL/tube of PBS and analyzed on a flow cytometer (BD Accuri™ C6 Plus, USA).

*Gene expression analysis*

Quantitative analysis of messenger RNA (mRNA) expression levels of VDR, NF-κB, p53, and cyclooxygenase-2 (COX-2) was performed using Real-time PCR (Applied Biosystems, Foster City, CA, USA). After administration of doses of calcitriol following RF exposure, cells were incubated for 24 hours and then removed from the flasks by trypsinization. RNA extraction (ELK Biotechnology, Wuhan) was performed according to the manufacturer's instructions. Purity and quantity were measured using a multi-mode microplate reader (BioTek Synergy HTX). Complementary DNA synthesis (ELK Biotechnology EntiLink 1$^{st}$ strand, Wuhan) was performed according to the manufacturer's instructions. GAPDH was used as the housekeeping gene. The real-time PCR thermal cycling conditions were set as follows: 95 °C for 1 min, 95 °C for 15 sec, 60 °C for 1 min, and 72 °C for 30 sec, repeated for 35 cycles. Primary designs are generated using the National Center for Biotechnology Information (NCBI) and Primer3 sites. The primers used are given in Table 1.

**Table 1. Forward and reverse primers of genes.**

| | | |
|---|---|---|
| GAPDH | F: GAAGGTGAAGGTCGGAGTCAAC | R: CAGAGTTAAAAGCAGCCCTGGT |
| VDR | F: TCTCCTGCCTACTCACGATAA | R: GCTACTGCCCGTGAGAATATAA |
| NF-κB | F: TGGCCCCTATGTGGAGATCA | R: AGGGGTTGTTGTTGGTCTGG |
| COX-2 | F: CAATATCACAGCAGGCCACC | R: GCGTGAGTTTGGTGTGTCAT |
| p53 | F: TTCTCATCACCGGCATCACG | R: GCTATCACAAACTGCAAGACG |

VDR, vitamin D receptor; COX-2, cyclooxygenase-2.

NCBI GenBank. Primer-Blast® (Basic Local Alignment Search Tool) was designed and evaluated by sequence-matching analysis.

*Statistical analysis*

Mean and standard deviation (SD) (mean ± SD) were used for continuous data as descriptive statistics. The distributions of variables in three or more groups were analyzed using the Kruskal–Wallis test, and the formula developed by Conover (1980) was used as the multiple comparison test. Data were analyzed using IBM SPSS 23 (IBM SPSS Inc., Chicago, IL) software. MTT test results were analyzed by GraphPad Prism (GraphPad Software Inc., La Jolla, USA). The significance level was set at $p < 0.05$.

## RESULTS

*MTT results*

Cell proliferation was examined to determine the effect of RF exposure on breast cancer cells. For this purpose, cell cultures were subjected to 2.1 GHz RF at 0.632 W/kg for 24 hours. In the MDA-MB-231 cell line (Figure 2a), PC (RF-exposed cells without calcitriol treatment) were exposed for 24 hours, and cell viability decreased from 100% to 89% compared to the NC group. Similarly, in the MCF-7 cell line (Figure 2b), cell viability decreased from 100% to 69% compared with that of the NC group (Figure 2). After the MTT test, we selected appropriate doses of calcitriol (0.1 μM, 1 μM, and 10 μM).

Figure 2 shows the cell viability of MDA-MB-231 and MCF-7 cell lines at the end of the 24-hour RF exposure following application of various doses of calcitriol. Compared with the NC group, 1 μM and 10 μM calcitriol decreased cell viability from 100% ± 1.82 ($p < 0.001$) to 91% ± 1.43% ($p < 0.005$) and 85% ± 3.11% ($p < 0.001$), respectively. When the 24-hour exposure of the MCF-7 cell line to calcitriol was evaluated using the MTT test, a significant decrease in proliferation was observed at a concentration of 0.1 μM. Compared to the PC group, 0.1, 1, and 10 μM calcitriol decreased MCF-7 cell viability from 100 ± 2.32% ($p < 0.001$) to 85 ± 3.44% ($p < 0.001$), to 68 ± 1.97% ($p < 0.001$), to 68 ± 3.14 ($p < 0.001$), respectively. Compared with the PC group, treatment with 0.1 μM calcitriol was associated with increased cell viability, whereas higher calcitriol concentrations (1 and 10 μM) produced a reduction in cell viability, indicating a biphasic, dose-dependent response in MCF-7 cells. No significant difference in MDA-MB-231 cell viability was observed with increasing doses of calcitriol compared with the control and PC ($p > 0.05$).

*Apoptosis results*

Percentages of apoptotic cells were determined by the annexin-V assay (Figure 3). The percentage of live MDA-MB-231 cells in the control group is 72.1% (Figure 3). After 24 hours of RF exposure and calcitriol application at 0.1 μM, 1 μM, and 10 μM, cell viability percentages were 82.8%, 92.2%, and 90.2%, respectively (Figure 3). In MDA-MB-231 cells, although the percentage of viable cells increased following calcitriol treatment compared with the PC group, these differences were not statistically significant ($p > 0.05$).

According to the annexin-V assay, the percentage of live cells in the control group was 31.5%. After calcitriol application

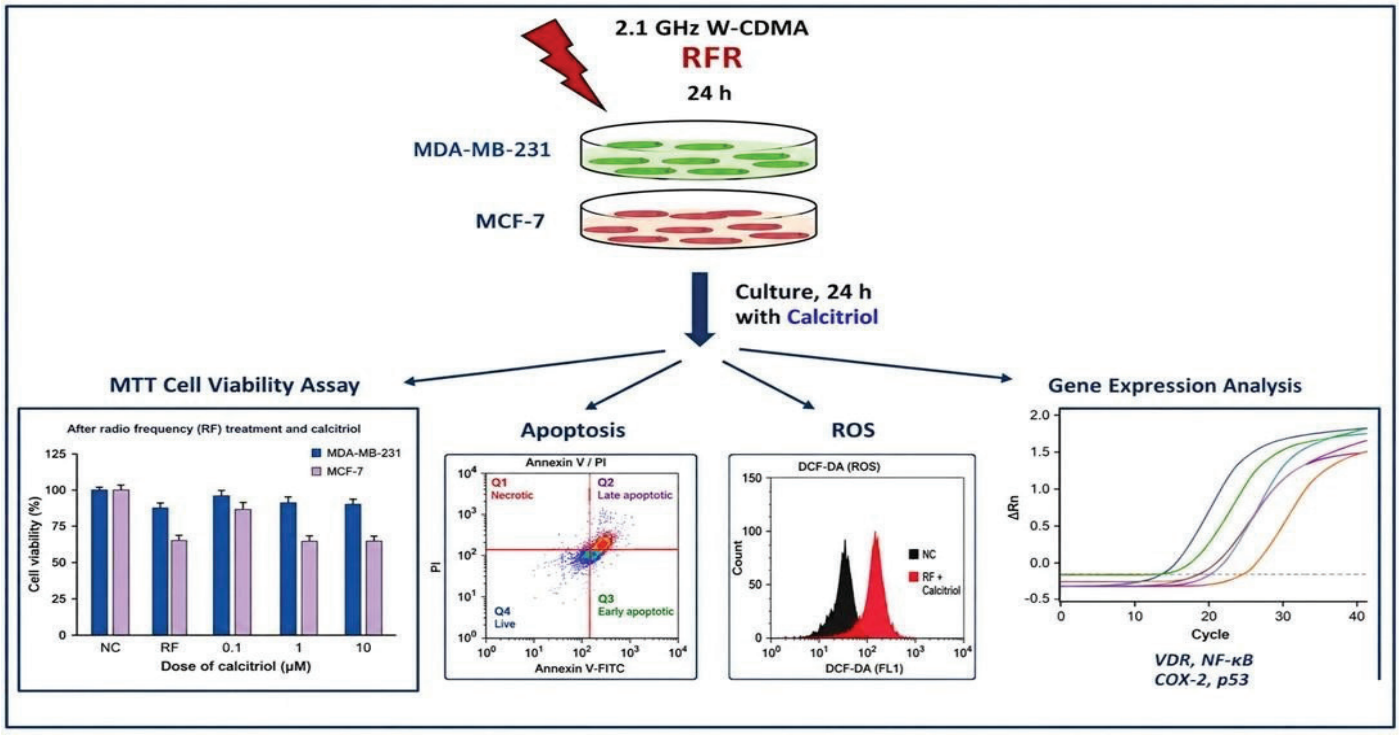



**Figure 1.** Schematic representation of study design.

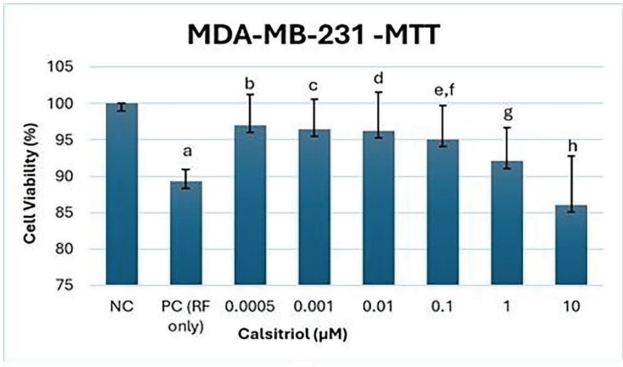
ROS, reactive oxygen species; VDR, vitamin D receptor; COX-2, cyclooxygenase-2.

(0.1 µM, 1 µM, and 10 µM), the percentages of live cells were 97.6%, 94.1%, and 89.7%, respectively (Figure 4). In MCF-7 cells, there was no statistically significant increase or decrease in apoptosis levels at 0.1, 1, and 10 µM doses compared to the control group and between doses ($p > 0.05$).

*ROS results*

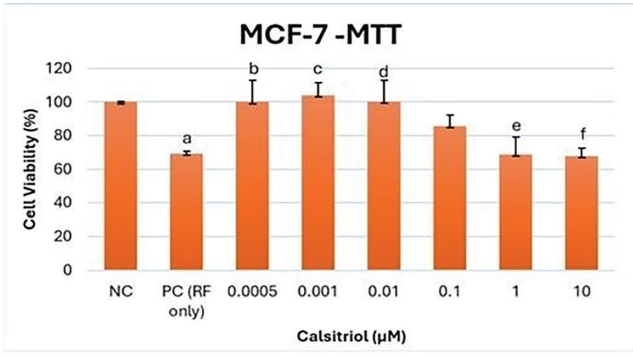
Intracellular ROS levels were determined following RF exposure and subsequent calcitriol treatment. In MDA-MB-231 cells, the relative ROS level in the PC was 76.3%, whereas levels of 76.2%, 65.7%, and 49.4% were observed after treatment with 0.1, 1, and 10 µM calcitriol, respectively (Figure 5). Although a dose-dependent decrease in ROS levels was observed compared with the PC group, these differences were not statistically significant ($p > 0.05$).

In MCF-7 cells, the relative ROS level in the positive control PC was 80.9%, whereas ROS levels following treatment with calcitriol at 0.1, 1, and 10 µM were 46.4%, 56.1%, and 39.2%, respectively (Figure 6). Although lower ROS levels were observed in the calcitriol-treated groups compared with the PC group, the differences did not reach statistical significance ($p > 0.05$).




(a)

[a] $p < 0.001$ comparing the NC and PC.
[b,c,d,e] $p < 0.005$, 0.005, 0.01, 0.05 comparing the PC with cells treated with 0.0005 µM, 0.001 µM, 0.01, and 0.1 µM of calcitriol, respectively.
[f,g,h] $p < 0.5$, 0.001, 0.005 comparing the NC with cells treated with 0.1 µM, 1 µM, 10.0 µM of calcitriol, respectively.




(b)

[a] $p < 0.001$ comparing the NC and PC.
[b,c,d] $p < 0.001$, 0.001, 0.005 Significance level obtained from comparing the PC and the cells treated with 0.0005 µM, 0.001 µM, and 0.01 µM of calcitriol (respectively).
[e,f] $p < 0.005$, 0.001 Significance level obtained from comparing the NC group and the cells treated with 1.0µM and 10.0µM of calcitriol (respectively).

**Figure 2.** Cell viability of MDA-MB-231 (a) and MCF-7 (b) cells in the negative control (NC; cells without RF-exposure or calcitriol treatment), positive control (PC; RF-exposed cells without calcitriol treatment), and calcitriol-treated groups following 24 h of RF-exposure.
RF, radiofrequency.

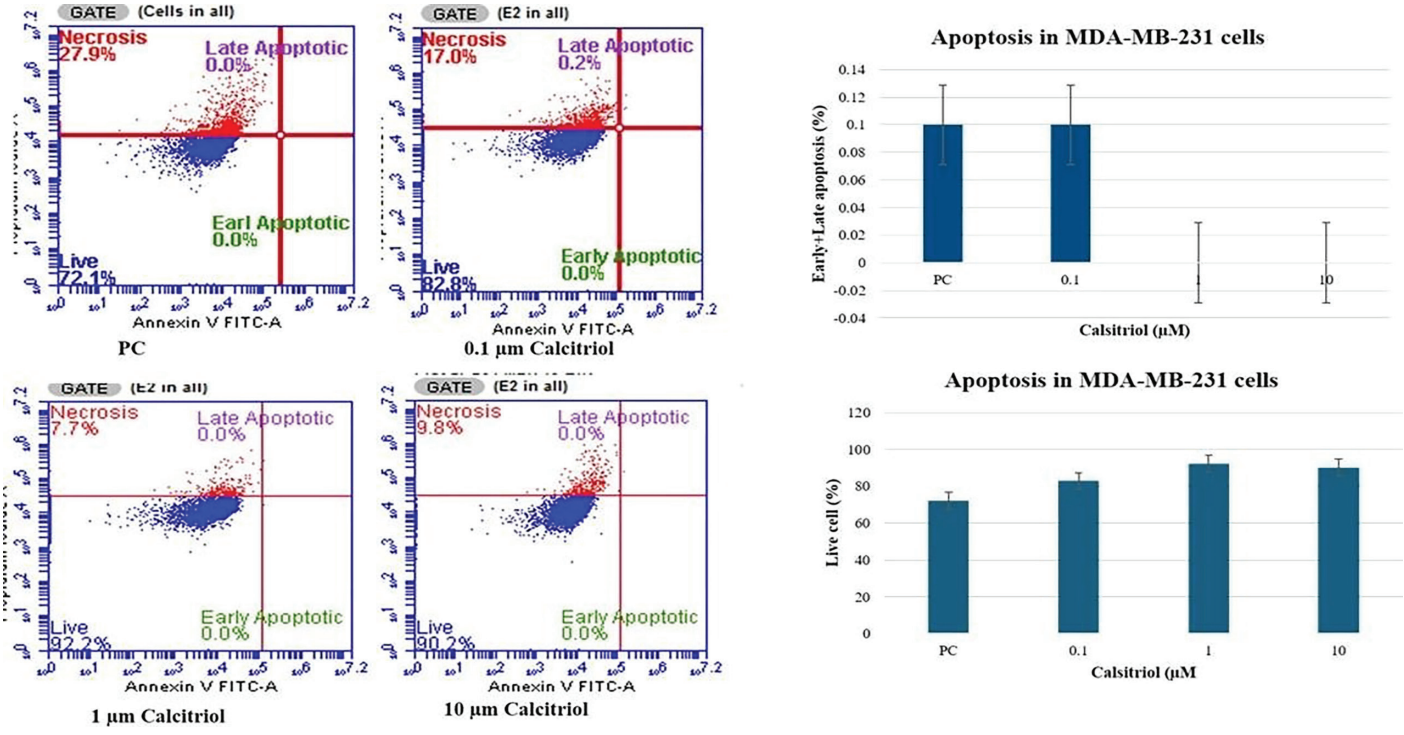



**Figure 3.** Percentage of apoptotic and viable MDA-MB-231 cells.

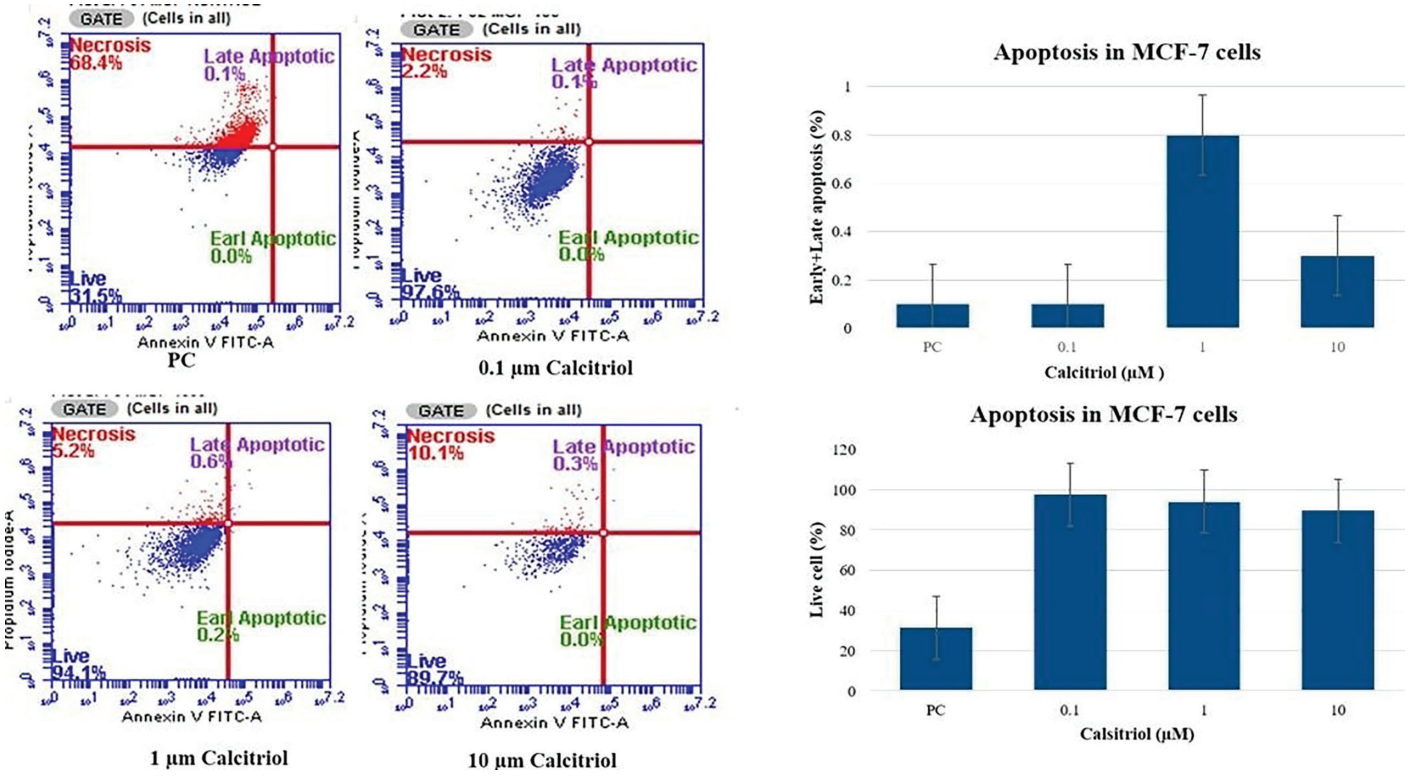



**Figure 4.** Percentage of apoptotic and viable MCF-7 cells.

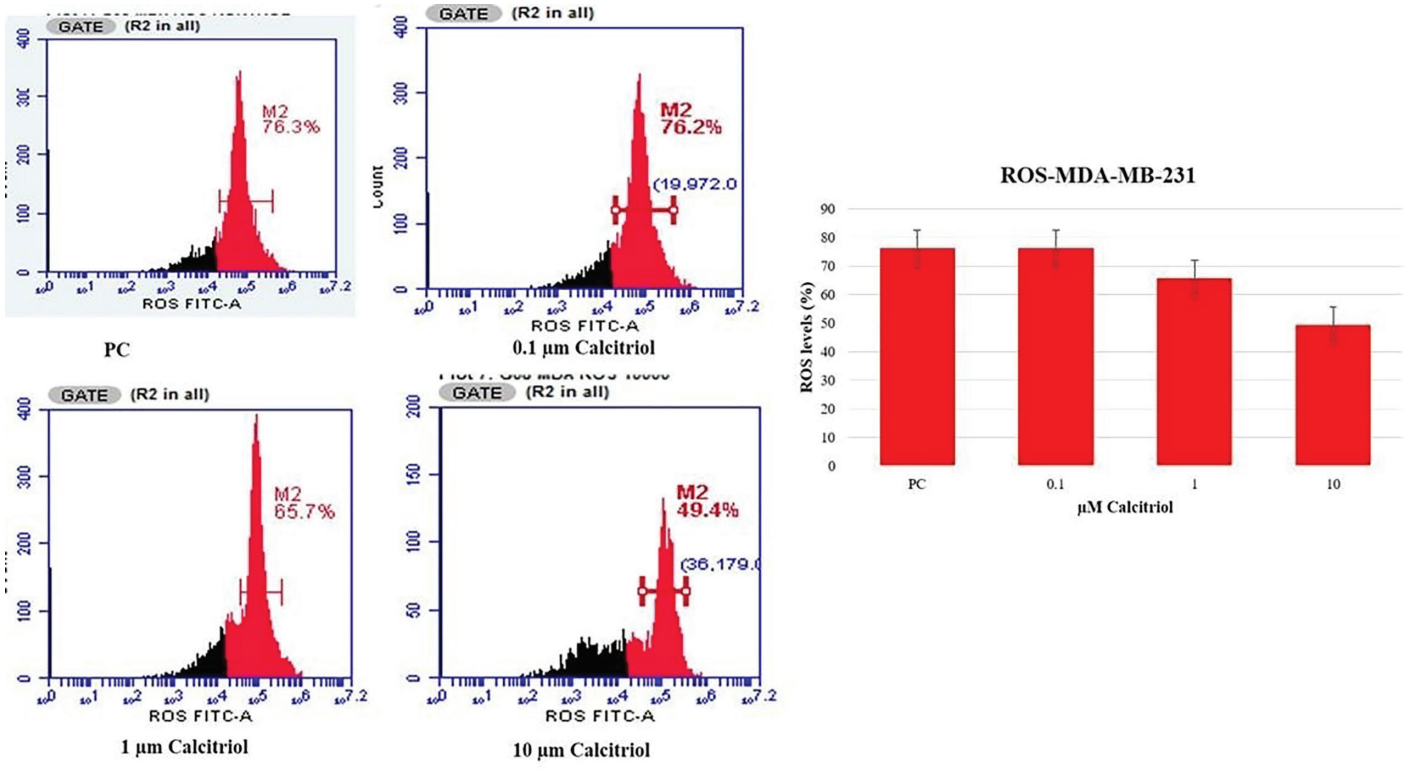



**Figure 5.** Intracellular ROS levels in MDA-MB-231 cells.
ROS, reactive oxygen species.

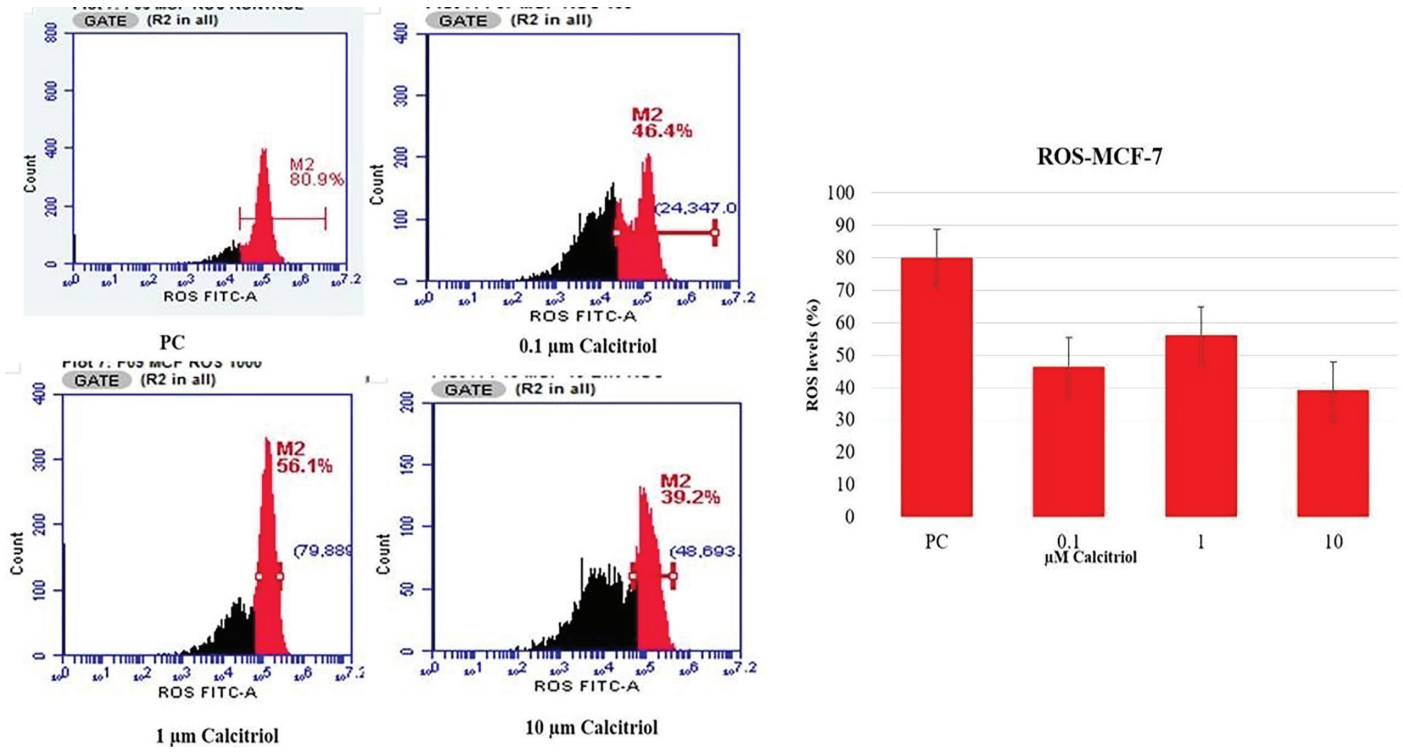



**Figure 6.** Intracellular ROS levels in MCF-7 cells. ROS, reactive oxygen species.

*Gene expression results*

To evaluate the genomic effects of calcitriol following RF exposure, the mRNA expression levels of VDR, NF-κB, COX-2, and p53 were determined by RT-qPCR (Figure 7). In MDA-MB-231 cells, the mRNA expression levels of VDR, NF-κB, and COX-2 did not differ significantly between the PC group and the calcitriol-treated groups (0.1, 1, and 10 µM) or among the calcitriol doses ($p > 0.05$). Although NF-κB expression tended to decrease and COX-2 expression tended to increase with increasing calcitriol concentrations, these changes did not reach statistical significance. Likewise, treatment with 0.1 µM calcitriol did not significantly alter p53 mRNA expression compared with the PC group ($p > 0.05$). However, 1 µM and 10 µM calcitriol significantly increased p53 mRNA expression by approximately 3.2- and 4.3-fold, respectively, compared with the PC group ($p < 0.05$) (Figure 7).

Expression levels of VDR, NF-κB, COX-2, and p53 were also evaluated in MCF-7 cells following 24 h of RF exposure and subsequent 24 h calcitriol treatment (Figure 8). VDR mRNA expression increased 2.38-fold, 2.62-fold, and 2.25-fold following treatment with 0.1, 1, and 10 µM calcitriol, respectively, compared with the PC group ($p < 0.05$) (Figure 8). However, no statistically significant differences were observed among the

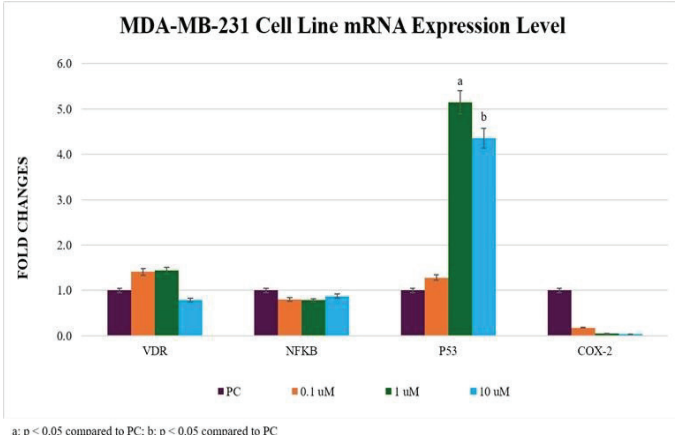



**Figure 7.** VDR, NF-κB, COX-2, and p53 mRNA expression levels in the MDA-MB-231 cell line.

VDR, vitamin D receptor; COX-2, cyclooxygenase-2; mRNA, messenger RNA.

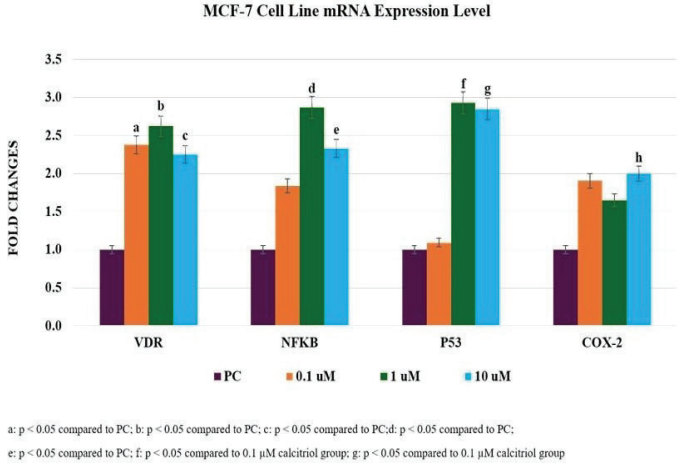



**Figure 8.** VDR, NF-κB, COX-2, and p53 mRNA expression levels in the MCF-7 cell line.

VDR, vitamin D receptor; COX-2, cyclooxygenase-2; mRNA, messenger RNA.

calcitriol-treated groups ($p > 0.05$). NF-κB mRNA expression was not significantly altered following treatment with 0.1 μM calcitriol compared with the PC group ($p > 0.05$). In contrast, treatment with 1 μM and 10 μM calcitriol increased NF-κB mRNA expression by 2.87- and 2.33-fold, respectively, compared with the PC group ($p < 0.05$). No statistically significant differences were observed between the 1 μM and 10 μM calcitriol-treated groups ($p > 0.05$). p53 mRNA expression was significantly higher in cells treated with 1 μM and 10 μM calcitriol than in those treated with 0.1 μM calcitriol ($p < 0.05$). COX-2 mRNA expression increased approximately 2-fold following treatment with 10 μM calcitriol compared with the PC group; however, this increase did not reach statistical significance ($p > 0.05$).

## DISCUSSION

The present study investigated the cellular responses of breast cancer cells to calcitriol treatment following RF exposure. We evaluated whether post-RF administration of calcitriol modulates RF-associated changes in cell viability, oxidative stress, apoptosis, and inflammation-related gene expression in MDA-MB-231 and MCF-7 cells. To interpret these findings, it is important to consider the well-established anticancer properties of calcitriol reported in the literature.

Many published studies associate low vitamin D levels not only with ischemic diseases but also with non-ischemic cancers, metabolic syndrome, infections, and autoimmune diseases.[20] Studies show that calcitriol can potentially influence cancer development and growth by regulating multiple signaling pathways involved in proliferation, apoptosis, differentiation, inflammation, invasion, angiogenesis, and metastasis.[21,22] Vitamin D and its metabolites reduce the incidence of many types of cancer by inhibiting tumor angiogenesis, enhancing cell-to-cell communication, and increasing contact inhibition of proliferation.

When calcitriol's regulation of specific signaling pathways involved in the growth of colon, breast, and prostate cancers was examined, calcitriol exerted a broad effect on cancer cells across multiple cancer types.[23] The anticancer effects of vitamin D can be analyzed in terms of antiproliferative, anti-inflammatory, and proapoptotic activities. The antiproliferative effect of vitamin D is achieved by interrupting cell cycle progression.[24] The cell cycle, which occurs in four stages, is regulated by cyclin-dependent kinases and their inhibitors, both of which are involved in specific processes such as cellular transcription. Vitamin D exerts this effect by suppressing kinase activity or inducing kinase inhibitors.[25]

Vitamin D also exerts its anti-inflammatory effect by modulating prostaglandin metabolism, which is implicated in the development and progression of many cancers. This is accomplished by $NAD^+$-dependent up-regulation of the *15-hydroxyprostaglandin dehydrogenase* gene and COX-2, thereby reducing prostaglandin levels.[24] Increased COX-2 expression has been reported to inhibit apoptosis, stimulate cell division, and inhibit antitumor immune responses and protein synthesis in cells, as well as inhibit cell adhesion and promote metastasis by stimulating neovascularization, thereby affecting cancer development.[26] Vitamin D exerts its proapoptotic effect in many cancer cells by suppressing the expression of anti-apoptotic proteins or by inducing apoptosis through the expression of apoptosis-inducing proteins.[27] However, in our study, COX-2 expression was suppressed at low doses in MDA-MB-231 cells, whereas it was re-induced at higher doses. COX-2 expression in MCF7 cells was higher at all doses than in the PC. In a similar study, COX-2 expression increased in MCF-7 cells and decreased in MDA-MB-231 cells after application of 1 μM calcitriol.[28] However, in MCF-7 cells the protein expression profile was generally consistent with mRNA expression, whereas in MDA-MB-231 cells protein expression appeared to increase despite relatively low mRNA expression.

The organism is constantly exposed to ROS that occur as byproducts of cellular processes and to exogenous ROS. Endogenous ROS at low and moderate concentrations effectively protect cells against infectious agents, regulate signal transduction pathways, and initiate responses to mitogenic stimuli. On the other hand, the oxidant/antioxidant imbalance resulting from excessive ROS production may favor oxidants, leading to oxidative stress.[8] Cancer cells produce elevated ROS levels due to their rapid metabolism and impaired cellular signaling mechanisms. Following RF exposure, calcitriol treatment showed a dose-dependent tendency toward lower ROS levels in both cell lines. However, these decreases did not reach statistical significance ($p > 0.05$). Although the observed trend may suggest an antioxidant effect of calcitriol, the present data do not provide sufficient evidence to conclude that it significantly reduced ROS levels under the experimental conditions used in this study. Although calcitriol treatment showed a tendency to reduce ROS levels following RF exposure, these changes did not reach statistical significance. Therefore, alterations in ROS should be interpreted cautiously, as the biological role of ROS in cancer is highly context-dependent. Depending on the cellular environment, reduced ROS levels may contribute to either enhanced cell survival or modulation of signaling pathways involved in apoptosis. In the present study, the tendency toward lower ROS levels was accompanied by increased apoptosis, particularly in MCF-7 cells, suggesting that the observed cellular responses cannot be explained solely by changes in oxidative stress but may also involve other apoptosis- and inflammation-related molecular pathways. Numerous studies have investigated the effects of vitamin D and its analogs, such as tacalcitol and calcipotriol, in cancer treatment. In a study by Milczarek et al.[29] in rats, vitamin D analogs were reported to inhibit tumor cell growth by enhancing anticancer effects. In another study by Ajibade et al.[2] in mice, vitamin D analogs reduced cancer cell numbers, suggesting that vitamin D is a reversible risk factor for cancer. 1α,25(OH)2D3 inhibits mitosis and induces apoptosis in breast cancer cells.[30] Following RF exposure, calcitriol treatment was associated with increased apoptosis, particularly in MCF-7 cells.

Activation of NF-κB in immune cells leads to the production of cytokines that activate NF-κB in cancer cells. NF-κB is

involved in angiogenesis, invasiveness, motility, chemokine and cytokine production, as well as in the regulation of genes that control cell survival, proliferation, and growth. The sustained activation of key inflammatory signaling pathways, such as NF-κB, COX-2, and Janus kinase/signal transducer and activator of the transcription, has been shown to contribute to the initiation of inflammatory breast cancer (IBC). Some inflammatory molecules, such as interleukin (IL)-6, tumor necrosis factor-alpha (TNF-α), and γ-interferon, function mainly in the process of malignant transformation of IBC, while transforming growth factor-β, IL-8, IL-1β, and TNF-α are involved in cancer cell proliferation, survival, epithelial-to-mesenchymal transition, invasion, and metastasis.[31] NF-κB appears to have a complex role in cancer. Although NF-κB is a critical molecule in the initiation and progression of cancer, it is also an essential player in the immune response to cancer. While inhibition of NF-κB is undesirable during the tumor elimination phase of the immune response, it is expected to have positive effects during the chronic inflammation phase of tumor progression, when the immune system targets transformed cells.[32] Following RF exposure, we observed a slight increase in NF-κB mRNA expression in MDA-MB-231 cells and a significant decrease at the 10 μM dose. In MCF-7 cells, NF-κB levels increased significantly and then showed slight dose-dependent declines.

p53 is a transcription factor that regulates the cell cycle. It is a protein that plays a key role in cancer suppression across many organisms. It is also involved in cell growth arrest, programmed cell death, cell differentiation, and initiation of DNA repair. It has been emphasized that p53 activity is impaired in cancerous cells and that its expression is decreased. Calcitriol has been shown to induce p53 expression.[33] Following RF exposure, calcitriol treatment significantly increased p53 expression in both cell lines, particularly at doses above 1 μM.

An additional finding of the present study was that the two breast cancer cell lines differed in their responses to calcitriol. While MCF-7 cells exhibited a more pronounced increase in apoptosis and a biphasic pattern of cell viability, MDA-MB-231 cells showed more modest changes in these parameters. These differences may reflect the distinct molecular characteristics of the two cell lines. Gx1A notable finding of the present study was a biphasic response in MCF-7 cells. Lower-dose calcitriol partially improved cell viability following RF exposure, whereas higher concentrations reduced viability. This pattern may reflect concentration-dependent cellular responses to calcitriol, suggesting that different signaling pathways may predominate at different doses. However, the underlying mechanisms were not investigated in the present study and should be explored in future studies.

*Study limitations*

A limitation of this study is that calcitriol-only treatment groups (without RF exposure), a separate vehicle (ethanol) control group, and non–malignant breast epithelial cells were not included. Therefore, the direct effects of calcitriol could not be determined based on its effects observed following RF exposure; the potential contribution of the vehicle could not be excluded; and the findings could not be directly extrapolated to normal breast epithelial cells. Future studies incorporating additional control groups may clarify the respective contributions of calcitriol and RF exposure under the experimental conditions used.

## CONCLUSION

The present findings suggest that calcitriol modulates cellular and transcriptional responses in RF-exposed breast cancer cells. Following RF exposure, calcitriol treatment was associated with increased apoptosis and p53 and NF-κB mRNA expression levels, whereas ROS levels showed a decreasing trend that did not reach statistical significance. These findings indicate that calcitriol may modulate apoptosis- and inflammation-related pathways following RF exposure. However, additional studies, particularly those including calcitriol-only treatment groups and protein-level analyses, are required to further clarify the underlying mechanisms.

*Ethics*

**Ethics Committee Approval:** Not applicable. This study involved only *in vitro* cell culture experiments and did not include human participants or animals. Therefore, ethics committee approval was not required.

**Informed Consent:** Not applicable.

*Footnotes*

*Authorship Contributions*

Concept: E.M.S., M.P.E., S.Y., Design: E.M.S., M.P.E., S.Y., Data Collection or Processing: E.M.S., M.P.E., T.F., S.Ö., M.E., Analysis or Interpretation: E.M.S., M.P.E., S.Y., Literature Search: E.M.S., M.P.E., S.Y., Writing: E.M.S., M.P.E., S.Y.

**Conflict of Interest:** The authors declare no conflicts of interest.

**Financial Disclosure:** The authors declared that this study received no financial support.

## REFERENCES

1. Challis LJ. Mechanisms for interaction between RF fields and biological tissue. Bioelectromagnetics. 2005;Suppl 7:S98-S106.
2. Ajibade AA, Kirk JS, Karasik E, Gillard B, Moser MT, Johnson CS, Trump DL, Foster BA. Early growth inhibition is followed by increased metastatic disease with vitamin D (calcitriol) treatment in the TRAMP model of prostate cancer. PLoS One. 2014;9:e89555.
3. International Commission on Non-Ionizing Radiation Protection (ICNIRP). Guidelines for limiting exposure to electromagnetic fields (100 kHz to 300 GHz). Health Phys. 2020;118:483-524.
4. Pacini S, Ruggiero M, Sardi I, Aterini S, Gulisano F, Gulisano M. Exposure to global system for mobile communication (GSM) cellular phone radiofrequency alters gene expression, proliferation, and morphology of human skin fibroblasts. Oncol Res. 2002;13:19-24.
5. Sirav B, Seyhan N. Blood-brain barrier disruption by continuous-wave radio frequency radiation. Electromagn Biol Med. 2009;28:215-222.

6. Baan R, Grosse Y, Lauby-Secretan B, El Ghissassi F, Bouvard V, Benbrahim-Tallaa L, Guha N, Islami F, Galichet L, Straif K; WHO International Agency for Research on Cancer Monograph Working Group. Carcinogenicity of radiofrequency electromagnetic fields. Lancet Oncol. 2011;12:624-626.
7. Karabulut H, Gülay MŞ. Antioksidanlar. Veterinary Journal of Mehmet Akif Ersoy University. 2016;1:65-76.
8. Pham-Huy LA, He H, Pham-Huy C. Free radicals, antioxidants in disease and health. Int J Biomed Sci. 2008;4:89-96.
9. Mittler R. ROS are good. Trends Plant Sci. 2017;22:11-19.
10. Cairns RA, Harris IS, Mak TW. Regulation of cancer cell metabolism. Nat Rev Cancer. 2011;11:85-95.
11. de Visser KE, Eichten A, Coussens LM. Paradoxical roles of the immune system during cancer development. Nat Rev Cancer. 2006;6:24-37.
12. Coussens LM, Werb Z. Inflammation and cancer. Nature. 2002;420:860-867.
13. National Cancer Institute. Vitamin D and Cancer. Reviewed May 9, 2023. Available from: https://www.cancer.gov/about-cancer/causes-prevention/risk/diet/vitamin-d-fact-sheet
14. Berretta M, Quagliariello V, Bignucolo A, Facchini S, Maurea N, Di Francia R, Fiorica F, Sharifi S, Bressan S, Richter SN, Camozzi V, Rinaldi L, Scaroni C, Montopoli M. The multiple effects of vitamin D against chronic diseases: from reduction of lipid peroxidation to updated evidence from clinical studies. Antioxidants (Basel). 2022;11:1090.
15. Mokhtari Z, Hekmatdoost A, Nourian M. Antioxidant efficacy of vitamin D. J Parathyr Dis. 2017;5:11-16.
16. Grant WB, Lahore H, McDonnell SL, Baggerly CA, French CB, Aliano JL, Bhattoa HP. Evidence that vitamin D supplementation could reduce risk of influenza and COVID-19 infections and deaths. Nutrients. 2020;12:988
17. Zerwekh JE. Blood biomarkers of vitamin D status. Am J Clin Nutr. 2008;87:1087S-1091S.
18. Wesa KM, Segal NH, Cronin AM, Sjoberg DD, Jacobs GN, Coleton MI, Fleisher M, Dnistrian AM, Saltz LB, Cassileth BR. Serum 25-hydroxy vitamin D and survival in advanced colorectal cancer: a retrospective analysis. Nutr Cancer. 2015;67:424-430.
19. Salle BL, Delvin EE, Lapillonne A, Bishop NJ, Glorieux FH. Perinatal metabolism of vitamin D. Am J Clin Nutr. 2000;71:1317S-1324S.
20. Holick MF. Vitamin D: a D-lightful health perspective. Nutr Rev. 2008;66:S182-S194.
21. Fatsa T, Hosbul T, Elçi PM, Ören S, Unat İ, Yılmaz C. Antiproliferative, anti-inflammatory, antitumoral, and proapoptotic effects of calcitriol on MCF-7 and MCF-10A cell lines. Indian J Exp Biol. 2023;61:320-328.
22. Feldman D, Krishnan AV, Swami S, Giovannucci E, Feldman BJ. The role of vitamin D in reducing cancer risk and progression. Nat Rev Cancer. 2014;14:342-357.
23. de La Puente-Yagüe M, Cuadrado-Cenzual MA, Ciudad-Cabañas MJ, Hernández-Cabria M, Collado-Yurrita L. Vitamin D: and its role in breast cancer. Kaohsiung J Med Sci. 2018;34:423-427.
24. Ylikomi T, Laaksi I, Lou YR, Martikainen P, Miettinen S, Pennanen P, Purmonen S, Syvälä H, Vienonen A, Tuohimaa P. Antiproliferative action of vitamin D. Vitam Horm. 2002;64:357-406.
25. Chiang KC, Chen TC. The anti-cancer actions of vitamin D. Anticancer Agents Med Chem. 2013;13:126-139.
26. Grösch S, Maier TJ, Schiffmann S, Geisslinger G. Cyclooxygenase-2 (COX-2)-independent anticarcinogenic effects of selective COX-2 inhibitors. J Natl Cancer Inst. 2006;98:736-747.
27. Chiang KC, Yeh CN, Chen MF, Chen TC. Hepatocellular carcinoma and vitamin D: a review. J Gastroenterol Hepatol. 2011;26:1597-1603.
28. Friedrich M, Reichert K, Woeste A, Polack S, Fischer D, Hoellen F, Rody A, Köster F, Thill M. Effects of combined treatment with vitamin D and COX2 inhibitors on breast cancer cell Lines. Anticancer Res. 2018;38:1201-1207.
29. Milczarek M, Psurski M, Kutner A, Wietrzyk J. Vitamin D analogs enhance the anticancer activity of 5-fluorouracil in an in vivo mouse colon cancer model. BMC Cancer. 2013;13:294.
30. Chen P, Hu P, Xie D, Qin Y, Wang F, Wang H. Meta-analysis of vitamin D, calcium and the prevention of breast cancer. Breast Cancer Res Treat. 2010;121:469-477.
31. Fouad TM, Kogawa T, Reuben JM, Ueno NT. The role of inflammation in inflammatory breast cancer. Adv Exp Med Biol. 2014;816:53-73.
32. Hoesel B, Schmid JA. The complexity of NF-κB signaling in inflammation and cancer. Mol Cancer. 2013;12:86.
33. Diesing D, Cordes T, Fischer D, Diedrich K, Friedrich M. Vitamin D--metabolism in the human breast cancer cell line MCF-7. Anticancer Res. 2006;26:2755-2759.

Turk J Pharm Sci 2026;23(3):140-149
**DOI:** 10.4274/tjps.galenos.2026.92428

ORIGINAL ARTICLE

# Polypharmacy and Glycemic Status in Individuals with Diabetes and Pre-diabetes: Iranian Multi-Center Osteoporosis Study 2021

Sarmad SALEHI[1], Azin RASHIDI[3], Mohanna KHOJASTE[2], Pardis ZAREPOUR[1], Neda CHERAGHLOO[1], Safoora GHARIBZADEH[4], Ozra TABATABAEI MALAZY[5]*, Afshin OSTOVAR[6]

[1]Non-Communicable Diseases Research Center, Endocrinology and Metabolism Population Sciences Institute, Tehran University of Medical Sciences, Tehran, Iran
[2]Department of Epidemiology and Biostatistics, School of Public Health, Tehran University of Medical Sciences, Tehran, Iran
[3]School of Medicine, Tehran University of Medical Sciences, Tehran, Iran
[4]Leicester Real World Evidence Unit, Diabetes Research Centre, Leicester General Hospital, University of Leicester, Leicester, UK
[5]Endocrinology and Metabolism Research Center, Endocrinology and Metabolism Clinical Sciences Institute, Tehran University of Medical Sciences, Tehran, Iran
[6]Osteoporosis Research Center, Endocrinology and Metabolism Clinical Sciences Institute, Tehran University of Medical Sciences, Tehran, Iran

## ABSTRACT

**Objectives:** This study examined the association between polypharmacy and glycemic status among adults aged ≥ 50 years.

**Materials and Methods:** This cross-sectional analysis included 1,117 participants from the 2021 Iranian Multi-center Osteoporosis Study (XXX). Data on sociodemographic characteristics, lifestyle factors, clinical and biochemical measures, and medication use were collected using standardized questionnaires, physical examinations, laboratory assessments, and direct observation of medication packages. Polypharmacy was assessed using thresholds of ≥ 3 and ≥ 5 concurrent medications. Weighted prevalence estimates with 95% confidence intervals (CIs) were calculated, and multivariable logistic regression models were used to examine the association between polypharmacy and glycemic status, with adjustment for relevant demographic and health-related factors.

**Results:** Polypharmacy was more common in individuals with diabetes than in those with pre-diabetes (≥ 3 medications: 49.89% vs. 28.25%; ≥ 5 medications: 26.28% vs. 9.82%).The mean number of medications was also higher among individuals with diabetes than among those with pre-diabetes (2.94 vs. 1.58). Among individuals receiving antidiabetic medications, polypharmacy defined as ≥ 5 medications was associated with higher odds of uncontrolled diabetes [adjusted odds ratio (AOR) = 2.21; 95% CI: 1.49, 3.29]. Each additional medication was also associated with higher odds of uncontrolled diabetes (AOR = 1.20; 95% CI: 1.12, 1.28).

**Conclusion:** Polypharmacy was associated with poorer glycemic control among adults aged ≥ 50 years. The association between polypharmacy and uncontrolled diabetes was particularly evident among those using ≥ 5 medications. These findings highlight the importance of considering overall medication burden when managing diabetes in this population.

**Keywords:** Polypharmacy, diabetes, pre-diabetes, Iran

***Correspondence:** tabatabaeiml@sina.tums.ac.ir, **ORCID-ID:** orcid.org/0000-0003-0188-9721

**Received:** 31.01.2026 **Accepted:** 17.09.2026 **Publication Date:** 27.10.2026

**Cite this article as:** Salehi S, Rashidi A, Khojaste M, Zarepour P, Cheraghloo N, Gharibzadeh S, Tabatabaei Malazy O, Ostovar A. Polypharmacy and glycemic status in individuals with diabetes and pre-diabetes: Iranian multi-center osteoporosis study 2021. Turk J Pharm Sci. 2026;23(3):140-149

Copyright© 2026 The Author(s). Published by Galenos Publishing House on behalf of Turkish Pharmacists' Association.
This is an open access article under the Creative Commons Attribution-NonCommercial-NoDerivatives 4.0 (CC BY-NC-ND) International License.

## INTRODUCTION

Diabetes is a major public health concern among older adults and is frequently accompanied by multiple chronic conditions that require the use of several medications.[1] The coexistence of diabetes and other chronic conditions often results in complex treatment regimens and increases the likelihood of polypharmacy. In addition to the challenges associated with managing multiple medications, polypharmacy may increase the risk of drug–drug interactions, adverse drug reactions, treatment burden, and poor health outcomes.[2] Therefore, understanding the relationship between polypharmacy and glycemic status is clinically important, particularly among older adults with diabetes who are more likely to have multiple comorbidities and complex medication regimens.

Among the various definitions of polypharmacy, the use of five or more medications simultaneously is the most common.[3] However, according to a recent report from the World Health Organization (WHO), there is no generally accepted definition of polypharmacy.[4] Polypharmacy is prevalent among individuals with diabetes, with approximately two–thirds of older people with diabetes taking multiple medications at the same time.[5]

The reported prevalence of polypharmacy across different studies ranged from 47% to 97.5% in older adults with diabetes, and the pooled prevalence in the study by Remelli et al.[5] was 64%. A survey conducted in Finland showed that patients with type 2 diabetes used considerably more medications and had a significantly greater medication burden than non–diabetic patients.[6] The need to add multiple medications to an individual's treatment regimen is strongly influenced by diabetes-related comorbidities and advanced age.[7]

Polypharmacy is clinically important because of its potential implications for overall health, quality of life, and life expectancy.[7] Although the use of multiple medications may reflect a greater burden of disease, it may also independently increase the risk of drug interactions and adverse events.[7,8] Individuals with diabetes and multiple chronic conditions are more vulnerable to the adverse effects of polypharmacy because of neuropathy, dysautonomia, and vascular disease.[7] Although it's reported that a statistically significant relationship exists between polypharmacy and mortality and myocardial infarction, a non-statistically significant relationship was found between polypharmacy and stroke and hospitalization in a systematic review and meta-analysis study.[9]

Previous studies have provided important evidence regarding polypharmacy among individuals with diabetes. For instance, the survey by Remelli et al.[5] reported a high prevalence of polypharmacy among older adults with diabetes and highlighted its association with several health-related outcomes, including glycemic control, syncope, hospitalization, and mortality. However, most studies in Iran on polypharmacy among individuals with diabetes have been hospital–based and have primarily focused on the prevalence of polypharmacy rather than the relationship between polypharmacy and glycemic status. Therefore, this study aimed to explore the association between polypharmacy and both glycemic status among adults aged ≥ 50 years with diabetes or pre-diabetes, using data from the 2021 Iranian Multi-center Osteoporosis Study (IMOS).

## MATERIALS AND METHODS

### *Study population*

IMOS is a national and population-based, cross-sectional survey which has been administered in Iran to estimate the prevalence of osteoporosis and its risk factors.[6] A multi-stage stratified random sampling approach was applied, in which the 31 provinces of Iran were stratified into five homogeneous strata based on potential osteoporosis risk factors, and one or two provinces were randomly selected from each stratum. Ultimately, eight provinces (Tehran, Isfahan, Mazandaran, West Azerbaijan, North Khorasan, Fars, Kermanshah, and Khuzestan) were included. Details of the IMOS study were published previously.[6]

The inclusion criteria for IMOS comprised sufficient physical and mental health abilities, including both females and males aged ≥ 50 years who reside in rural and urban areas. The exclusion criteria of the study were cystic fibrosis, inability to measure bone mineral density, pregnancy, weighing more than 150 kg, and having undergone X-ray imaging with contrast in the last 14 days. In the IMOS study, 1450 individuals aged 50 years and older participated. Of these, 260 participants with normal blood glucose levels (fasting blood sugar < 100 mg/dL), no previous diagnosis of diabetes, and no current use of glucose-lowering medications were excluded from the study population. After removing 73 cases with missing data, we retained a sample of 1117 individuals for analysis. Figure 1 summarizes the selection process and variable-specific missing data.

### *Study instruments and validation*

Data were collected using version 3.2 of the WHO questionnaires, which were translated and standardized for use in Iran.[10] The instruments were evaluated for internal consistency, face validity, and content validity and pilot–tested prior to their implementation.

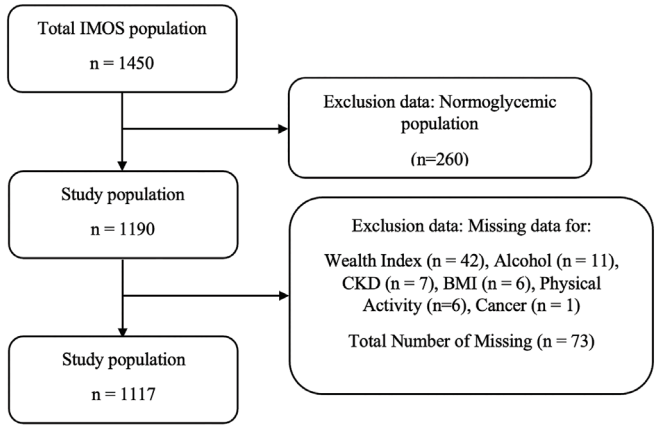



**Figure 1.** Missing and inclusion flowchart of the study
CKD, chronic kidney disease; BMI, body mass index.

*Sociodemographic and lifestyle variables measurements*

Demographic data included age, sex, residential area, wealth index (WI), employment status, marital status, and years of schooling. WI was measured using a questionnaire consisting of 36 questions that evaluated household assets and covered different dimensions of participants' assets. Principal component analysis (PCA), a statistical method, was employed to simplify and condense this information.[11] PCA utilizes all the collected data to derive new summary variables, termed principal components. The initial principal component, which explained the largest variation in wealth, was WI.[11] WI was categorized as 0 (lowest), 1 (moderate), and 2 (highest). The question used to determine participants' employment status was: "What has been your employment status during the past 12 months?" Years of schooling were divided into three groups: 6 years or less, 7 to 11 years, and 12 years or more of successfully completed schooling.

Anthropometric factors included body mass index (BMI) and waist circumference (WC). BMI, defined as the weight (kg) to the square of height (M) ratio, was divided into three categories: less than 25 as underweight or normal weight, 25 to 30 as overweight, and more than 30 as obese.[12] WC was divided into two categories of less than 95 cm as non-central obesity and ≥ 95 as central obesity.[12]

Systolic and diastolic blood pressures were measured three times with standard Beurer sphygmomanometers at the brachial artery; the interval between measurements was three minutes, and measurements were taken in a sitting position after 15 minutes of rest. The second and third measurements' average was reported as the final blood pressure

Lifestyle factors included alcohol consumption, smoking, and physical activity. Alcohol consumption was evaluated using the question: "During the past 12 months, how often did you drink alcohol?" The question "do you currently smoke any tobacco products?" was used to evaluate tobacco use during the past 12 months. Based on their responses, participants were classified into two groups: current smokers and non–current smokers. To evaluate physical activity, the Global Physical Activity Questionnaire version two, developed by WHO, was used.[13] This study measured physical activity in minutes per week.[14] Participants were classified as engaging in 150 minutes or more per week or less than 150 minutes per week.

*Biochemical assessments*

Laboratory measurements—glycosylated hemoglobin A1C (HbA1C), fasting plasma glucose (FPG), and creatinine—were assessed using the auto-analyzer (Roche-Hitachi Cobas C311, High-Technologies Corporation, Tokyo, Japan).[10] Blood samples were obtained after a 12-hour fasting period. The prestige premium 24i analyzer was used to assess urinary albumin. The estimated glomerular filtration rate (eGFR) was calculated using patients' age, sex, and the measured serum creatinine.[10] GFR was estimated from calibrated serum creatinine values using equations such as the Modification of Diet in Renal Disease (MDRD) Study equation and the Cockcroft-Gault formula.[15]

*Definitions of clinical conditions*

Diabetes was defined as fasting blood sugar levels ≥ 126 mg/dL, HbA1c ≥ 6.5%, or self-reported medical diagnosis or use of glucose-lowering medications, including oral medications or insulin.[16] Pre-diabetes was defined as fasting blood sugar levels between 100 mg/dL and 126 mg/dL, HbA1c between 5.7% and 6.5%, and not being on medication for diabetes.[16]

Individuals with diabetes were classified into two main categories: those who were unaware of their condition and those who were aware. The aware group was further divided into individuals not receiving treatment and those receiving treatment. Among those receiving treatment, glycemic status was categorized as controlled or uncontrolled based on HbA1c levels. HbA1c < 7.0% was considered controlled diabetes, whereas HbA1c ≥ 7.0% was considered uncontrolled diabetes, consistent with the glycemic target recommended by the American Diabetes Association.[17]

The variable "multiple long-term conditions" was defined as the co-occurrence of at least two chronic conditions in the same individual, including cardiovascular diseases (CVDs), cancer, hypertension, chronic kidney disease (CKD), and diabetes. CVD was evaluated by a self-reported response to the question: "Have you ever had a heart attack or chest pain from heart disease (angina) or a stroke (cerebrovascular accident or incident)?" The history of cancer was also assessed by self-report, using the question: "During the past 12 months, did a doctor or other health worker tell you that you had cancer?. Hypertension can be defined by any of the following criteria: systolic blood pressure of 140 mmHg or higher, diastolic blood pressure of 90 mmHg or higher, or a history of antihypertensive medication use. CKD was defined as an eGFR < 60 mL/min/1.73 $m^2$ or urine albumin excretion > 30 mg/g in individuals with diabetes.[15]

*Assessment of polypharmacy*

Polypharmacy in this study is defined both as taking three or more medications at one time and as taking five or more medications. In the main analysis, vitamin supplements are included in the list of medications and in the definition of polypharmacy. However, tables presenting polypharmacy data excluding vitamins from the list of medications are provided in the supplementary file. Participants were asked to bring their medication packages with them to the interview, and the interviewer recorded medication information after directly observing the medications.

*Statistical analysis*

All analyses used weighted data to reflect the national population accurately. The final weight was derived by combining sampling, response, and post-stratification weights. Detailed procedures for weight construction are described in the study protocol.[6] By excluding observations with missing values (6.13%), a complete-case approach was used in the analyses. Descriptive statistics, including weighted prevalence estimates and 95% confidence intervals (CIs), were calculated. The association between polypharmacy and diabetes control among individuals receiving antidiabetic medication was examined using three

models: a crude model, a model adjusted for age and sex, and a fully adjusted model that included all demographic and health–related variables assessed in the study. The variables included in the adjustment were age, sex, WI, years of schooling, physical activity, and multiple long-term conditions. A stepwise backward-elimination method was applied to fully adjusted models, and a *p*-value threshold of less than 0.2 was used for inclusion. All the statistical analyses were conducted via Stata version 14.2 (Stata Corp LLC, College Station, TX, USA)[18] and the figures were produced via Microsoft Excel 2016.[19]

*Ethical considerations*

Prior to participation, all individuals gave written informed consent. The study protocol was reviewed and approved by Tehran University of Medical Sciences Ethics Committee (approval ID: IR.TUMS.EMRI.REC.1403.144, date: 23.02.2025). The research was conducted in accordance with the ethical standards set forth in the Declaration of Helsinki.

## RESULTS

In the total population, the mean age of participants was 61.18 (95% CI: 60.65–61.70), and 53.46% (95% CI: 50.08–56.82) of participants were female. Of the 1,117 participants included in the analysis, 670 had pre-diabetes and 447 had diabetes. Among individuals with pre-diabetes, 69 used ≥ 5 medications and 180 used ≥ 3 medications. In the diabetic group, 111 participants used ≥ 5 medications and 212 used ≥ 3. After excluding vitamins and supplements from the medication list, the number of individuals with polypharmacy was slightly lower, with 63 pre-diabetic and 103 diabetic participants used ≥ 5 medications, and 168 and 205, respectively, used ≥ 3 medications.

*Association between polypharmacy and diabetes or pre-diabetes*

Polypharmacy was more prevalent among females than males in both glycemic groups. In pre-diabetics, 32.75% (95% CI: 27.23–38.79) of females and 23.50% (95% CI: 18.32–29.61) of males used ≥ 3 medications; corresponding figures in diabetics were 51.46% (95% CI: 44.69–58.17) and 47.82% (95% CI: 39.63–56.12), respectively. Use of ≥ 5 medications was also higher in females (pre-diabetics: 10.22% (95% CI: 7.17–14.37) vs. 9.40% (95% CI: 6.29–13.83); diabetics: 29.13% (95% CI: 23.29–35.75) vs. 22.54% (95% CI: 16.23–30.40). Polypharmacy was also more prevalent among participants aged ≥ 60 years than among those aged < 60 years, particularly among individuals with diabetes (56.20% vs. 40.44% for ≥ 3 medications) (Table 1).

The prevalence estimates in Table 1 describe the distribution of polypharmacy across participant characteristics and should not be interpreted as statistically significant associations in the absence of corresponding inferential tests.

The prevalence of polypharmacy varied across educational categories, but the pattern was not clearly linear. For example, for ≥ 5 medications, prevalence was 31.16% (95% CI: 25.21–37.80) among participants with ≤ 6 years of schooling, 13.36% (95% CI: 6.63–25.10) among those with 7–11 years, and 21.10% (95% CI: 13.75–30.97) among those with ≥ 12 years of schooling. Polypharmacy was also more prevalent among unemployed than among employed participants in both glycemic groups.

The prevalence of polypharmacy varied across WI categories. In the pre-diabetic group, the prevalence of ≥ 3 medication use ranged from 24.95% (95% CI: 19.09–31.90) in the lowest wealth category to 31.26% (95% CI: 24.27–39.22) in the highest category. Among individuals with diabetes, the prevalence ranged from 45.62% (95% CI: 37.02–54.49) in the lowest wealth category to 52.69% (95% CI: 43.59–61.62) in the middle wealth category.

Polypharmacy also varied across BMI and WC categories. Among pre-diabetic individuals, the highest prevalence of ≥ 3 medication use was observed among those with BMI ≥ 30 kg/m$^2$ (35.71%; 95% CI: 28.17–44.02). Among individuals with diabetes, the prevalence of ≥ 3 medication use was 55.76% (95% CI: 47.83–63.41) among those with BMI >30 kg/m$^2$. Participants with WC ≥ 95 cm had a prevalence of 30.19% (95% CI: 25.19–35.72) and 51.21% (95% CI: 45.17–57.23) for ≥ 3 medications among pre-diabetic and diabetic groups, respectively, while the corresponding prevalence for ≥ 5 medications was 10.74% (95% CI: 7.77–14.67) and 29.84% (95% CI: 24.49–35.81).

Polypharmacy prevalence was lower among participants reporting ≥ 150 minutes of physical activity per week than among those reporting < 150 minutes per week. For ≥ 3 medications, the corresponding prevalence was 21.70% (95% CI: 16.92–27.39) versus 34.16% (95% CI: 28.46–40.36) in pre-diabetic individuals and 47.50% (95% CI: 38.91–56.23) versus 51.21% (95% CI: 44.63–57.74) in individuals with diabetes.

The strongest descriptive gradient was observed across categories of multiple long-term conditions. Among pre-diabetic individuals, the prevalence of ≥ 3 medications increased from 15.04% (95% CI: 10.60–20.92) among those without multiple long-term conditions to 55.86% (95% CI: 45.43–65.80) among those with two or more conditions. Among individuals with diabetes, the corresponding prevalence increased from 37.09% (95% CI: 26.80–48.72) to 63.75% (95% CI: 55.13–71.57). A similar pattern was observed for the ≥ 5-medication threshold.

In the Supplementary Table S1, the prevalence of polypharmacy was re-evaluated separately in diabetic and pre-diabetic groups, with vitamins and dietary supplements excluded from the medication list.

Figure 2 illustrates the prevalence of polypharmacy in individuals with diabetes and pre-diabetes, stratified by comorbid conditions. The highest prevalence estimates for both polypharmacy thresholds were observed among participants with CVD.

*Cumulative prevalence and categories of medication use among diabetic and pre-diabetic population*

According to Table 2, the mean number of medications used was 1.58 (95% CI: 1.39–1.77) for individuals with pre-diabetes and 2.94 (95% CI: 2.66–3.21) for individuals with diabetes. The prevalence of medication use was consistently higher among individuals with diabetes across the medication-count categories. For example, 35.52% (95% CI: 30.56–40.80) of

**Table 1. Prevalence of polypharmacy among pre-diabetics and diabetics population.**

| | Pre-diabetes population | | Diabetic population | |
|---|---|---|---|---|
| Polypharmacy | ≥ 3 | ≥ 5 | ≥ 3 | ≥ 5 |
| | % (95% CI) | % (95% CI) | % (95% CI) | % (95% CI) |
| Total | 28.25 (24.36, 32.49) | 9.82 (7.54, 12.71) | 49.89 (44.64, 55.13) | 26.28 (21.86, 31.25) |
| Age | | | | |
| < 60 | 23.79 (18.90, 29.49) | 6.75 (4.28, 10.48) | 40.44 (32.63, 48.77) | 17.78 (12.29, 25.02) |
| ≥ 60 | 33.06 (27.24, 39.45) | 13.15 (9.49, 17.92) | 56.20 (49.50, 62.69) | 31.97 (25.90, 38.73) |
| Sex | | | | |
| Female | 32.75 (27.23, 38.79) | 10.22 (7.17, 14.37) | 51.46 (44.69, 58.17) | 29.13 (23.29, 35.75) |
| Male | 23.50 (18.32, 29.61) | 9.40 (6.29, 13.83) | 47.82 (39.63, 56.12) | 22.54 (16.23, 30.40) |
| BMI [kg/(m)$^2$] | | | | |
| < 25 | 19.01 (13.18, 26.61) | 5.52 (3.07, 9.74) | 46.95 (35.46, 58.77) | 21.11 (12.86, 32.64) |
| 25-30 | 28.82 (23.05, 35.38) | 12.47 (8.57, 17.78) | 45.23 (36.77, 53.98) | 22.82 (16.18, 31.18) |
| > 30 | 35.71 (28.17, 44.02) | 9.37 (5.98, 14.38) | 55.76 (47.83, 63.41) | 32.23 (25.24, 40.12) |
| Waist (cm) | | | | |
| < 95 | 25.36 (19.51, 32.26) | 8.46 (5.32, 13.20) | 46.30 (35.98, 56.95) | 16.68 (10.27, 25.92) |
| ≥ 95 | 30.19 (25.19, 35.72) | 10.74 (7.77, 14.67) | 51.21 (45.17, 57.23) | 29.84 (24.49, 35.81) |
| Residential area | | | | |
| Rural | 23.24 (17.05, 30.84) | 7.97 (4.77, 13.04) | 41.74 (31.89, 52.30) | 20.17 (13.20, 29.56) |
| Urban | 30.14 (25.44, 35.29) | 10.52 (7.73, 14.16) | 52.47 (46.43, 58.44) | 28.23 (22.99, 34.13) |
| Wealth index | | | | |
| 0 (lowest) | 24.95 (19.09, 31.90) | 10.87 (7.05, 16.40) | 45.62 (37.02, 54.49) | 22.33 (15.89, 30.44) |
| 1 | 28.72 (22.15, 36.34) | 8.94 (5.27, 14.78) | 52.69 (43.59, 61.62) | 29.59 (21.78, 38.81) |
| 2 (highest) | 31.26 (24.27, 39.22) | 9.67 (6.34, 14.49) | 51.32 (42.04, 60.51) | 26.78 (19.29, 35.88) |
| Employment status | | | | |
| Unemployed | 30.68 (26.18, 35.57) | 12.03 (9.07, 15.78) | 53.70 (47.74, 59.55) | 28.62 (23.49, 34.37) |
| Employed | 21.68 (14.60, 30.93) | 3.87 (1.95, 7.53) | 35.28 (25.64, 46.30) | 17.34 (10.30, 27.71) |
| Marital status | | | | |
| Single | 26.02 (17.18, 37.37) | 10.49 (5.87, 18.06) | 53.49 (41.32, 65.26) | 29.20 (19.16, 41.78) |
| Married | 28.62 (24.41, 33.25) | 9.71 (7.23, 12.93) | 49.04 (43.26, 54.85) | 25.60 (20.80, 31.07) |
| Years of schooling (years) | | | | |
| ≤ 6 | 27.60 (22.82, 32.95) | 10.91 (7.95, 14.81) | 52.05 (45.43, 58.59) | 31.16 (25.21, 37.80) |
| 7-11 | 25.39 (16.00, 37.82) | 7.89 (3.83, 15.54) | 38.76 (26.13, 53.11) | 13.36 (6.63, 25.10) |
| ≥ 12 | 31.21 (23.54, 40.08) | 8.68 (4.67, 15.59) | 50.62 (39.84, 61.35) | 21.10 (13.75, 30.97) |
| Alcohol consumption during past 12 months | | | | |
| No | 28.77 (24.81, 33.07) | 10.05 (7.72, 13.00) | 50.26 (44.95, 55.57) | 26.40 (21.92, 31.42) |
| Yes | 6.02 (0.80, 33.82) | 0 | 35.63 (12.16, 68.86) | 22.08 (4.66, 62.18) |
| Current smoking | | | | |
| No | 29.23 (25.04, 33.81) | 9.53 (7.26, 12.42) | 50.30 (44.75, 55.86) | 25.96 (21.31, 31.22) |

**Table 1. Continued.**

| | Pre-diabetes population | | Diabetic population | |
|---|---|---|---|---|
| Yes | 22.07 (13.14, 34.64) | 11.65 (5.02, 24.73) | 46.48 (31.53, 62.09) | 28.95 (16.63, 54.44) |
| Physical activity | | | | |
| < 150 min/week | 34.16 (28.46, 40.36) | 12.73 (9.39, 17.04) | 51.21 (44.63, 57.74) | 30.15 (24.39, 36.61) |
| ≥ 150 min/week | 21.70 (16.92, 27.39) | 6.60 (3.91, 10.93) | 47.50 (38.91, 56.23) | 19.28 (13.23, 27.22) |
| Multiple long-term Conditions | | | | |
| No disease | 15.04 (10.60, 20.92) | 3.89 (2.13, 7.00) | 37.09 (26.80, 48.72) | 12.66 (6.60, 22.90) |
| One disease | 29.06 (23.32, 35.56) | 9.25 (6.05, 13.89) | 43.60 (35.60, 51.94) | 21.32 (15.33, 28.85) |
| Two or more diseases | 55.86 (45.43, 65.80) | 24.26 (16.38, 34.36) | 63.75 (55.13, 71.57) | 39.18 (31.11, 47.90) |

CI, confidence interval; BMI, body mass index.

individuals with diabetes used ≥ 5 medications compared with 16.01% (95% CI: 13.08–19.45) of those with pre-diabetes. Similar results were observed when excluding vitamins from the list of medications (Supplementary Table S2).

Supplementary Table S3 in the supplementary files presents the five therapeutic drug groups most frequently used by individuals with diabetes and pre-diabetes. Cardiovascular medications were the most commonly reported class of drugs in both groups.

*Diabetes status according to polypharmacy*

Among pre-diabetic individuals, mean HbA1c was 5.93% (95% CI: 5.83–6.03) among those using ≥ 5 medications and 5.91% (95% CI: 5.88–5.93) among those using < 5 medications. A similar, difference was observed when polypharmacy was defined as ≥ 3 medications (5.93% vs. 5.90%). Given the overlap in CIs, these findings are best interpreted as descriptive differences rather than as evidence of meaningful differences in glycemic measures (Table 3).

Among individuals with diabetes, mean HbA1c was 8.30% (95% CI: 7.94–8.66) among those using ≥ 5 medications compared with 8.06% (95% CI: 7.81–8.31) among those using < 5 medications. Mean FPG was also higher among participants using ≥ 5 medications (156.36 mg/dL; 95% CI: 148.08–164.65) than among those using < 5 medications (151.00 mg/dL; 95% CI: 141.69–161.00).

Regarding diabetes status, the proportion of unaware individuals with diabetes was lower among those using ≥ 5 medications (27.03%; 95% CI: 18.72–37.33) than among those using < 5 medications (52.52%; 95% CI: 46.46–58.50). A similar pattern was observed using the ≥ 3-medication threshold (34.32% vs. 57.27%). In individuals receiving treatment, the prevalence of uncontrolled diabetes was higher in those meeting either of the polypharmacy thresholds. For the ≥ 5-medication definition, 56.58% (95% CI: 46.05–66.56) had uncontrolled diabetes compared with 35.15% (95% CI: 29.68–41.05) among those using < 5 medications. For the ≥ 3-medication definition, the corresponding figures were 51.96% (95% CI: 44.35–59.48) and 29.66% (95% CI: 23.51–36.65), respectively (Table 3).

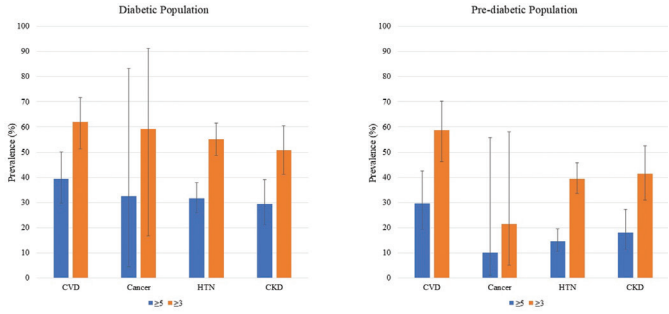



**Figure 2.** Prevalence of polypharmacy stratified by comorbidity status in diabetic and pre-diabetic individuals; Polypharmacy was defined in this figure as the use of ≥ 5 medications and alternatively as ≥ 3 medications

CKD, chronic kidney disease; CVD, cardiovascular diseases; HTN, hypertension.

*Association between polypharmacy and uncontrolled diabetes among individuals using antidiabetic medications*

Table 4 presents the association between polypharmacy and uncontrolled diabetes among 243 individuals using antidiabetic medications, of whom 188 had uncontrolled diabetes. In the crude analysis, both polypharmacy definitions were associated with higher odds of uncontrolled diabetes. For ≥ 5 medications, the crude odds ratio (OR) was 3.16 (95% CI: 2.19–4.56; $p < 0.001$), while for ≥ 3 medications it was 2.84 (95% CI: 2.07–3.90; $p < 0.001$).

Model 1 was adjusted for age and sex to account for the two basic demographic factors that may be associated with both medication burden and glycemic control. After this adjustment, the associations remained similar: the adjusted OR (AOR) was 2.99 (95% CI: 2.06–4.36; $p < 0.001$) for ≥ 5 medications and 2.78 (95% CI: 2.01–3.83; $p < 0.001$) for ≥ 3 medications.

Model 2 was additionally adjusted for years of schooling, physical activity, multiple long-term conditions, and WI. Following this more extensive adjustment, the association between ≥ 5 medications and uncontrolled diabetes remained statistically significant (AOR = 2.21; 95% CI: 1.49–3.29; p < 0.001). In contrast, the association for ≥ 3 medications was attenuated and was no longer statistically significant (AOR = 1.58; 95% CI: 0.81–3.09; $p = 0.178$).

**Table 2. Cumulative prevalence of medication use among pre-diabetics and diabetics population**

| | Number of medication use | |
|---|---|---|
| | Pre-diabetic population | Diabetic population |
| | % (95% CI) | % (95% CI) |
| **Mean** | 1.58 (1.39, 1.77) | 2.94 (2.66, 3.21) |
| 0 | 47.20 (42.85, 51.60) | 23.77 (19.77, 28.29) |
| ≥ 1 | 52.80 (48.40, 57.15) | 76.23 (71.71, 80.23) |
| ≥ 2 | 38.20 (34.01, 42.57) | 64.68 (59.61, 69.45) |
| ≥ 3 | 28.25 (24.37, 32.48) | 49.89 (44.66, 55.12) |
| ≥ 4 | 16.01 (13.08, 19.45) | 35.52 (30.56, 40.80) |
| ≥ 5 | 9.82 (7.54, 12.70) | 26.28 (21.86, 31.25) |
| ≥ 6 | 5.72 (3.92, 8.26) | 16.61 (13.08, 20.87) |
| ≥ 7 | 3.07 (1.88, 4.96) | 9.01 (6.50, 12.35) |
| ≥ 8 | 1.50 (0.67, 3.33) | 6.35 (4.29, 9.31) |
| ≥ 9 | 1.20 (0.46, 3.13) | 3.00 (1.67, 5.34) |
| ≥ 10 | 1.12 (0.40, 3.10) | 2.12 (1.03, 4.28) |

Data have been weighted to account for overall non-response, non-response at each step, and sample distribution across provinces, adjusted for age, sex, and area of residence.
The reported percentages represent column-wise prevalence.
CI, confidence interval.

**Table 3. Diabetes status according to polypharmacy**

| | | | Number of medication use | | | |
|---|---|---|---|---|---|---|
| **Variable** | | | **< 5** | **≥ 5** | **< 3** | **≥ 3** |
| **Pre-diabetes population (n = 670)** | | | | | | |
| **Mean HbA1c, % (95% CI)** | | | 5.91 (5.88, 5.93) | 5.93 (5.83, 6.03) | 5.90 (5.87, 5.92) | 5.93 (5.88, 5.98) |
| **Mean FPG, mg/dL (95% CI)** | | | 97.97 (97.18, 98.76) | 99.82 (97.35, 102.28) | 98.09 (97.24, 98.94) | 98.31 (96.75, 99.87) |
| **Diabetes population (n = 447)** | | | | | | |
| **Mean HbA1c, % (95% CI)** | | | 8.06 (7.81, 8.31) | 8.30 (7.94, 8.66) | 7.95 (7.63, 8.27) | 8.30 (8.04, 8.57) |
| **Mean FPG, mg/dL (95% CI)** | | | 151.00 (141.69, 161.00) | 156.36 (148.08, 164.65) | 153.80 (146.78, 160.82) | 156.28 (145.09, 167.48) |
| **Diabetes status** | | | | | | |
| **Unaware, % (95% CI)** | | | 52.52 (46.46, 58.50) | 27.03 (18.72, 37.33) | 57.27 (49.98, 64.25) | 34.32 (27.28, 42.12) |
| **Aware** | **No treatment, % (95% CI)** | | 2.10 (1.05, 4.17) | 3.60 (1.12, 10.95) | 1.89 (0.80, 4.40) | 3.10 (1.33, 7.06) |
| | **Under treatment** | **Uncontrolled, % (95% CI)** | 35.15 (29.68, 41.05) | 56.58 (46.05, 66.56) | 29.66 (23.51, 36.65) | 51.96 (44.35, 59.48) |
| | | **Controlled, % (95% CI)** | 10.23 (7.13, 14.46) | 12.79 (7.44, 21.09) | 11.18 (7.25, 16.85) | 10.62 (7.02, 15.75) |

Data have been weighted to account for overall non-response, non-response at each step, and sample distribution across provinces, adjusted for age, sex, and area of residence. The reported percentages represent column-wise prevalence.
CI, confidence interval; HbA1c, glycosylated hemoglobin A1C; FPG, fasting plasma glucose.

**Table 4. Relationship between polypharmacy and uncontrolled diabetes (n = 188) in anti-diabetic medication consumers (n = 243) using stepwise logistic regression**

| | Crude | | Model 1 | | Model 2 | |
|---|---|---|---|---|---|---|
| | OR (95% CI) | *p*-value | AOR (95% CI) | *p*-value | AOR (95% CI) | *p*-value |
| **Polypharmacy** | | | | | | |
| **< 5** | Reference | | Reference | | Reference | |
| **≥ 5** | 3.16 (2.19, 4.56) | < 0.001 | 2.99 (2.06, 4.36) | < 0.001 | 2.21 (1.49, 3.29) | < 0.001 |
| **Polypharmacy** | | | | | | |
| **< 3** | Reference | | Reference | | Reference | |
| **≥ 3** | 2.84 (2.07, 3.90) | < 0.001 | 2.78 (2.01, 3.83) | < 0.001 | 1.58 (0.81, 3.09) | 0.178 |
| **Medication use (per each medication)** | 1.27 (1.19, 1.34) | < 0.001 | 1.26 (1.18, 1.34) | < 0.001 | 1.20 (1.12, 1.28) | < 0.001 |

Model 1: adjusted for age and sex; Model 2: adjusted for age, sex, years of schooling, physical activity, comorbidity and wealth index; OR, odds ratio; CI, confidence interval; AOR, adjusted odds ratio.

When medication count was analyzed as a continuous variable, each additional medication was associated with higher odds of uncontrolled diabetes. This association remained statistically significant after adjustment, with an AOR of 1.20 (95% CI: 1.12–1.28; $p < 0.001$) in Model 2, corresponding to approximately 20% higher odds of uncontrolled diabetes for each additional medication.

## DISCUSSION

Polypharmacy was more prevalent in individuals with diabetes than in those with pre-diabetes. The mean number of medications was also higher in individuals with diabetes than in those with pre-diabetes (2.94 vs. 1.58), indicating a greater medication burden in the diabetes group. The prevalence of polypharmacy also varied by age, sex, anthropometric characteristics, residential area, physical activity, and comorbidity. Mean HbA1c and FPG levels were higher among individuals with polypharmacy. Uncontrolled diabetes was more common among individuals with polypharmacy. Among individuals receiving antidiabetic medications, the association between polypharmacy and uncontrolled diabetes remained statistically significant after adjustment when polypharmacy was defined as ≥ 5 medications.

The substantially higher medication burden observed among individuals with diabetes compared with those with pre-diabetes is consistent with the greater complexity of disease management in diabetes. In our study, individuals with diabetes used nearly twice as many medications on average as those with pre-diabetes, and the prevalence of both ≥ 3 and ≥ 5 medication use was considerably higher in the diabetes group. This difference is also consistent with previous evidence indicating a high prevalence of polypharmacy among individuals with diabetes and a greater medication burden compared with individuals without diabetes.[5] The higher medication burden among individuals with diabetes may partly reflect the need for glucose-lowering therapy together with medications for diabetes-related comorbidities and other chronic conditions. Clinically, these findings highlight the importance of considering overall medication burden when managing individuals with diabetes, particularly those with multiple chronic conditions.

Polypharmacy was more common among adults older than 60 years in our study. This may be because older adults often have multiple coexisting medical conditions and take several medications concurrently.[20] Women may also be at greater risk of receiving potentially inappropriate medications. There are several reasons for this matter; for instance, women seek more medical care than men.[21] They have better social aptitude for expressing their symptoms to their healthcare practitioner. Therefore, women are more likely to be diagnosed with multiple medical conditions. On the other hand, for some men, masculine ideologies act as a barrier to seeking healthcare, thereby reducing their likelihood of being diagnosed with chronic conditions.[22-27]

As stated previously, the prevalence of polypharmacy varied across educational categories, without a clear linear pattern. The literature suggests that there are various reasons for this. Firstly, individuals with less education tend to be less involved in preventive health measures, thereby placing them at greater risk of conditions that may require polypharmacy.[28,29] Secondly, people with lower education are less proactive in shared decision making.[30] Therefore, are more likely to take multiple medications without asking for further explanation.[31,32] However, given the non–linear pattern observed in our study, these potential explanations should be interpreted cautiously.

As indicated in the study results, individuals with different levels of socioeconomic status (SES) showed variation in the prevalence of polypharmacy. People with higher SES may still have as much multimorbidity but because of their social status they benefit from better access to healthcare services and preventive care, which may influence medication usage.[33] Some reviews have indicated that low SES is related to medication non-adherence, which may be associated with a greater burden of chronic conditions and polypharmacy.[34-37] Also, people with better social status use more preventive services, diagnostic services, and receive better treatment quality.[38]

Obesity and overweight which is a manifestation of high BMI and large WC, were associated with higher prevalence of polypharmacy in our study. This may partly reflect the coexistence of obesity with several non–communicable diseases and metabolic conditions, which may increase the overall medication burden.[39,40] In this study, alcohol consumption also showed differences in polypharmacy prevalence across categories. However, some studies have found that in women exclusively, alcohol consumption is related to lower risk of polypharmacy.[41,42]

This study also revealed that polypharmacy prevalence was higher among individuals with a greater number of comorbidities. Clinical condition of individuals is one of the major factors of physical function.[43] The coexistence of multiple chronic conditions may require management with several medications and may therefore contribute to a greater medication burden.[39]

As indicated in the results, polypharmacy was associated with uncontrolled diabetes among individuals receiving antidiabetic medications, particularly when polypharmacy was defined as the use of ≥ 5 medications. This association may have several possible explanations. A higher medication burden may reflect greater disease complexity and a higher prevalence of comorbid conditions, which may also be related to poorer glycemic control. In addition, treatment adherence may influence glycemic control, and several factors, including forgetfulness, financial constraints, disappearance of symptoms, and being busy, have been reported as reasons for non–adherence to treatment.[44] However, medication adherence and drug–drug interactions were not assessed in the present study; therefore, their potential roles in the observed association cannot be directly evaluated.

### *Study limitations*

This study is based on IMOS survey as a nationwide study which includes participants aged ≥ 50 years across provinces of Iran, enhancing the generalizability of findings. Simultaneous assessment of diabetes and pre-diabetes allows for comparison and early recognition of risk patterns associated with polypharmacy. The main limitation of this study is its cross-sectional design, which does not allow the establishment of temporal or causal relationships between polypharmacy and associated factors. Medication use and comorbidities were self-reported, which may introduce recall bias. Although antidiabetic medications were included in the polypharmacy definition to capture the overall medication burden among individuals receiving treatment for diabetes, this approach may partly reflect treatment intensity and influence the observed association with glycemic control. This should be considered when interpreting the findings. This study did not include an evaluation of medication appropriateness or adherence.

## CONCLUSION

Uncontrolled diabetes was associated with polypharmacy among adults aged ≥ 50 years receiving antidiabetic medications, particularly when polypharmacy was defined as the use of ≥ 5 medications. The observed association does not establish a causal relationship, and the potential roles of medication adherence and drug–drug interactions could not be assessed in this study. These findings highlight the relevance of considering overall medication burden in the clinical management of individuals with diabetes.

### *Ethics*

*Ethics Committee Approval: The study protocol was reviewed and approved by Tehran University of Medical Sciences Ethics Committee (approval ID: IR.TUMS.EMRI.REC.1403.144, date: 23.02.2025)*

**Informed Consent:** Prior to participation, all individuals gave written informed consent.

### *Acknowledgements*

We sincerely acknowledge the contributions of all individuals and organizations who supported this work. We are particularly thankful for the collaboration and support from the teams involved in the STEPS survey and the previous IMOS survey. The IMOS study was approved by the Iranian National Institute for Medical Research Development (NIMAD) Ethics Committee under code IR.NIMAD.REC.1398.056, and the STEPS survey was approved by the National Institute for Health Research Ethics Committee (IR.TUMS.NIHR.REC.1398.006 code). We also extend our appreciation to the medical universities across Iran for their efforts in data collection, and to the staff members of the Non-Communicable Diseases Research Center (NCDRC) and the Osteoporosis Research Center at Tehran University of Medical Sciences for their valuable assistance and collaboration throughout the project.

### *Footnotes*

### *Authorship Contributions*

Surgical and Medical Practices: O.T.M., A.O., Concept: O.T.M., A.O., Design: O.T.M., Data Collection or Processing: M.K., P.Z., Analysis or Interpretation: S.S., N.C., S.G., Literature Search: A.R., Writing: S.S., A.R.

S.S. and A.R. contributed equally as first authors.

Supplementary Table Link: https://d2v96fxpocvxx.cloudfront.net/25021570-dd5c-48cc-b052-771af43e75cc/content-images/bc3d88fe-a8cb-4c72-9bd5-6e53e1bee2cc.pdf

## REFERENCES

1. Hajiuni K, Salehi S, Rajabli Z, Azadnajafabad S, Akbarpour S, Asgari S, Rezaei N. Prevalence and factors associated with comorbidities in Iranian patients with type 2 diabetes: a national study. PLoS One. 2026;21:e0343690.
2. S H, Tripathi S, Venuturumilli R, K SP, Reddy GHV, Mukherjee B, Lakhani HA. Adverse drug reactions and drug interactions in multimorbid patients: a review of current evidence. Cureus. 2025;17:e97640.
3. Masnoon N, Shakib S, Kalisch-Ellett L, Caughey GE. What is polypharmacy? A systematic review of definitions. BMC Geriatr. 2017;17:230.
4. Pazan F, Wehling M. Polypharmacy in older adults: a narrative review of definitions, epidemiology and consequences. Eur Geriatr Med. 2021;12:443-452.
5. Remelli F, Ceresini MG, Trevisan C, Noale M, Volpato S. Prevalence and impact of polypharmacy in older patients with type 2 diabetes. Aging Clin Exp Res. 2022;34:1969-1983.

6. Khalagi K, Fahimfar N, Hajivalizadeh F, Sanjari M, Mansourzadeh MJ, Gharibzadeh S, Shafiee G, Kamali K, Alaeddini F, Farzadfar F, Mohseni S, Namazi N, Razi F, Gorgani K, Kateb Saber K, Panahi N, Heshmat R, Raeisi A, Larijani B, Ostovar A. Iranian Multi-center Osteoporosis Study (IMOS), 2021-2022: the study protocol. BMC Geriatr. 2022;22:818.
7. Good CB. Polypharmacy in elderly patients with diabetes. Diabetes Spectrum. 2002;15:240-248.
8. Hanlon JT, Schmader KE, Ruby CM, Weinberger M. Suboptimal prescribing in older inpatients and outpatients. J Am Geriatr Soc. 2001;49:200-209.
9. Al-Musawe L, Martins AP, Raposo JF, Torre C. The association between polypharmacy and adverse health consequences in elderly type 2 diabetes mellitus patients; a systematic review and meta-analysis. Diabetes Res Clin Pract. 2019;155:107804.
10. Djalalinia S, Azadnajafabad S, Ghasemi E, Yoosefi M, Rezaei N, Farzi Y, Kazemi A, Ahmadi N, Nasserinejad M, Fattahi N, Rezaei S, Abdolhamidi E, Foroutan Mehr E, Haghshenas R, Rezaei N, Abdi J, Moghisi A, Mahdavihezaveh A, Akbari Sari A, Raeisi A, Jamshidi H, Larijani B, Farzadfar F. Protocol design for surveillance of risk factors of non-communicable diseases during the COVID-19 pandemic: an experience from Iran STEPS survey 2021. Arch Iran Med. 2022;25:634-646.
11. Rutstein SO. Steps to constructing the new DHS Wealth Index. Rockville, MD: ICF International. 2015; 6.
12. Azizi F, Hadaegh F, Khalili D, Esteghamati A, Hosseinpanah F, Delavari A, Larijani B, Mirmiran P, Zabetian A, Mehrabi Y, Kelishadi R, Aghajani H. Appropriate definition of metabolic syndrome among Iranian adults: report of the Iranian National Committee of Obesity. Arch Iran Med. 2010;13:426-428.
13. Armstrong T, Bull F. Development of the World Health Organization Global Physical Activity Questionnaire (GPAQ). J Public Health. 2006;14:66-70.
14. Piercy KL, Troiano RP, Ballard RM, Carlson SA, Fulton JE, Galuska DA, George SM, Olson RD. The Physical Activity Guidelines for Americans. JAMA. 2018;320:2020-2028.
15. Levey AS, Eckardt KU, Tsukamoto Y, Levin A, Coresh J, Rossert J, De Zeeuw D, Hostetter TH, Lameire N, Eknoyan G. Definition and classification of chronic kidney disease: a position statement from Kidney Disease: Improving Global Outcomes (KDIGO). Kidney Int. 2005;67:2089-2100.
16. American Diabetes Association. 2. Classification and diagnosis of diabetes: standards of medical care in diabetes-2021. Diabetes Care. 2021;44(Suppl 1):S15-S33. Erratum in: Diabetes Care. 2021;44:2182.
17. American Diabetes Association. 6. Glycemic targets: standards of medical care in diabetes-2021. Diabetes Care. 2021;44(Suppl 1):S73-S84.
18. StataCorp, L. StataCorp stata statistical software: Release 14. StataCorp LP.: College Station, TX, USA. 2015.
19. Excel CMM. Redmond, WA: Microsoft Corporation. 2016.
20. Milton JC, Hill-Smith I, Jackson SH. Prescribing for older people. BMJ. 2008;336:606-609.
21. Bertakis KD, Azari R, Helms LJ, Callahan EJ, Robbins JA. Gender differences in the utilization of health care services. J Fam Pract. 2000;49:147-152.
22. Courtenay WH. Constructions of masculinity and their influence on men's well-being: a theory of gender and health. Soc Sci Med. 2000;50:1385-1401.
23. Addis ME, Mahalik JR. Men, masculinity, and the contexts of help seeking. Am Psychol. 2003;58:5-14.
24. Murtagh KN, Hubert HB. Gender differences in physical disability among an elderly cohort. Am J Public Health. 2004;94:1406-1411.
25. Galdas PM, Cheater F, Marshall P. Men and health help-seeking behaviour: literature review. J Adv Nurs. 2005;49:616-623.
26. Hammond WP, Matthews D, Mohottige D, Agyemang A, Corbie-Smith G. Masculinity, medical mistrust, and preventive health services delays among community-dwelling African-American men. J Gen Intern Med. 2010;25:1300-1308.
27. Braybrook DE, Witty KR, Robertson S. Men and lung cancer: a review of the barriers and facilitators to male engagement in symptom reporting and screening. Journal of Men's Health. 2011;8:93-99.
28. Rosemann T, Laux G, Szecsenyi J, Grol R. The chronic care model: congruency and predictors among primary care patients with osteoarthritis. Qual Saf Health Care. 2008;17:442-446.
29. Cramm JM, Nieboer AP. A longitudinal study to identify the influence of quality of chronic care delivery on productive interactions between patients and (teams of) healthcare professionals within disease management programmes. BMJ Open. 2014;4:e005914.
30. Protheroe J, Nutbeam D, Rowlands G. Health literacy: a necessity for increasing participation in health care. Br J Gen Pract. 2009;59:721-723.
31. Abdulrahman KA. What do patient's expect of their general practitioners? J Family Community Med. 2003;10:39-45.
32. Plaza-Zamora J, Legaz I, Osuna E, Pérez-Cárceles MD. Age and education as factors associated with medication literacy: a community pharmacy perspective. BMC Geriatr. 2020;20:501.
33. Iqbal A, Richardson C, Iqbal Z, O'Keefe H, Hanratty B, Matthews FE, Todd A. Are there socioeconomic inequalities in polypharmacy among older people? A systematic review and meta-analysis. BMC Geriatr. 2023;23:149.
34. Mann DM, Woodward M, Muntner P, Falzon L, Kronish I. Predictors of nonadherence to statins: a systematic review and meta-analysis. Ann Pharmacother. 2010;44:1410-1421.
35. Lemstra M, Blackburn D, Crawley A, Fung R. Proportion and risk indicators of nonadherence to statin therapy: a meta-analysis. Can J Cardiol. 2012;28:574-580.
36. Yeam CT, Chia S, Tan HCC, Kwan YH, Fong W, Seng JJB. A systematic review of factors affecting medication adherence among patients with osteoporosis. Osteoporos Int. 2018;29:2623-2637.
37. Kvarnström K, Westerholm A, Airaksinen M, Liira H. Factors contributing to medication adherence in patients with a chronic condition: a scoping review of qualitative research. Pharmaceutics. 2021;13:1100.
38. Assari S, Saqib M, Wisseh C, Bazargan M. Social determinants of polypharmacy in first generation Mexican immigrants in the United States. Int J Travel Med Glob Health. 2019;7:86-90.
39. Cantlay A, Glyn T, Barton N. Polypharmacy in the elderly. InnovAiT. 2016;9:69-77.
40. Al-Dahshan A, Al-Kubiasi N, Al-Zaidan M, Saeed W, Kehyayan V, Bougmiza I. Prevalence of polypharmacy and the association with non-communicable diseases in Qatari elderly patients attending primary healthcare centers: A cross-sectional study. PLoS One. 2020;15:e0234386. Erratum in: PLoS One. 2020;15:e0238343.
41. San José B, van de Mheen H, van Oers JA, Mackenbach JP, Garretsen HF. The U-shaped curve: various health measures and alcohol drinking patterns. J Stud Alcohol. 1999;60:725-731.
42. Cebrino J, Portero de la Cruz S. Polypharmacy and associated factors: a gender perspective in the elderly Spanish population (2011-2020). Front Pharmacol. 2023;14:1189644.
43. Painter P, Stewart AL, Carey S. Physical functioning: definitions, measurement, and expectations. Adv Ren Replace Ther. 1999;6:110-123.
44. Aminde LN, Tindong M, Ngwasiri CA, Aminde JA, Njim T, Fondong AA, Takah NF. Adherence to antidiabetic medication and factors associated with non-adherence among patients with type-2 diabetes mellitus in two regional hospitals in Cameroon. BMC Endocr Disord. 2019;19:35.

Turk J Pharm Sci 2026;23(3):150-164
**DOI:** 10.4274/tjps.galenos.2026.39953

ORIGINAL ARTICLE

# Nadifloxacin-Loaded Thermosensitive *In Situ* Gel Formulations with a Quality by Design Approach

**Ece ÖZCAN BÜLBÜL[1,2], Burçin İZBUDAK[3], Ayça BAL ÖZTÜRK[3,4,5] Neslihan ÜSTÜNDAĞ OKUR[6]***

[1]University of Health Sciences Faculty of Pharmacy, Department of Radiopharmacy, İstanbul, Türkiye
[2]İstinye University Faculty of Pharmacy, Department of Pharmaceutical Technology, İstanbul, Türkiye
[3]İstinye University, Institute of Graduate Education, Department of Stem Cell and Tissue Engineering, İstanbul, Türkiye
[4]İstinye University, Stem Cell and Tissue Engineering Application and Research Center (ISUKOK), İstanbul, Türkiye
[5]İstinye University Faculty of Pharmacy, Department of Analytical Chemistry, İstanbul, Türkiye
[6]University of Health Sciences Faculty of Pharmacy, Department of Pharmaceutical Technology, İstanbul, Türkiye

## ABSTRACT

**Objectives:** In our study, we aimed to prepare topical in situ gels containing nadifloxacin (NDF), used in the treatment of acne and superficial skin infections, and to evaluate them using characterization studies.

**Materials and Methods:** Thermosensitive (temperature-sensitive) *in situ* gels were produced by the cold method using poloxamer 188 (P188) and poloxamer 407 (P407) after methylcellulose (MC) and gellan gum (GG) were dissolved. Finally, the NDF concentration in the gels was 1% (w/w). The prepared gels exhibited desirable properties, as shown by Fourier-transform infrared spectroscopy, and in clarity, pH, gelation temperature, gelling capacity, viscosity, mechanical properties (springiness, resilience, and cohesiveness), spreadability (work of adhesion, work of shear, stickiness, and firmness), drug content uniformity, *in vitro* release, and cytocompatibility (MTT cytotoxicity assay). The impact of critical materials in the formulation on the results was evaluated using quality by design.

**Results:** The gelation temperatures of all NDF-included *in situ* gels were found to be in the range of 30–35.2 °C. Furthermore, the cytotoxicity of these gels was evaluated using MTT analysis. Based on the observed results, the most suitable gel was identified as N3, which contains 17.5% P407, 7% P188, 0.7% MC, 0.1% GG, and 1% NDF.

**Conclusion:** After further studies to determine its effectiveness against acne, it could become an alternative to existing creams for acne and superficial skin infections on the market.

**Keywords:** Nadifloxacin, thermosensitive, *in situ* gel, quality by design, poloxamer

## INTRODUCTION

The skin is the largest organ in adults (surface area: ~2 $m^2$ and weight: ~3.6 kg), and has three layers: dermis, hypodermis, and epidermis.[1,2] Skin diseases include scabies, superficial mycoses, eczema (dermatitis), pigment anomalies, and acne.[3] Acne involves inflammatory lesions (papules and pustules), noncomedones, and seborrhea.[4] Acne vulgaris (acne) is a chronic inflammatory disease that affects the pilosebaceous follicles. It ranks eighth among skin diseases and affects 9.4% of the world's population.[5] Clinical and psychological consequences can occur, including negative psychological effects resulting from potential scarring and pigmentary changes.[6]

Nadifloxacin (NDF) is a newer quinolone-derivative antibiotic commonly used topically to treat inflammatory acne lesions.[7,8] NDF is antibacterial and anti-inflammatory, making it beneficial for treating inflammatory acne. It is highly effective

***Correspondence:** neslihanustundag.okur@sbu.edu.tr, **ORCID-ID:** orcid.org/0000-0002-3210-3747

**Received:** 23.09.2025 **Accepted:** 23.09.2026 **Publication Date:** 27.10.2026

**Cite this article as:** Özcan Bülbül E, İzbudak B, Bal Öztürk A, Üstündağ Okur N. Nadifloxacin-loaded thermosensitive *in situ* gel formulations with a quality by design approach. Turk J Pharm Sci. 2026;23(3):150-164

Copyright© 2026 The Author(s). Published by Galenos Publishing House on behalf of Turkish Pharmacists' Association.
This is an open access article under the Creative Commons Attribution-NonCommercial-NoDerivatives 4.0 (CC BY-NC-ND) International License.

against Gram-negative and Gram-positive bacteria, such as *Propionibacterium acnes*. NDF 1% cream is available for the treatment of acne.[8] It is applied twice a day for 1 or 2 weeks.[7] However, NDF has very low water solubility (Log $p$ = 2.47), and, because of the large droplet size of dermal creams, penetration into the skin layers is limited, which has led to patient non-compliance with treatment. These problems may be overcome by different drug delivery systems.[8]

*In situ* gel *is* a drug-delivery system that transitions from "sol to gel" upon application, providing sustained drug release. While their advantages include extended drug residence time, improved patient compliance, and localized drug delivery, they also have some known disadvantages, such as limited mechanical strength and drug degradation. *In situ* gels are divided into three groups: temperature-sensitive (thermosensitive), pH-sensitive, and ion-sensitive.[9,10] Temperature-sensitive *in situ* gel systems are in the "sol" state at room temperature. Depending on the application site, they transition from sol to gel at different temperatures (32–37 °C). As the temperature increases, polymer-water interactions change. Polymers undergo gelation as temperature increases at concentrations above the critical micelle concentration.[11] Poloxamers, well-known polymers, are thermosensitive and are liquid at 4–5 °C, turning into a gel as temperature rises. Poloxamers are suitable for topical, nasal, ophthalmic, and vaginal application routes.[12] NDF was homogeneously dispersed within the prepared *in situ* gels. Compared with conventional cream formulations, this formulation offers the advantage of prolonged residence time at the application site due to its adhesive properties and *in situ* gelation behavior. *In situ* gel systems are a special class of polymeric sustained-release formulations that are prepared in liquid form and transform into a gel after administration via various physicochemical triggers. In these systems, the drug may be present in the polymeric matrix either in dissolved form or as a suspension.[13] *In situ* gels transform from a solution or suspension into a gel at the target site under the influence of factors such as interactions with body fluids, temperature, pH, ion concentration, UV radiation, and the presence of specific molecules and ions.[10] In the literature, dexamethasone-dispersed *in situ* gels for oral mucosal application,[14] fusidic acid-loaded ophthalmic *in situ* gels 9, and econazole nitrate-loaded vaginal *in situ* gels[15] prepared using this approach have been reported.

Gellan gum (GG) is a microbial polysaccharide produced by Pseudomonas elodea, characterized by its water solubility and mucoadhesive properties.14 Initially utilized in the food industry as a stabilizing, thickening, and gelling agent, this biopolymer has recently attracted considerable attention in pharmaceutical applications due to its biocompatibility, biodegradability, low toxicity, and structural stability.[14,16,17] In the present study, GG was preferred not only because of these advantageous properties but also due to its ability to form soft gels even at low concentrations.[14]

Quality by design (QbD) is an approach to development that emphasizes understanding of process and product through quality risk management and starts with predefined targets. Pharmaceutical development includes the critical quality attribute (CQA) and the quality target product profile (QTPP).[18-20] Critical material attributes (CMAs) may include excipients, such as polymers in the formulation, and these affect the CQAs.[21]

Our study aims to propose a novel approach for the topical application of NDF by preparing temperature-sensitive *in situ* gel formulations to treat acne and superficial skin infections. *In situ* gels were prepared using poloxamers (Poloxamer 407 and 188) and different polymers [methyl cellulose (MC) and GG] for evaluation using the QbD approach. Fourier-transform infrared (FTIR) were recorded, and the gels were characterized for gelation temperature (Tsol-gel, sol-gel temperature), clarity, gelling capacity, pH, viscosity, mechanical properties (springiness, cohesiveness, and resilience), spreadability (work of adhesion, work of shear, firmness, and stickiness), drug content, cytotoxicity, and drug release assays.

## MATERIALS AND METHODS

Ethics committee approval and informed consent were not required for this study because the study did not involve human participants or animals.

### *Materials*

Medium-viscosity MC was obtained from BioBasic (Canada). GG was obtained from Thermo Scientific. Poloxamers 188 (P188) and 407 (P407) were provided by BASF. NDF was provided by Berko Pharmaceutical Company (İstanbul, Türkiye) and Santa Farma Pharmaceutical Company (İstanbul, Türkiye). Dialysis membrane (diameter 16 mm, Spectra/Por® 2, Vol/Lg 2 mL/cm, molecular weight of 12–14 kDa) was obtained from Spectrumlabs. Methanol was supplied by Isolab. The phosphate-buffered saline (PBS, pH 7.4) tablet was obtained from Sigma–Aldrich (United States). The L929 mouse fibroblast cell line was obtained from the American Type Culture Collection (ATCC, Manassas, VA, USA). Penicillin-streptomycin solution (10,000 U/mL penicillin, 10,000 µg/mL streptomycin) and fetal bovine serum (FBS) were also acquired from Gibco (Thermo Fisher Scientific, Waltham, MA, USA). Dulbecco's modified Eagle medium (DMEM) was purchased from Gibco (Thermo Fisher Scientific, Waltham, MA, USA). Dimethyl sulfoxide (DMSO) was supplied by Tekkim (Ankara, Türkiye). Trypsin-EDTA solution (0.25%) was purchased from Gibco (Thermo Fisher Scientific, Waltham, MA, USA). MTT reagent [3-(4,5-dimethylthiazol-2-yl)-2,5-diphenyltetrazolium bromide] was supplied by Biomatik (Wilmington, DE, USA).

### *Implementation of the QbD*

The first step in development using the QbD approach is to define the target product profile (TPP), which includes the intended characteristics such as the dosage form, route of administration, and dosage strength.[22] To achieve the quality properties, we must summarize the QTPP.[19,20,23] The QTPP includes dosage form (*in situ* thermosensitive gel), route of administration (topical), drug content (90–110%), dosage strength (1%), pH (~5), gelling capacity (immediate), and gelation temperature (32–35 °C) for dermal application of *in situ* gels. According to the QTPP, the CQAs were determined. Then, CMAs were determined. In our study, different types and

ratios of polymers (GG and MC) were considered inputs (CMAs), and gelation temperature, pH, viscosity, mechanical properties, drug content, spreadability, and *in vitro* drug release (CQAs) were considered outputs.[21,24] CQAs were tested. The results were imported into Minitab® software, and the relationships between input and output were evaluated.

*Preparation of NDF loaded in situ gel formulations*

Gels were produced by mixing distilled water and polymers. First, 2/3 of the required distilled water was preheated to 90 °C. MC was added in portions as it dissolved slowly, and the mixture was continuously stirred for 1 hour. Then the remaining distilled water, at room temperature, was added, and the mixture was continuously stirred using a magnetic stirrer until it appeared clear.[25] The temperature was reduced to 50 °C, GG was added, and stirring continued for about 20 minutes. The drug was dispersed at 25 °C with continuous stirring.[14] After that, poloxamers were added using the cold technique.[26,27] The mixture was cooled by covering the outside of the beaker with ice, and the required amounts of P188 and P407 were added while stirring continuously with a magnetic stirrer for about 1 hour. It was stored overnight in the refrigerator until all the polymers were completely dissolved. The gel formulations are presented in Table 1.

*Characterization of NDF loaded in situ gel formulations*

Gels were characterized using FTIR and by measuring gelation temperature, pH, clarity, viscosity, drug content, mechanical properties, spreadability, cytotoxicity, and in vitro drug release.

*FTIR spectroscopy analysis*

The infrared spectra of the drug (NDF), the polymers (GG, MC, P188, and P407), drug-free *in situ* gels and NDF-loaded *in situ* gels were recorded using an FTIR spectrometer (FT/IR-4600, Jasco, Tokyo, Japan). Samples were placed on the sample plate. The study was performed at room temperature with 32 scans over the spectra range from 4,000 to 400 $cm^{-1}$ at a resolution of 4.0 $cm^{-1}$.[28-30]

*Clarity*

Clarity was determined by visual inspection as follows: very clear (glassy), +++; clear, ++; and turbid, +.[31]

*Determination of gelation temperature (Tsol-gel, sol-gel temperature)*

After the prepared gels were refrigerated overnight, a magnetic bar was placed inside the container, which was then placed on a magnetic stirrer at 80 °C. The temperature at which the magnetic bar stopped was recorded (n = 3).[32]

**Table 1. Formulations of the NDF-loaded thermosensitive *in situ* gels (%w/w).**

| Formulation | P407 | P188 | MC | GG | NDF |
|---|---|---|---|---|---|
| **N1** | 17.5 | 7 | 0.3 | 0.1 | 1 |
| **N2** | 17.5 | 7 | 0.3 | 0.3 | 1 |
| **N3** | 17.5 | 7 | 0.7 | 0.1 | 1 |
| **N4** | 17.5 | 7 | 0.7 | 0.3 | 1 |

P407, poloxamer 407; P188, poloxamer 188; MC, methyl cellulose; GG, gellan gum; NDF, nadifloxacin.

*Gelling capacity*

The gelation capacity of the formulation was evaluated by introducing a drop of the sample into a beaker maintained at 32–34 °C, and the gel formation time was determined visually. The results were categorized according to gel behavior as follows: #, gel developed after a short delay but quickly liquefied; ##, gel formed instantly and lasted for several minutes; ###, rapid gel formation that remained intact for approximately one hour.[31-34]

*Determination of pH*

The pH was determined using a pH meter (Mettler Toledo S220-K, Switzerland). The device probe was directly immersed in the gel, and after 10 seconds, the value read from the device was recorded (n = 4).

*Viscosity*

The viscosity was measured using a Brookfield DVE digital viscometer. To ensure that the torque value was between 10% and 90% and did not cause errors, the speed value was determined experimentally.[35] *In situ* gels were placed in a 100 mL beaker, and the measurement was performed.[31-33] Formulations were analyzed at 32 °C, at speeds of 60 rpm (for N1, N2, and N3) and 10 rpm (for N4), using spindle number s03 (n = 4).

*Mechanical properties*

The mechanical properties (springiness, resilience, and cohesiveness) were measured using a TA-XT plus texture analyzer. The test was performed with a Perspex probe (P/25P, $\theta$: 25 mm) and at 32 ± 0.5 °C (n = 4). The pre-test, test, and post-test speeds were each 2.00 mm/s with a trigger force of 0.001 N; the target mode distance and the compression depth in each run were 10.00 mm; and the delay time between two compressions was 10 s.[12,36]

*Spreadability*

Spreadability (work of shear, stickiness, work of adhesion, and firmness) was measured using the TA-XT plus texture analyzer. Both female and male cones were used. The gel was placed into the female cone. The distance was 23.00 mm, the test speed was 3 mm/s, and the post-test speed was 10.00 mm/s at 32 ± 0.5 °C (n = 3).[36]

*Drug content uniformity*

For the drug content experiment, a 100 µg/mL solution was prepared by dissolving 100 mg of the NDF-loaded gels (N1, N2, N3, and N4) in 10 ml of methanol, was then diluted to 6 µg/mL with methanol: pH 7.4 PBS (30:70, v/v) solution, and was analyzed by UV spectrophotometry using a spectrophotometer (JASCO V-730 BIO, Tokyo, Japan).[37,38] A stock solution of NDF (100 µg/mL) was prepared by sonication in methanol. The calibration standards were prepared at concentrations of 6–16 µg/mL. A wavelength of 290 nm was used, and methanol: PBS (30:70 v/v) was used as a blind (n = 3).

*In vitro drug release studies*

Dialysis membrane method was used for *in vitro* drug release studies for N1, N2, N3, N4 formulations and the commercially available marketed product (MP) (Magnis,© Santa Farma Pharmaceutical Company, İstanbul, Türkiye). In this method, physical separation of the dosage forms is achieved by using a dialysis membrane, which facilitates sampling at periodic intervals. *In vitro* release experiment of formulations was performed in 100 mL methanol and pH 7.4 PBS (30:70 v/v ratio) at 320 rpm. Methanol and pH 7.4 PBS (30:70 v/v ratio) to ensure sink conditions were used as a medium in the study. The beakers were sealed with parafilm to prevent evaporation. The temperature was adjusted at 34 ± 1 ˚C to imitate skin temperature.[31] Two g of formulations were separated from the medium by means of a dialysis membrane (Spectra/por, MW of 12–14 kDa). 0.1 mL of sample was withdrawn at predetermined time intervals of 0.5, 1, 2, 3, 4, 6, 8, 24, 30, and 46 h, and the same volume of fresh medium was replaced.[31,36,39] Gels were measured using the UV method as described above.

*Cytotoxicity studies*

*Cell culture*

The murine fibroblast cell line (L929) was used. The cells were cultured in high-glucose DMEM supplemented with 1% (v/v) penicillin-streptomycin and 10% (v/v) FBS. Cultures were maintained at 37 ˚C in a humidified atmosphere containing 5% CO2. When the cells reached 70–80% confluence, they were detached with 0.25% trypsin-EDTA and used for subsequent studies.

*MTT cytotoxicity assay*

L929 cells were seeded in 96-well plates at a density of 1 × $10^4$ cells/well and incubated for 24 hours at 37 ˚C, 5% $CO_2$. Following this period, four hydrogel formulations containing NDF (N1, N2, N3, and N4) were extracted by incubation in cell culture medium for 24 hours at 37 ˚C. After release, the hydrogel extracts were sterilized using a membrane filter (pore size of 0.22 µm). The resulting sterile hydrogel extracts were applied to the cells at concentrations of 50, 125, 250, 500, 750, and 1000 ppm, and the cells were incubated for 24 hours. Cells treated only with cell culture medium were used as negative controls. At the end of the incubation period, 10 µL of MTT solution (5 mg/mL prepared in PBS) was added to each well, and the plates were incubated for an additional 4 hours at 37 ˚C. The medium was then carefully removed, and 100 µL of DMSO was added to each well to dissolve the formed formazan crystals. Absorbance values were determined with a BMG SPECTROstar microplate reader at a wavelength of 570 nm. Cell viability (%) was calculated using the following formula:[40]

Statistical analysis was performed using two-way analysis of variance (ANOVA) followed by Tukey's multiple comparisons test in GraphPad Prism version 8.4.3. A *p*-value of less than 0.05 was considered statistically significant.

*Statistical analysis*

All data are expressed as mean ± standard deviation (SD); the number of replicates (n = 3 or 4) is given in each table legend. Physicochemical, spreadability, and mechanical parameters were analyzed using ordinary one-way ANOVA followed by Tukey's multiple comparisons test. *In vitro* release data were analyzed by two-way ANOVA followed by Dunnett's multiple comparisons test. Multiplicity-adjusted *p*-values are reported (*$p < 0.05$, **$p < 0.01$, ***$p < 0.001$). Analyses were performed with GraphPad Prism 10.2.1 (GraphPad Software, Boston, MA, USA); $p < 0.05$ was considered significant.

## RESULTS

*Preparation of NDF loaded in situ gel formulations*

The United States Food and Drug Administration has approved two poloxamers (P407 and P188), which are widely used in the preparation of thermosensitive *in situ* gels. The sol-gel temperature of the formulation varies with the polymer concentration. Normally, they are liquid at room temperature and undergo gelation at physiological temperatures.[41] During the preparation of *in situ* gels, MC was dispersed at 90 ˚C according to the method in the literature.[25] The temperature was reduced to 50 ˚C, and GG was added and mixed.[14] Poloxamers were added to this mixture using a cold technique.[26,27]

In this study, we formulated thermosensitive *in situ* gels that can be effortlessly applied to the skin and are appropriate for use in treating acne vulgaris and superficial bacterial skin infections. *In situ* gels contain 1% NDF, 17.5% P407, and 7% P188. The effect of CMAs was investigated within the framework of QbD, using variable ratios of MC and GG. *In situ gels* are carrier systems that can be prepared using poloxamers and that play a vital role in delivering drugs to a specific area of the skin.[31,42] In our study, opaque, white, and homogeneous *in situ* gels were produced (Figure 1).

*FTIR spectroscopy analysis*

FTIR studies were conducted on the pure drug (NDF), the polymers (GG, MC, P188, and P407), and the prepared drug-free

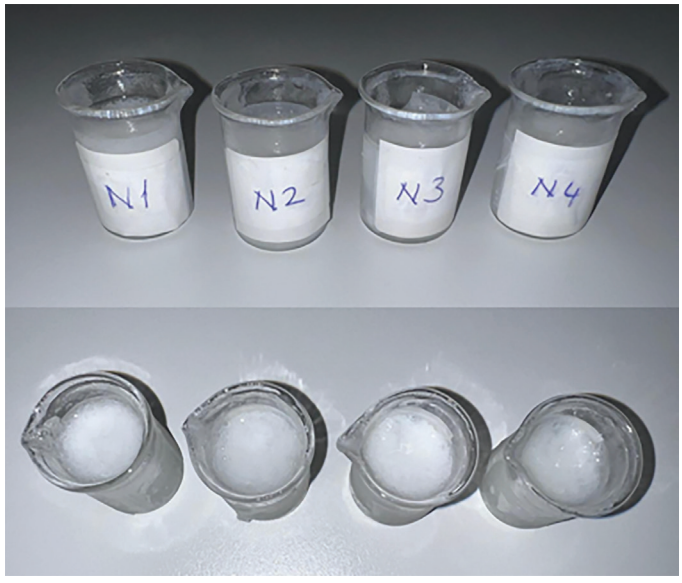



**Figure 1.** Photo of prepared nadifloxacin-loaded thermosensitive *in situ* gel formulations.

and NDF-loaded gels (Figure 2). No peak shift or peak loss was observed in the spectra of the gels and substances, indicating that the excipients and the drug were compatible.

*Determination of gelation temperature, gelling capacity, clarity, viscosity, and pH*

The gelation temperatures, pH, and viscosity of the gels prepared with NDF are presented in Table 2. Results of the clarity evaluation, showing that all the gels were turbid, are presented in Table 2. The photograph of the four formulations, which provides an idea of their clarity, is presented in Figure 1.

*Mechanical properties*

The textural parameters of the four prepared dermal gel formulations, including springiness, cohesiveness, and resilience, were evaluated using a texture analyzer. Table 3 shows the TPA data of the formulations.

*Spreadability*

Table 4 presents the results of our study on spreadability. The spreadability study characterizes the formulation's work of adhesion and work of shear, as well as its stickiness and firmness by measuring force fluctuations over time.[36]

*Drug content uniformity*

The maximum wavelength observed with the method was 290 nm. The average NDF values were 97.1% and 100.3% (Table 2).

*In vitro drug release studies*

Release from NDF gels of N1, N2, N3, N4, and the MP was carried out and is shown in Figure 3. During the first hour of the study, the NDF release rates were observed for N4 (6.1%), N3 (9.5%), N2 (10.4%), N1 (11.1%), and MP (11.9%), in ascending order (Table 5). Within 8 h, *in vitro* NDF release from N1, N2, N3, N4, and MP was 96.1%, 95.1%, 92.4%, 77.5%, and 42.8%, respectively. Within 24 h, approximately 100% of the NDF was released from all *in situ* gels, and 78.9% was released from MP.

*Cytotoxicity studies*

The cytotoxic effects of the developed NDF-loaded hydrogel formulations on L929 fibroblast cells were evaluated using MTT analysis. The results are presented in Figure 4. Cells were exposed to increasing concentrations of hydrogel extracts (50–1000 ppm), and cell viability remained above 90% in all groups, indicating that the formulations are generally well tolerated and highly biocompatible.

*Evaluation of quality by design approach*

Table 6 shows that the $R^2$ values and *p*-values.

Contour plots show the effects of MC and GG concentrations on various parameters (Figure 5).

## DISCUSSION

In the literature, the peaks of the polymers used and of NDF have already been reported. GG FTIR spectra described O–H stretching vibration (hydroxyl groups, hydrogen bonding) at 3200 $cm^{-1}$ 3400 $cm^{-1}$. The band at about 2927 $cm^{-1}$ is due to–$CH_2$ group, and 1153 and 1024 $cm^{-1}$ are due to C–O stretchings. Bending vibration of the carboxylate group appeared at about 1627 and 1409 $cm^{-1}$.[43] MC had an absorption band at about

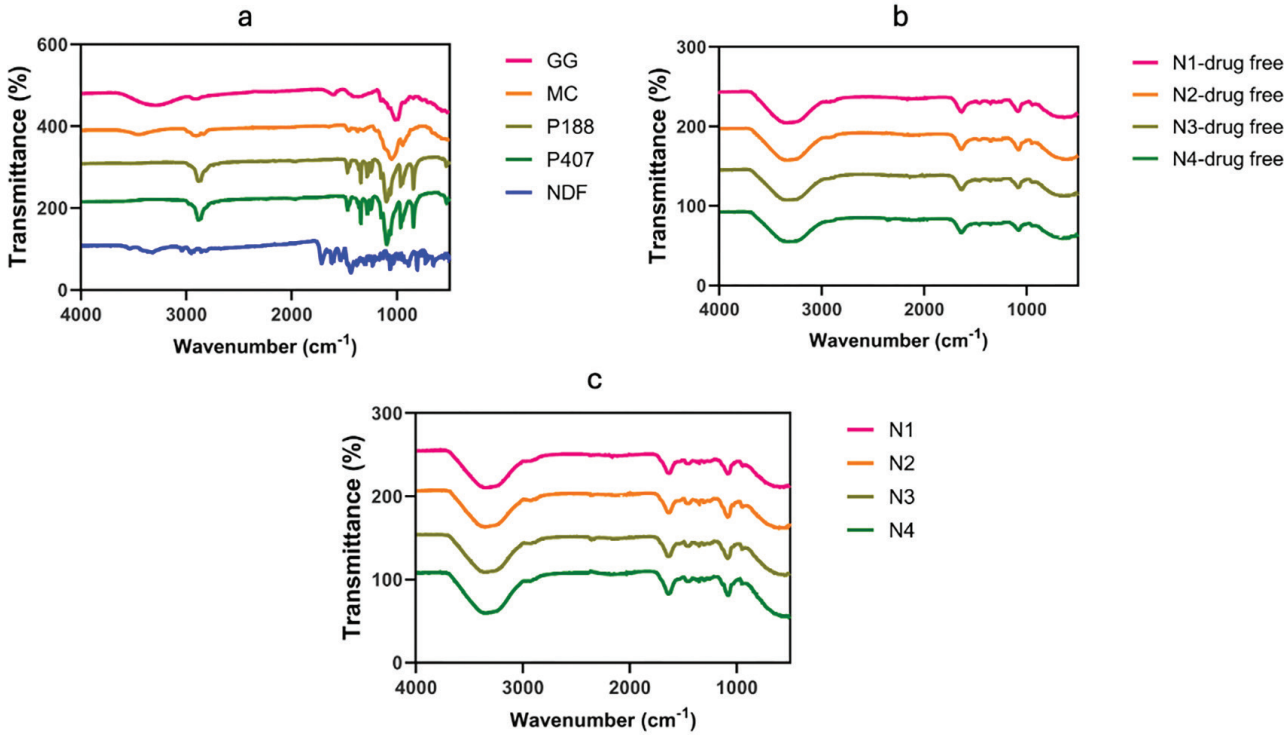



**Figure 2.** FTIR spectra of a) the different starting components (GG, MC, P188, P407, and NDF); b) drug-free *in situ* gels and c) NDF-loaded *in situ* gels.
MC, methyl cellulose; GG, gellan gum; NDF, nadifloxacin.

**Table 2. Values of gelation temperature (n = 3), gelling capacity (n = 3), pH (n = 4), viscosity (n = 4), drug content (n = 3), and score of clarity (n = 3).**

| Formulation | Gelling capacity | Gelling temperature (°C) | Clarity | pH | Viscosity (cP) | Drug content (%) |
|---|---|---|---|---|---|---|
| N1 | ### | 35.167 ± 0.289$^{A}$ | + | 7.095 ± 0.013$^{B}$ | 422.425 ± 0.846$^{D}$* | 98.686 ± 0.315$^{B}$ |
| N2 | ### | 32.500 ± 0.500$^{B}$ | + | 7.085 ± 0.013$^{B}$ | 883.750 ± 3.676$^{C}$* | 97.697 ± 0.116$^{C}$ |
| N3 | ### | 32.000 ± 0.000$^{B}$ | + | 7.093 ± 0.036$^{B}$ | 1196.250 ± 4.272$^{B}$* | 97.072 ± 0.075$^{D}$ |
| N4 | ### | 30.000 ± 0.000$^{C}$ | + | 7.198 ± 0.005$^{A}$ | 3622.500 ± 15.000$^{A}$** | 100.348 ± 0.046$^{A}$ |

Values are expressed as mean ± standard deviation.
$^{A-D}$Within each column, values not sharing a common superscript letter differ significantly (one-way ANOVA followed by Tukey's multiple comparisons test, $p < 0.05$). Letters are assigned in descending order of the mean and are independent for each column. Gelling capacity and clarity were scored qualitatively and were identical for all formulations; therefore no statistical comparison was performed for these parameters.
#, gel developed after a short delay but quickly liquefied; ##, gel formed instantly and lasted for several minutes; ###, rapid gel formation that remained intact for approximately one hour.
+++, very clear (glassy); ++, clear; +, turbid.
*measured at 60 rpm; **measured at 10 rpm. These symbols denote the rotational speed of the measurement only and carry no statistical meaning.
ANOVA, analysis of variance.

**Table 3. The mechanical properties of the NDF-loaded thermosensitive *in situ* gels (n = 4).**

| Formulation | Springiness (%) | Cohesiveness | Resilience (%) |
|---|---|---|---|
| N1 | 3.985 ± 0.001$^{A}$ | 2.227 ± 0.104$^{A}$ | 0.005 ± 0.000$^{C}$ |
| N2 | 2.656 ± 0.161$^{B}$ | 0.957 ± 0.039$^{B}$ | 0.005 ± 0.001$^{C}$ |
| N3 | 0.997 ± 0.000$^{C}$ | 0.805 ± 0.031$^{C}$ | 0.038 ± 0.002$^{B}$ |
| N4 | 0.977 ± 0.003$^{C}$ | 0.770 ± 0.029$^{C}$ | 0.080 ± 0.004$^{A}$ |

Values are expressed as mean ± standard deviation (n = 4).
$^{A-C}$Within each column, values not sharing a common superscript letter differ significantly (one-way ANOVA followed by Tukey's multiple comparisons test, $p < 0.05$). Letters are assigned in descending order of the mean and are independent for each column.
ANOVA, analysis of variance; NDF, nadifloxacin.

**Table 4. The spreadability results of the NDF-loaded thermosensitive *in situ* gels (n = 3).**

| Formulation | Work of shear (g.sec) | Stickiness (g) | Firmness (g) | Work of adhesion (g.sec) |
|---|---|---|---|---|
| N1 | 13.312 ± 0.294$^{C}$ | -60.250 ± 1.578$^{C}$ | 35.289 ± 0.545$^{C}$ | -8.155 ± 0.218$^{C}$ |
| N2 | 27.500 ± 0.357$^{C}$ | -79.102 ± 0.938$^{B}$ | 50.959 ± 0.192$^{C}$ | -12.327 ± 0.078$^{C}$ |
| N3 | 71.756 ± 11.401$^{B}$ | -110.277 ± 2.354$^{A}$ | 135.704 ± 12.501$^{B}$ | -33.512 ± 4.539$^{B}$ |
| N4 | 104.857 ± 3.550$^{A}$ | -110.579 ± 5.881$^{A}$ | 162.308 ± 10.204$^{A}$ | -43.721 ± 3.699$^{A}$ |

Values are expressed as mean ± standard deviation (n=3).
$^{A-C}$Within each column, values not sharing a common superscript letter differ significantly (one-way ANOVA followed by Tukey's multiple comparisons test, $p < 0.05$). Letters are assigned independently for each column, with "A" denoting the highest magnitude of the corresponding property.
Stickiness and work of adhesion are reported as negative values because they are derived from the withdrawal phase of the probe; more negative values therefore indicate stronger adhesive interaction. Superscript letters for these two parameters were assigned according to the absolute magnitude of the response.
ANOVA, analysis of variance.

3400 $cm^{-1}$ associated to hydrogen bonding. The bands at about 2900 cm,$^{-1}$ 2800 $cm^{-1}$ are attributed to vibration of C–H. The pics at 1063 $cm^{-1}$ are assigned to C-O-C stretching mode from glycosidic units. The absorption band at 944 $cm^{-1}$ is ascribed to $OCH_3$ groups.[44,45] P188 and P407 peaks at around 2800-2900 $cm^{-1}$ (C–H stretch). Other peaks are seen at 1341 $cm^{-1}$ (in-plane O–H bend) and around 1100 $cm^{-1}$ (C–O stretch). Our spectra of P188 and P407 were comparable to previously recorded spectra.[46,47] The characteristic peak of P188 and P407 shifted from 2856 $cm^{-1}$ (Figure 2a) to 2871 $cm^{-1}$ (Figure 2c) as previously reported, which was shown to the physical interaction between drug and water-soluble polymers.[47] The spectrum of NDF demonstrated an intense vibration observed at 2976 $cm^{-1}$ can be associated with the carboxyl O–H stretching. At the same time was observed the presence of large bands at 1748 $cm^{-1}$ was observed, attributed with ketone C = O stretching. Other large vibrations observed at 1624 $cm^{-1}$ can be related to the aromatic C = C stretching.[48] All characteristic bands were shown in the FTIR spectra of polymers, NDF, and gels with or without the drug and all excipients (Figure 2). The FTIR spectra of drug-free gels and NDF-containing gels did not show significant differences across formulations, indicating that the polymer blends do not support the formation of additional interactions among their components.[30]

**Table 5. *In vitro* cumulative release (%) of NDF from the thermosensitive *in situ* gel formulations and the marketed product (n=3).**

| Time (h) | N1 | N2 | N3 | N4 | Product |
|---|---|---|---|---|---|
| 0.5 | 4.2 ± 0.4 | 4.3 ± 1.2 | 4.5 ± 1.5 | 2.3 ± 0.5 | 7.7 ± 2.0 |
| 1 | 11.1 ± 0.6 | 10.4 ± 3.6 | 9.5 ± 4.5 | 6.1 ± 1.5 | 11.9 ± 2.9 |
| 2 | 27.6 ± 1.4 | 27.6 ± 8.6 | 24.6 ± 6.2 | 18.2 ± 2.3 | 20.4 ± 4.0 |
| 3 | 42.9 ± 2.9* | 43.9 ± 12.3 | 43.8 ± 4.4 | 27.0 ± 5.5 | 27.2 ± 3.9 |
| 4 | 51.4 ± 5.4* | 57.7 ± 3.1*** | 58.2 ± 4.7 | 35.8 ± 3.2 | 28.5 ± 1.4 |
| 6 | 76.9 ± 4.4 | 74.5 ± 3.7 | 70.8 ± 11.1 | 65.1 ± 15.8 | 37.0 ± 1.4 |
| 8 | 96.1 ± 11.8* | 95.1 ± 7.4* | 92.4 ± 2.3** | 77.5 ± 8.7 | 42.8 ± 5.1 |
| 24 | 100.5 ± 1.3** | 100.2 ± 1.9*** | 98.8 ± 2.6 | 98.5 ± 0.6 | 78.9 ± 2.4 |
| 30 | 100.5 ± 1.3** | 100.2 ± 5.0 | 103.6 ± 1.7 | 98.5 ± 0.5 | 90.5 ± 0.5 |
| 46 | 100.5 ± 1.3 | 100.2 ± 7.0 | 102.9 ± 0.1 | 98.5 ± 0.5 | 102.5 ± 2.3 |

Values are expressed as mean ± standard deviation (n = 3). Statistical comparisons were performed by two-way ANOVA followed by Dunnett's multiple comparisons test, with each formulation compared against the marketed product at every sampling time.
*$p < 0.05$, **$p < 0.01$, ***$p < 0.001$ versus the marketed product. Absence of a symbol indicates no statistically significant difference.
ANOVA, analysis of variance.

**Table 6. Regression equation, model summary, and *p*-values of NDF-loaded *in situ* gels.**

| CQA | Regression equation | Model summary | | | *p*-value | |
|---|---|---|---|---|---|---|
| | | $R^2$ (%) | $R^2$ adj (%) | $R^2$ pred (%) | *p*-value of MC | *p*-value of GG |
| **Gelation temperature (°C)** | 38.338 - 7.125 MC% (w/w) - 11.75 GG% (w/w) | 99.11 | 97.33 | 85.76 | 0.078 | 0.094 |
| **pH** | 7.008 + 0.125 MC% (w/w) + 0.250 GG% (w/w) | 58.14 | 0.00 | 0.00 | 0.558 | 0.558 |
| **Viscosity 32°C (cps)** | -2108 + 4391 MC% (w/w) + 7219 GG% (w/w) | 84.26 | 52.79 | 0.00 | 0.325 | 0.380 |
| **Springiness (%)** | 5.75 - 5.83 MC% (w/w) - 3.37 GG% (w/w) | 93.23 | 79.69 | 0.00 | 0.174 | 0.490 |
| **Cohesiveness** | 2.85 - 2.01 MC% (w/w) - 3.26 GG% (w/w) | 73.78 | 21.34 | 0.00 | 0.417 | 0.482 |
| **Resilience (%)** | -0.0565 + 0.1350 MC% (w/w) + 0.105 GG% (w/w) | 88.39 | 65.17 | 0.00 | 0.236 | 0.500 |
| **Firmness (g)** | -57.43 + 264.7 MC% (w/w) + 105.7 GG% (w/w) | 99.74 | 99.23 | 95.90 | 0.033 | 0.161 |
| **Work of shear (g.sec)** | -54.2 + 169.8 MC% (w/w) + 118.2 GG% (w/w) | 98.30 | 94.90 | 72.80 | 0.088 | 0.242 |
| **Stickiness (g)** | -29.5 - 101.9 MC% (w/w) - 47.9 GG% (w/w) | 95.32 | 85.96 | 25.14 | 0.142 | 0.490 |
| **Work of adhesion (g.sec)** | 18.24 - 70.94 MC% (w/w) - 36.0 GG% (w/w) | 98.95 | 96.85 | 83.21 | 0.067 | 0.253 |
| **Drug content (%)** | 96.73 + 1.25 MC% (w/w) + 5.5 GG% (w/w) | 24.87 | 0.00 | 0.00 | 0.851 | 0.693 |
| **Release 6$^{th}$ hour (%)** | 85.56 - 19.38 MC% (w/w) - 20.25 GG% (w/w) | 96.56 | 89.69 | 44.99 | 0.134 | 0.246 |

MC, methyl cellulose; GG, gellan gum; NDF, nadifloxacin; CQA, critical quality attribute.

All four formulations (N1–N4) exhibited rapid sol-to-gel conversion upon exposure to the simulated physiological conditions, and the resulting gels remained structurally intact for approximately one hour (###). None of the formulations liquefied prematurely, indicating that the concentrations employed in this study were sufficient to establish a coherent gel network in every composition tested. With respect to visual appearance, all four formulations were scored as turbid (+); no formulation reached the clear (++) or glassy (+++) levels on the clarity scale. The *in situ* gels produced were turbid. The literature reports that the clarity of drug-loaded *in situ* gels reaches this level.[32]

Rapid gel formation, which maintained structural integrity for approximately one hour, was observed in all formulations. If the gelation temperature is below 25 °C, the gel may form at room temperature before application. When the gelation temperature is above 38 °C, it remains liquid at body temperature and therefore does not gel. Therefore, an average gelation temperature of 32 °C–35 °C is preferred.[49] The gelation temperature decreased progressively from N1 to N4, and the differences among the

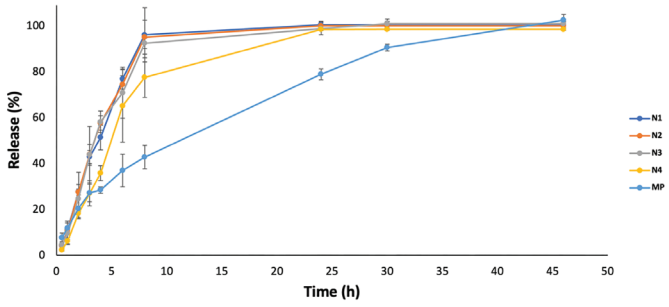



**Figure 3.** *In vitro* drug release profiles of NDF-loaded *in situ* gels (N1, N2, N3, and N4) and marketed product (MP) (n = 3, ± SD).

NDF, nadifloxacin; SD, standard deviation.

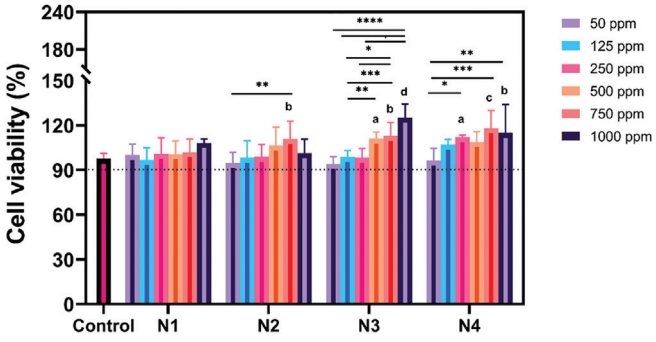



**Figure 4.** The cell viability (%) of L929 fibroblast cells treated with NDF-loaded hydrogel extracts (N1–N4) at various concentrations (50–1000 ppm) for 24 hours. Datas are shown as average ± standard deviation (n = 7). Statistical significance: *$p < 0.05$, **$p < 0.01$, ***$p < 0.001$, ****$p < 0.0001$ according to the hydrogel content at different concentrations and $^{a}p < 0.05$; $^{b}p < 0.01$; $^{c}p < 0.001$; $^{d}p < 0.0001$, compared with the control group.

NDF, nadifloxacin.

formulations were statistically significant (one-way ANOVA, $F(3,8) = 163.0$, $p < 0.0001$). Tukey's multiple comparisons test showed that N1 (35.167 ± 0.289 °C) gelled at a significantly higher temperature than all other formulations ($p < 0.0001$), whereas N4 (30.000 ± 0.000 °C) gelled at the lowest temperature and differed significantly from N1, N2 ($p < 0.0001$) and N3 ($p = 0.0001$). The only pairwise comparison that did not reach statistical significance was that between N2 (32.500 ± 0.500 °C) and N3 (32.000 ± 0.000 °C) (adjusted $p = 0.2252$), indicating that these two compositions behave equivalently with respect to the sol-gel transition.

The pH value is a significant factor in dermal applications. The normal pH range for non-neonatal skin is acidic, typically between 4 and 6.[50] Accordingly, the formulations' skin-nonirritating pH and the pH of the gels are suitable for topical application. The formulations had pH values of approximately 7.1–7.2. These values were compatible with the skin pH, which ranges from 5.0 to 7.0.[51,52] Although the average pH of healthy skin is around 5.5, the pH of wounded, burned, or acne-affected skin may shift toward neutral or slightly alkaline values. Previous studies have reported that the wound surface pH is around 7 during the healing process. Therefore, the pH values of the developed formulations (7.1–7.2) were considered acceptable for dermal *in situ* gel application and were not expected to cause irritation.[53] In other dermally applied *in situ* gel studies, the pH values were reported to range from 5.777 ± 0.07 to 6.027 ± 0.06.[31] If gels contain GG, their pH is primarily determined by the pH of the solution used and by the presence of acidic or basic additives. GG is a weak acid, and when used at concentrations of 0.1–2% w/w, as in our study, increasing GG concentration in a formulation has only a minor effect on the pH of the final gel.[54] Another study reported that altering the proportion of methylcellulose in gels did not significantly change the pH of the formulation within the typical operating range. pH is primarily determined by the solvent and any acidic or basic components, but not by the methylcellulose concentration itself.[55] The pH values of all formulations were within the near-neutral range (7.085–7.198). Although one-way ANOVA indicated a statistically significant difference among the groups ($p < 0.0001$), Tukey's test revealed that this effect was driven entirely by N4 (7.198 ± 0.005), which differed significantly from N1, N2 and N3 ($p < 0.0001$ for all three comparisons). No significant differences were detected among N1, N2, and N3 (adjusted $p = 0.8965$, 0.9980, and 0.9521 for N1 vs. N2, N1 vs. N3, and N2 vs. N3, respectively). The absolute magnitude of the difference attributable to N4 was only 0.10–0.11 pH units.

Similar studies in the literature on *in situ* gel formulations report viscosity measurements performed at 32 °C. For example, viscosity analyses were also carried out at 32 °C in pycnogenol-loaded[42] and vanillic acid-loaded[56] *in situ* gel formulations. In the vanillic acid-loaded *in situ* gel study, the gelation temperature was below 32 °C, but the viscosity was evaluated at 32 °C, as in our study. As observed in other gel studies, viscosity increased with the increase in polymer content.[57,58] Viscosity increased markedly across the formulation series, and all six pairwise comparisons were statistically significant ($p < 0.0001$ for each). The measured values followed the order N1 (422.425 ± 0.846 cP) < N2 (883.750 ± 3.676 cP) < N3 (1196.250 ± 4.272 cP) < N4 (3622.500 ± 15.000 cP). It should be noted that N1-N3 were measured at 60 rpm, whereas N4 was measured at 10 rpm because its consistency exceeded the working range of the spindle at the higher rotational speed (inference). Because *in situ*-gelling systems of this type typically display pseudoplastic (shear-thinning) flow, the apparent viscosity recorded for N4 at the lower shear rate is expected to be higher than the value obtained at 60 rpm; the difference between N4 and the remaining formulations should therefore be interpreted as a combined effect of composition and measurement conditions, rather than a composition effect alone.

Suitable mechanical properties are crucial for dermal formulations. TPA is a standard technique for assessing mechanical properties.[59] Springiness is a textural parameter attributed to the flexibility of the product.[60] The gel sample deforms during initial compression and restructures to regain elasticity.[59] In our study, the springiness decreased as GG increased in the N3 and N4 formulations, which were in gel form at 32 °C. Similarly, one study reported that the addition of GG increased hardness but significantly decreased springiness

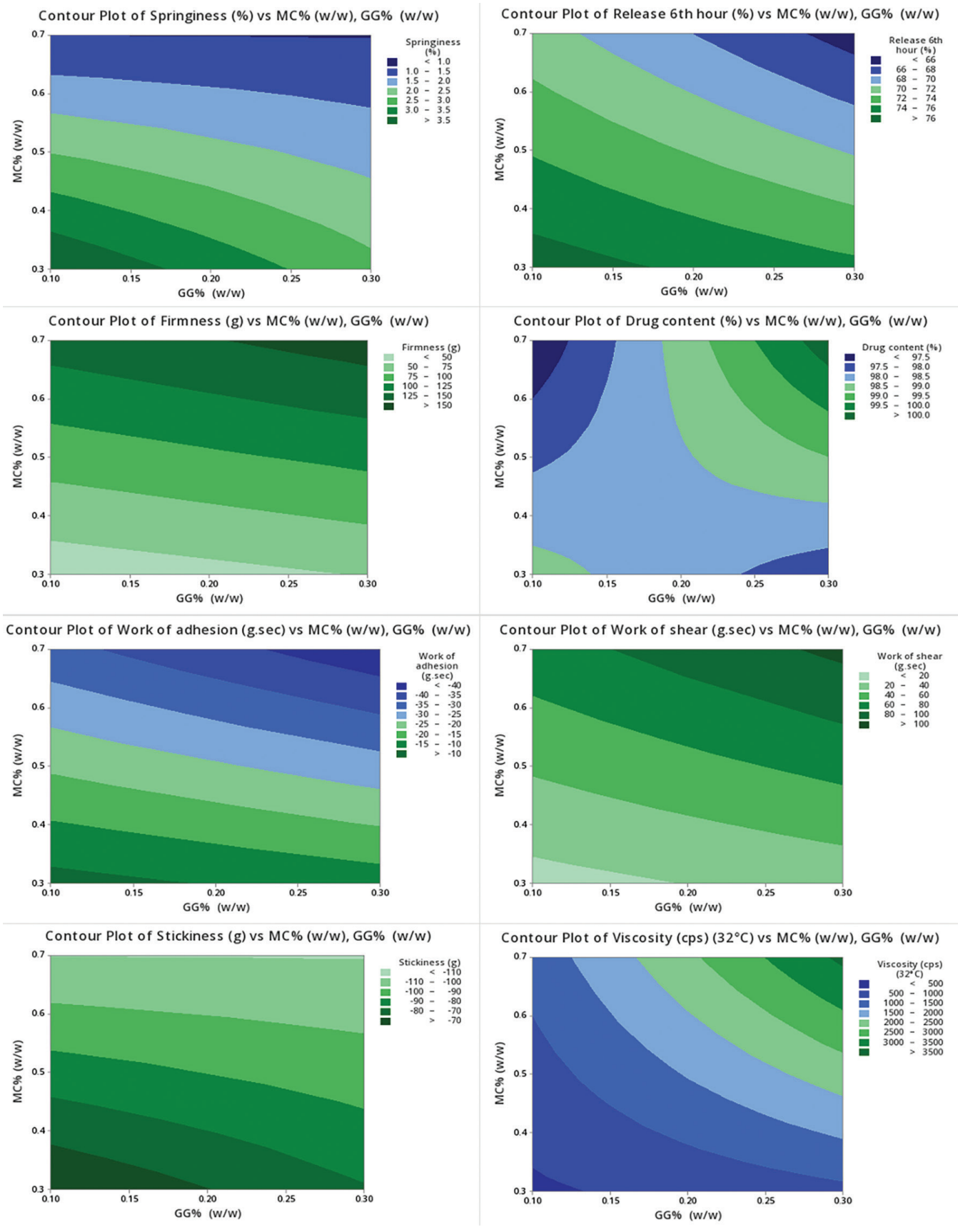



**Figure 5.** Contour plot graphics on various CQAs of NDF-loaded *in situ* gels.

CQA, critical quality attribute; MC, methyl cellulose; GG, gellan gum; NDF, nadifloxacin.

compared to the control group.[61] Similarly, as MC increased, springiness decreased. Cohesion describes how well a sample resists a second deformation relative to its resistance to the first deformation.[59] Elasticity indicates the rate at which a sample returns to its original form after deformation, while cohesiveness provides insight into the sample's response to repeated stresses. Higher values indicate lower sample elasticity.[9] A lower cohesion value indicates a weaker gel structure that breaks more readily.[62] As can be seen from Table 3, cohesiveness values range from 0.770 to 2.227. In our study, cohesiveness decreased as the MC ratio increased (N2: 0.3% and N4: 0.7%). This decrease was also observed in another *in situ* gel study prepared with 0.1% and 0.5% Na CMC.[9] In our study, cohesiveness decreased as the GG ratio increased (N3, 0.1% and N4, 0.3%). A similar decrease was observed in GG/Chitosan formulations and in GG formulations. While GG alone exhibited lower cohesiveness, the addition of chitosan increased cohesiveness.[62] Resilience reflects the capacity of gels to recover their shape after penetration.[63] Resilience is an indicator of how quickly and forcefully a product recovers from deformation. It's the product's elastic recovery.[60] The elastic recovery was highest in N4 gels, which had the highest polymer concentration in the sample. In our study, we observed that resilience increased with increasing MC (N2, 0.3% and N4, 0.7%). Similarly, other studies reported that the MC in hydrogels showed improved resilience as weight percentage increased.[64,65] In our study, resilience increased as the GG ratio increased (N3, 0.1%; N4, 0.3%). One study reported that increasing the GG content improved resilience and reduced swelling and water uptake.[66] The mechanical properties of the NDF-loaded thermosensitive *in situ* gels were evaluated by texture profile analysis, and the results are summarized in Table 3. All three parameters—springiness, cohesiveness, and resilience—differed significantly among the formulations (one-way ANOVA, $p < 0.0001$).

Springiness decreased markedly across the formulation series. N1 exhibited the highest value (3.985 ± 0.001), followed by N2 (2.656 ± 0.161); both differed significantly from each other and from the remaining formulations ($p < 0.0001$ for all comparisons involving N1 or N2). N3 (0.997 ± 0.000) and N4 (0.977 ± 0.003) displayed the lowest springiness values and did not differ significantly from each other (adjusted $p = 0.9838$), indicating that the elastic recovery of the gel network reached a plateau in these two compositions. A similar pattern was observed for cohesiveness. N1 showed a distinctly higher value (2.227 ± 0.104) than all other formulations ($p < 0.0001$), while N2 (0.957 ± 0.039) differed significantly from both N3 (0.805 ± 0.031; adjusted $p = 0.0157$) and N4 (0.770 ± 0.029; adjusted $p = 0.0038$). As with springiness, no significant difference was detected between N3 and N4 (adjusted $p = 0.8424$). Resilience followed the opposite trend, increasing from N1 and N2 to N4. N1 (0.005 ± 0.000) and N2 (0.005 ± 0.001) exhibited the lowest values and were statistically indistinguishable from one another (adjusted $p = 0.9978$), whereas N3 (0.038 ± 0.002) and N4 (0.080 ± 0.004) showed significantly higher resilience than both of these formulations and than each other ($p < 0.0001$ for all remaining comparisons). N4, therefore, displayed approximately sixteenfold greater resilience than N1. Taken together, the texture profile data indicate an inverse relationship between the elastic parameters (springiness and cohesiveness) and resilience across the formulation series.

Spreadability is a fundamental property of topically applied dermal formulations. If the formulation is used in this manner, it should exhibit sufficient spreadability to enable the patient to apply it easily to the skin.[36,67] When the male cone is removed from the sample, a negative region is formed. The maximum negative value represents the gel's adhesion force; that is, the force needed to separate the gel from the tube.[68] In one study, stickiness and the work of adhesion of drug-loaded hydrogels prepared with Carbopol as the gelling polymer increased with increasing polymer ratio.[36] Similarly, in our study, the work of adhesion and stickiness of the formulations increased with increasing polymer ratios. Firmness is the maximum force required to deform the formulation, indicating its strength. Higher firmness values are more favorable for the formulation's power.[68] In our study, as the polymer content in the gels increased, the firmness and viscosity increased. As a result, the spreadability of the gels decreased. Another study emphasized this similar relationship between the polymer content, viscosity, firmness, and spreadability. The same study reported that higher firmness values corresponded to greater gel consistency, which negatively affected its spreadability.[69] The field up to the positive force represents the work of shear, indicating the spreadability of the formulation.[68] Spreadability is inversely related to both work of shear and firmness.[36] The suitability of a gel for the skin is related to its spreadability, which is influenced by its resistance to external forces. Even if two products have similar firmness, their skin applications may differ. Accordingly, shear work and firmness are usually evaluated together.[67] Shear work and firmness values are N4, N3, N2, and N1, in order from highest to lowest (Table 4). The spreadability follows an opposite order, i.e., from highest to lowest: N1, N2, N3, and N4. The data showed that the work of shear and firmness were higher in formulations N3 and N4 than in formulations N1 and N2, resulting in lower spreadability. The spreadability and adhesion-related mechanical characteristics of the NDF-loaded thermosensitive *in situ* gels are presented in Table 4. All four parameters differed significantly among the formulations (one-way ANOVA, $p < 0.0001$ in each case).

The work of shear, which reflects the energy required to spread the gel, increased markedly across the formulation series. N4 required the greatest energy (104.857 ± 3.550 g·sec) and differed significantly from all other formulations ($p < 0.0001$ versus N1 and N2; $p = 0.0006$ versus N3), while N3 (71.756 ± 11.401 g·sec) in turn differed significantly from both N1 and N2 ($p < 0.0001$). The two formulations at the lower end of the series, N1 (13.312 ± 0.294 g·sec) and N2 (27.500 ± 0.357 g·sec), were not statistically distinguishable from one another (adjusted $p = 0.0758$), although their means differed approximately twofold.

Firmness followed an essentially identical pattern. The highest value was recorded for N4 (162.308 ± 10.204 g), followed

by N3 (135.704 ± 12.501 g); these two formulations differed significantly from each other (adjusted $p$ = 0.0159) and from both N1 and N2 ($p < 0.0001$ for all four comparisons). As with work of shear, no significant difference was detected between N1 (35.289 ± 0.545 g) and N2 (50.959 ± 0.192 g) (adjusted $p$ = 0.1593).

Stickiness became progressively more negative from N1 to N4, indicating a stepwise increase in adhesive strength. N1 exhibited the weakest response (-60.250 ± 1.578 g) and differed significantly from N2 (-79.102 ± 0.938 g; adjusted $p$ = 0.0005) as well as from N3 and N4 ($p < 0.0001$). N3 (-110.277 ± 2.354 g) and N4 (-110.579 ± 5.881 g) produced almost identical values and were statistically indistinguishable (adjusted $p$ = 0.9994), indicating that the stickiness response reached a plateau in these two compositions.

The work of adhesion showed the same directional trend but a different grouping. N4 exhibited the highest adhesive work (-43.721 ± 3.699 g·sec) and differed significantly from all other formulations, including N3 (-33.512 ± 4.539 g·sec; adjusted $p$ = 0.0117). N1 (-8.155 ± 0.218 g·sec) and N2 (-12.327 ± 0.078 g·sec) displayed the lowest adhesive work and did not differ significantly from each other (adjusted $p$ = 0.3633). Stickiness reached a plateau between N3 and N4, whereas the work of adhesion continued to increase.

The within-group variability observed for N3 was consistently higher than that observed for the other formulations for work of shear, firmness, and work of adhesion (relative SDs of 15.9%, 9.2%, and 13.5%, respectively, compared with values below 5% for N1 and N2).

When considered together with the texture profile data (Table 3), the results indicate that N3 and N4 form denser and more strongly adhesive gels at the expense of markedly reduced spreadability, whereas N1 and N2 spread readily but adhere weakly.

Two hundred ninety nm is consistent with the 291 nm,[70] 294 nm,[37] 295 nm,[71] 296 nm,[39] and 296.5 nm[38] values found in the literature. The maximum SD for NDF content was found to be 0.3. NDF is homogeneously distributed in the gels. Drug content ranged from 97.072 ± 0.075% to 100.348 ± 0.046% across the four formulations. All six pairwise comparisons were statistically significant, with N4 showing the highest content and N3 the lowest (N1 vs. N2, p=0.0006; N2 vs. N3, p=0.0112; all remaining comparisons, p<0.0001). Despite these statistically significant differences, every formulation complied with the (90.0–110.0%) acceptance range specified in (Ph. Eur./USP monograph), confirming that the drug was distributed homogeneously and the preparation procedure was reproducible.

Taken together, these results indicate that all four formulations satisfy the basic requirements for an *in situ* gelling system in terms of gelling capacity, pH, and drug content, but differ substantially in gelation temperatures and viscosity profiles.

Release studies are commonly carried out in media such as water, PBS, mixtures of organic solvents with PBS, or combinations of inorganic components with PBS.[72] The choice of release medium is primarily determined by the solubility characteristics of the drug being investigated.[73] NDF is insoluble in ethanol[74] and soluble in methanol. In NDF studies, methanol was used as a solvent.[39,75] Therefore, a 30:70 (v/v) mixture of methanol and PBS (pH 7.4) was chosen as the release medium. Based on the release results, the gels sustained drug release for 8 hours. N1 and N2 formulations showed higher release than N3 and N4 formulations; this difference can be attributed to the polymer ratio. The *in vitro* cumulative release profiles of the four thermosensitive *in situ* gel formulations and the MP are presented in Table 5. Two-way ANOVA revealed significant effects of formulation, sampling time, and their interaction ($p < 0.0001$ in each case), and Dunnett's multiple comparisons test was subsequently applied at each sampling time to compare each formulation against the MP.

During the first two hours, all four formulations and the MP released comparable proportions of the incorporated drug (2.3-7.7% at 0.5 h and 18.2-27.6% at 2 h). The MP showed the highest initial release at 0.5 h (7.7 ± 2.0%), whereas N4 exhibited the slowest onset (2.3 ± 0.5%). The profiles began to diverge from the third hour onwards. Between 3 and 8 h, N1, N2 and N3 released the drug substantially faster than the MP, reaching 92.4–96.1% at 8 h compared with 42.8 ± 5.1% for the product. The differences were statistically significant for N1 at 3, 4 and 8 h ($p < 0.05$), for N2 at 4 h ($p < 0.001$) and 8 h ($p < 0.05$), and for N3 at 8 h ($p < 0.01$). Between 3 and 8 h, N4 released the drug more gradually than the other three formulations and did not differ significantly from the MP at any point.

At 6 h, none of the four comparisons reached statistical significance, despite mean differences of 28–34 percentage points in favour of the formulations. By 24 h all four formulations had released essentially their entire drug load (98.5–100.5%), whereas the MP had reached 78.9 ± 2.4%. The difference remained statistically significant for N1 ($p < 0.01$) and N2 ($p < 0.001$) at this time, and for N1 alone at 30 h ($p < 0.01$). At 46 h the MP had also achieved complete release (102.5 ± 2.3%) and no significant differences remained between any formulation and the product. Overall, the release data indicate that three of the four formulations (N1, N2, and N3) accelerated drug release relative to the MP over the 3–24 h interval, while N4 produced a profile that remained statistically indistinguishable from the MP throughout.

Viability increased with dose, particularly in the N3 group, suggesting that the methylcellulose and GG create a microenvironment supportive of cell proliferation. The literature reports that polymers such as MC and GG provide controlled drug release while supporting fibroblast activity and wound healing.[76] Although cells and medium were used as controls, the high viability values indicate that the carrier polymer system is not cytotoxic and provides a cell-friendly environment. It has been previously reported that MC and GG facilitate cell migration and proliferation by maintaining moisture balance at the wound surface.[77] The controlled release of NDF allows for local treatment while reducing the risk of systemic toxicity. Such topical systems offer benefits for both effective drug delivery and cell viability, particularly in infected or chronic wounds.[78]

The definitions of QbD and its elements are given in ICH Q8 (R2).[19] In our study, the effect of material properties on CQA was investigated.[19-21] Two different concentrations of MC (0.3% and 0.7%) and GG (0.1% and 0.3%) were used to prepare gels within the QbD framework. The adjusted $R^2$ ($R^2$ adj), regression coefficient ($R^2$), and predicted $R^2$ ($R^2$ pred) values were calculated from the program. The interaction between output and input variables can be assessed using *p*-values.[20] Based on the analysis results, $R^2$ is an estimate of the ratio of the input factors to the variance in the output response. The $R^2$ adj varies with the number of terms in the analysis. The $R^2$ pred indicates how well the analysis predicts the output responses. The $R^2$ pred and the $R^2$ adj are always less than $R^2$.[79] $R^2$ values for gelation temperature, viscosity, springiness, cohesiveness, resilience, firmness, stickiness, work of adhesion, work of shear, and release at 6 hours are greater than 70%, indicating that the model captures more variation in the results and is reliable.[80] A regression model is considered a good fit when $p < 0.05$.[79] The *p*-value for the firmness parameter for MC is <0.05. Therefore, MC is identified as an influential factor for this parameter. Consequently, the effects of the CMAs can be assessed using the QbD concept.

*Study limitations*

The present study focused on the development and characterization of NDF containing topical *in situ* gels. However, microbiological studies were not performed to evaluate the efficacy of the developed formulation against acne and superficial skin infections. Further investigations are therefore needed to assess its antimicrobial activity and determine its potential as an alternative to conventional creams used to treat these conditions.

## CONCLUSION

Our study evaluated the potential of *in situ* gels containing NDF as topical drug carriers. It was concluded that NDF *in situ* gels could be prepared successfully by hot dissolution of MC and GG followed by cold dissolution of poloxamers. The prepared formulations were investigated and evaluated using QbD. FTIR studies revealed compatibility between the excipients and the drug. The drug content, viscosity, and pH of all formulations were demonstrated to be satisfactory. Formulations with appropriate gelation temperatures (32 °C–35 °C) are N1, N2, and N3. The two formulations with the highest spreading parameters and redeformation capacity are N3 and N4, which both have high MC ratios (0.7%). Their release profiles were similar. Cytotoxic effects were assessed using MTT assays, and a dose-dependent increase in viability was observed, particularly in the N3 formulation. This study may open new avenues for the topical application of NDF-loaded *in situ* gels. It may serve as a superior alternative to traditional creams for acne and dermal infections. Furthermore, the impact of critical materials in the formulation on the results was evaluated using QbD, which has been shown to avoid unnecessary studies that waste time and money in industry.

*Ethics*

**Ethics Committee Approval:** Ethics committee approval was not required for this study because the study did not involve human participants or animals.

**Informed Consent:** Informed consent was not required for this study because the study did not involve human participants or animals.

**Acknowledgements**

The authors would like to thank Berko Pharmaceutical Company (İstanbul, Türkiye) and Santa Farma Pharmaceutical Company (İstanbul, Türkiye) for kindly providing nadifloxacin and BASF (Türkiye) for kindly getting poloxomers.

*Footnotes*

*Authorship Contributions*

Surgical and Medical Practices: E.Ö.B., B.İ., N.Ü.O., Concept: E.Ö.B., N.Ü.O., Design: E.Ö.B., N.Ü.O.,

Data Collection or Processing: E.Ö.B., B.İ., N.Ü.O., Analysis or Interpretation: E.Ö.B., B.İ., A.B.Ö., N.Ü.O., Literature Search: E.Ö.B., B.İ., A.B.Ö., N.Ü.O., Writing: E.Ö.B., B.İ., A.B.Ö., N.Ü.O.

**Conflict of Interest:** The authors declare no conflicts of interest.

**Financial Disclosure:** The authors declared that this study received no financial support.

## REFERENCES

1. Gilaberte Y, Prieto Torres L, Pastushenko I, Juarranz Á. Anatomy and function of the skin. Nanoscience in Dermatology, Elsevier. 2016. p.1-14.
2. Franco AC, Aveleira C, Cavadas C. Skin senescence: mechanisms and impact on whole-body aging. Trends Mol Med. 2022;28:97-109.
3. Hay R, Bendeck SE, Chen S, Estrada R, Haddix A, McLeod T, et al. Skin Diseases. In: Jamison D, Breman J, and Measham A, editors. Disease Control Priorities in Developing Countries, Washington (DC): Oxford University Press; 2006, p.1091-100.
4. Condrò G, Guerini M, Castello M, Perugini P. Acne vulgaris, atopic dermatitis and rosacea: the role of the skin microbiota-a review. Biomedicines. 2022;10:2523.
5. Vasam M, Korutla S, Bohara RA. Acne vulgaris: a review of the pathophysiology, treatment, and recent nanotechnology based advances. Biochem Biophys Rep. 2023;36:101578.
6. Layton AM, Ravenscroft J. Adolescent acne vulgaris: current and emerging treatments. Lancet Child Adolesc Health. 2023;7:136-144.
7. Muchhala S, Sarkar R, Lahiri K, Kharkar RD, Rathod R. Management of skin and soft-tissue infections and acne with topical nadifloxacin: a comprehensive review. Int J Res Dermatology. 2022;8:551-563.
8. Patil S, Dandagi PM, Kazi T, Hulyalkar S, Biradar P, Kumbar V. A DoE-based development and characterization of nadifloxacin-loaded transethosomal gel for the treatment of acne vulgaris. Futur J Pharm Sci. 2024;10:1-19.
9. Rençber S, Özcan Bülbül E, Üstündağ N, Senyiğit Z. Preparation and detailed characterization of fusidic acid loaded in situ gel formulations for ophthalmic application. J Res Pharm. 2025;25:1-12.
10. Garg A, Agrawal R, Singh Chauhan C, Deshmukh R. In-situ gel: a smart carrier for drug delivery. Int J Pharm. 2024;652:123819.

11. Vigani B, Rossi S, Sandri G, Bonferoni MC, Caramella CM, Ferrari F. Recent advances in the development of in situ gelling drug delivery systems for non-parenteral administration routes. Pharmaceutics. 2020;12:859.
12. Üstündağ Okur N, Yozgatlı V, Şenyiğit Z. Formulation and detailed characterization of voriconazole loaded in situ gels for ocular application. Ankara Ecz Fak Derg. 2020;44:33-49.
13. Ahmed TA, Alharby YA, El-Helw AR, Hosny KM, El-Say KM. Depot injectable atorvastatin biodegradable in situ gel: development, optimization, in vitro, and in vivo evaluation. Drug Des Devel Ther. 2016;10:405-415.
14. Rençber S, Karavana SY. Formulation and optimization of gellan gum-poloxamer based dexamethasone mucoadhesive in situ gel. J Res Pharm. 2025;24:529-538.
15. Baloglu E, Karavana SY, Senyigit ZA, Hilmioglu-Polat S, Metin DY, Zekioglu O, Guneri T, Jones DS. In-situ gel formulations of econazole nitrate: preparation and in-vitro and in-vivo evaluation. J Pharm Pharmacol. 2011;63:1274-1282.
16. Mahmood H, Khan IU, Asif M, Khan RU, Asghar S, Khalid I, Khalid SH, Irfan M, Rehman F, Shahzad Y, Yousaf AM, Younus A, Niazi ZR, Asim M. In vitro and in vivo evaluation of gellan gum hydrogel films: assessing the co impact of therapeutic oils and ofloxacin on wound healing. Int J Biol Macromol. 2021;166:483-495.
17. Feketshane Z, Alven S, Aderibigbe BA. Gellan gum in wound dressing scaffolds. Polymers (Basel). 2022;14:4098.
18. ICH Q8(R2). ICH Harmonised Tripartite Guideline Pharmaceutical Development Q8(R2), 2009.
19. Özcan Bülbül E, Mesut B, Cevher E, Öztaş E, Özsoy Y. Product transfer from lab-scale to pilot-scale of quetiapine fumarate orodispersible films using quality by design approach. J Drug Deliv Sci Technol. 2019;54:101358.
20. Özcan Bülbül E, Üstündağ Okur N, Mısırlı D, Cevher E, Tsanaktsis V, Bingöl Özakpınar Ö, Siafaka PI. Applying quality by design approach for the determination of potent paclitaxel loaded poly(lactic acid) based implants for localized tumor drug delivery. International Journal of Polymeric Materials and Polymeric Biomaterials. 2023;72:968-983.
21. Mohseni-Motlagh SF, Dolatabadi R, Baniassadi M, Baghani M. Application of the quality by design concept (QbD) in the development of hydrogel-based drug delivery systems. Polymers (Basel). 2023;15:4407.
22. Kis N, Kovács A, Budai-Sz□cs M, Gácsi A, Csányi E, Csóka I, Berkó S. Investigation of silicone-containing semisolid in situ film-forming systems using QbD tools. Pharmaceutics. 2019;11:660.
23. Özcan Bülbül E, Hussein HA, Yeğen G, Okur ME, Üstündağ Okur N, Aksu NB. Preparation and *in vitro-in vivo* evaluation of QbD based acemetacin loaded transdermal patch formulations for rheumatic diseases. Pharm Dev Technol. 2022;27:1016-1026.
24. Kovács A, Kis N, Budai-Sz□cs M, Gácsi A, Csányi E, Csóka I, Berkó S. QbD-based investigation of dermal semisolid in situ film-forming systems for local anaesthesia. Drug Des Devel Ther. 2020;14:5059-5076.
25. Kumar S, Haglund BO, Himmelstein KJ. In situ-forming gels for ophthalmic drug delivery. J Ocul Pharmacol. 1994;10:47-56.
26. Schmolka IR. Artificial skin. I. Preparation and properties of pluronic F-127 gels for treatment of burns. J Biomed Mater Res. 1972;6:571-582.
27. Schmolka IR. Physical basis for poloxamer interactions. Ann N Y Acad Sci. 1994;720:92-97.
28. Fumoto E, Sato S, Kawamata Y, Koyama Y, Yoshikawa T, Nakasaka Y, Tago T, Masuda T. Determination of carbonyl functional groups in lignin-derived fraction using infrared spectroscopy. Fuel. 2022;318:123530.
29. Kumar GP, Phani AR, Prasad RG, Sanganal JS, Manali N, Gupta R, Rashmi N, Prabhakara GS, Salins CP, Sandeep K, Raju DB. Polyvinylpyrrolidone oral films of enrofloxacin: film characterization and drug release. Int J Pharm. 2014;471:146-152.
30. Özcan-Bülbül E, Kalender Y, Bal-Öztürk A, Üstündağ-Okur N. Preparation and in vitro evaluation of montelukast sodium-loaded 3D printed orodispersible films for the treatment of asthma. AAPS PharmSciTech. 2024;25:218.
31. Aksu NB, Yozgatlı V, Okur ME, Ayla Ş, Yoltaş A, Üstündağ Okur N. Preparation and evaluation of QbD based fusidic acid loaded in situ gel formulations for burn wound treatment. J Drug Deliv Sci Technol. 2019;52:110-121.
32. Üstündağ Okur N, Yozgatlı V, Okur ME, Yoltaş A, Siafaka PI. Improving therapeutic efficacy of voriconazole against fungal keratitis: thermo-sensitive in situ gels as ophthalmic drug carriers. J Drug Deliv Sci Technol. 2019;49:323-333.
33. Okur NÜ, Yozgatli V, Okur ME. In vitro-in vivo evaluation of tetrahydrozoline-loaded ocular in situ gels on rabbits for allergic conjunctivitis management. Drug Dev Res. 2020;81:716-727.
34. Üstündağ Okur N, Yoltaş A, Yozgatli V. Development and characterization of voriconazole loaded in situ gel formulations for ophthalmic application. Turkish J Pharm Sci. 2016;13:311-317.
35. Brookfield Digital Viscometer Operating Instructions. Brookf Ametek Instrum Spec Control Div. n.d.:1-49.
36. Çağlar EŞ, Karaotmarlı Güven G, Üstündağ Okur N. Preparation and characterization of carbopol based hydrogels containing dexpanthenol. J Fac Pharm Ankara. 2023;47:770-783.
37. Kalantre UL, Pishwikar SA. Development and validation of multiwavelength method for simultaneous estimation of nadifloxacin and ibuprofen in formulated hydrogel. Int J PharmTech Res. 2012;4:1575-1580.
38. Kulkarni AA, Nanda RK, Ranjane Meenal N, Ranje PN. Spectrophotometric estimation of nadifloxacin in pharmaceutical dosage form. Res J Pharm Tech. 2010;3:429-431.
39. Parihar S, Dubey N, Choudhary B, Nema S. Formulation and characterization of nadifloxacin loaded microsponge for the tretment of acne vulgaris. Int J Pharm Sci. 2024;2:497-513.
40. Karaca ÖG, Moran B, Türk M, Bal-Öztürk A, İzbudak B, Aydin YA, Utkan G, Alemdar N. The comparison of contribution of GO and rGO produced by green synthesis to the properties of CMC-based wound dressing material. Int J Biol Macromol. 2024;271:132521.
41. Destruel PL, Zeng N, Maury M, Mignet N, Boudy V. In vitro and in vivo evaluation of in situ gelling systems for sustained topical ophthalmic delivery: state of the art and beyond. Drug Discov Today. 2017;22:638-651.
42. Okur ME, Ayla Ş, Batur Ş, Yoltaş A, Genç E, Pertek S, Okur NU. Evaluation of in situ gel containing pycnogenol for cutaneous wound healing. Medeni Med J. 2019;34:67-75.
43. Dixit R, Verma A, Singh UP, Soni S, Mishra AK, Bansal AK, Pandit JK. Preparation and characterization of gellan-chitosan polyelectrolyte complex beads. Lat Am J Pharm. 2011;30:1186-1195.

44. Nadour M, Boukraa F, Ouradi A, Benaboura A. Effects of methylcellulose on the properties and morphology of polysulfone membranes prepared by phase inversion. Mater Res. 2017;20.339-348.
45. Brahmaiah B, Desu PK, Nama S, Khalilullah S, Babu SS. Formulation and evaluation of extended release mucoadhesive microspheres of simvastatin. Int J Pharm Biomed Res. 2013;4:57-64.
46. M A Fathalla Z, Vangala A, Longman M, Khaled KA, Hussein AK, El-Garhy OH, Alany RG. Poloxamer-based thermoresponsive ketorolac tromethamine in situ gel preparations: Design, characterisation, toxicity and transcorneal permeation studies. Eur J Pharm Biopharm. 2017;114:119-134.
47. Pervaiz A, Saeed MA, Anwar M, Mansoor U, Shabbir U, Khalid M. Preparation and characterization of self emulsifying solid dispersions of mebendazole to improve solubility. Int J Pharm Integr Heal Sci. 2023;4:2-21.
48. Hutchins M, Bovill RA, Stephens PJ, Brazier JA, Osborn HMI. Glycosides of nadifloxacin-synthesis and antibacterial activities against methicillin-resistant *Staphylococcus aureus*. Molecules. 2022;27:1504.
49. Güven UM, Yakut Y, Çakır N, Demirci Kayıran S. Thermosensitive in situ gel formulation and characterization studies of Sambucus ebulus L. extract. iujp. 2023;53:30-38.
50. Panther DJ, Jacob SE. The importance of acidification in atopic eczema: an underexplored avenue for treatment. J Clin Med. 2015;4:970-978.
51. Basha M, AbouSamra MM, Awad GA, Mansy SS. A potential antibacterial wound dressing of cefadroxil chitosan nanoparticles in situ gel: fabrication, in vitro optimization and in vivo evaluation. Int J Pharm. 2018;544:129-140.
52. Plasencia I, Norlén L, Bagatolli LA. Direct visualization of lipid domains in human skin stratum corneum's lipid membranes: effect of pH and temperature. Biophys J. 2007;93:3142-3155.
53. Sharpe JR, Booth S, Jubin K, Jordan NR, Lawrence-Watt DJ, Dheansa BS. Progression of wound pH during the course of healing in burns. J Burn Care Res. 2013;34:e201-e208.
54. Siqueira C, Picone F, Lopes Cunha R. Influence of pH on formation and properties of gellan gels. Carbohydr Polym. 2011;84:662-668.
55. Bhowmik M, Das S, Sinha J, Bag S, Chattopadhyay D, Ghosh LK. Methyl cellulose based sustagned release thermosensitive in situ fast gelling ocular delivery of ketorolac tromethamine. Asian J Chem. 2010;22:2147-2154.
56. Mutlu Sonat G, Çağlar EŞ, Güreşçi D, Aydın A, Sipahi H, Üstündağ Okur N. Novel vanillic acid-loaded *in situ* gels: development, characterization, *in vitro* evaluation for enhanced wound healing and skin irritation test. Pharm Dev Technol. 2025;30:905-922.
57. Azad MS. Influence of polymer concentration on the viscous and (linear and non-linear) viscoelastic properties of hydrolyzed polyacrylamide systems in bulk shear field and porous media. Polymers (Basel). 2024;16:2617.
58. Rahman MN, Qader OA, Sukmasari S, Ismail AF, Doolaanea AA. Rheological characterization of different gelling polymers for dental gel formulation. J Pharm Sci Res. 2017;9:2633-2640.
59. Karakucuk A, Tort S, Han S, Oktay AN, Celebi N. Etodolac nanosuspension based gel for enhanced dermal delivery: *in vitro* and *in vivo* evaluation. J Microencapsul. 2021;38:218-232.
60. Chandra MV, Shamasundar BA. Texture profile analysis and functional properties of gelatin from the skin of three species of fresh water fish. Int J Food Prop. 2015;18:572-584.
61. Wang J, Zhao X, Zhou C, Wang C, Zheng Y, Ye K, Li C, Zhou G. Effects of gellan gum and inulin on mixed-gel properties and molecular structure of gelatin. Food Sci Nutr. 2021;9:1336-1346.
62. Khorshidi S, Khoobbakht F, Mirmoghtadaie L, Hosseini SM. Characterization of gellan gum-chitosan based hydrogel to evaluate as a potential gelatin substitute. Food Hydrocoll. 2023;145:109038.
63. Aday MS, Caner C, Yuceer YK. Instrumental and sensory measurements of ezine cheese texture. Akademik Gıda. 2010;8:6-46.
64. Karaca MA, Khalili V, Ege D. Highly flexible methyl cellulose/gelatin hydrogels for potential cartilage tissue engineering applications. Biopolymers. 2025;116:e23641.
65. Xu L, Liu S, Zhu L, Liu Y, Li N, Shi X, Jiao T, Qin Z. Hydroxypropyl methyl cellulose reinforced conducting polymer hydrogels with ultra-stretchability and low hysteresis as highly sensitive strain sensors for wearable health monitoring. Int J Biol Macromol. 2023;236:123956.
66. Ramburrun P, Kumar P, Choonara YE, du Toit LC, Pillay V. Design and characterization of neurodurable gellan-xanthan pH-responsive hydrogels for controlled drug delivery. Expert Opin Drug Deliv. 2017;14:291-306.
67. Polat Y, Aydın HH, Rençber S. Linezolid loaded nanoparticle for topical administration of diabetic foot treatment: formulation, in vitro and ex vivo characterization. Fabad J Pharm Sci. 2024;49:299-316.
68. Siafaka PI, Çağlar EŞ, Sipahi H, Charehsaz M, Aydın A, Üstündağ Okur N. Ocular microemulsion of brinzolamide: Formulation, physicochemical characterization, and in vitro irritation studies based on EpiOcularTM eye irritation assay. Pharmaceutical Development and Technology. 2021;26:765-778.
69. Ergin AD, İnal Ö, Barakat A. In vitro and ex vivo assessments of surfactant-free topical curcumin emulgel. J Res Pharm. 2025;27:544-556.
70. D'sa M, Bhogale D, Sawant S, Thakur P, Shukla S, Mahadik S, Patel N, Ukhade R, Shaikh J, Hatvate N. Spectrometric method for simultaneous quantification of nadifloxacin and salicylic acid in a novel topical dosage form. Green Anal Chem. 2024;11:100166.
71. Zanwar A, Sen DB, Vora AA, Maheshwari RA, Sen AK, Seth AK. Two spectrophotometric methods for the simultaneous analysis of nadifloxacin and mometasone furoate in cream. Int J Pharm Res. 2020;12:1594-1600.
72. Abbasnezhad N, Zirak N, Champmartin S, Shirinbayan M, Bakir F. An overview of in vitro drug release methods for drug-eluting stents. Polymers (Basel). 2022;14:2751.
73. Lusina Kregar M, Krtali I, Šagud I. An overview of in vitro release methods for long-acting injectable products based on PLGA. Methods and Protocols. 2026;9:87.
74. Selleck Chemicals. Nadifloxacin. Accessed March 13, 2025. https://www.selleckchem.com/products/nadifloxacin.html
75. ChemicalBook. Nadifloxacin (CAS No. 124858-35-1). Accessed March 13, 2025. https://www.chemicalbook.com/ChemicalProductProperty_EN_CB3301560.htm
76. Mendes AI, Fraga AG, Peixoto MJ, Aroso I, Longatto-Filho A, Marques AP, Pedrosa J. Gellan gum spongy-like hydrogel-based dual antibiotic therapy for infected diabetic wounds. Bioeng Transl Med. 2023;8:e10504.
77. Ismail NA, Amin KAM, Majid FAA, Razali MH. Gellan gum incorporating titanium dioxide nanoparticles biofilm as wound dressing: physicochemical, mechanical, antibacterial properties and wound healing studies. Mater Sci Eng C Mater Biol Appl. 2019;103:109770.

78. Kumar A, Agarwal SP, Ahuja A, Ali J, Choudhry R, Baboota S. Preparation, characterization, and in vitro antimicrobial assessment of nanocarrier based formulation of nadifloxacin for acne treatment. Pharmazie. 2011;66:111-114.

79. Fukuda IM, Pinto CFF, Moreira CDS, Saviano AM, Lourenço FR. Design of experiments (DoE) applied to pharmaceutical and analytical quality by design (QbD). Brazilian J Pharm Sci. 2018;54:1-16.

80. Amasya G, Badilli U, Aksu B, Tarimci N. Quality by design case study 1: design of 5-fluorouracil loaded lipid nanoparticles by the W/O/W double emulsion - solvent evaporation method. Eur J Pharm Sci. 2016;84:92-102.

Turk J Pharm Sci 2026;23(3):165-173
**DOI:** 10.4274/tjps.galenos.2026.23796

ORIGINAL ARTICLE

# Furanocoumarins from the Roots of *Cachrys cristata* DC.: Isolation, Anticholinesterase Activity, and Molecular Docking Studies

**Fadıl Kaan KURAN[1]*, Ceren KUŞ[1], Zehra Ezel DOLAP[2], Şule Nur KARAVUŞ KANTEMÜR[3], Kübra Şeyma ÖZTÜRK[1], Gülsüm ALTIPARMAK ÜLBEGİ[4], Mahmut MİSKİ[1]**

[1]İstanbul University Faculty of Pharmacy, Department of Pharmacognosy, İstanbul, Türkiye
[2]İstanbul University, Health Sciences Institute, Department of Pharmacognosy, İstanbul, Türkiye
[3]Istanbul Medipol University Faculty of Pharmacy, Department of Pharmacognosy, İstanbul, Türkiye
[4]İstanbul University Faculty of Pharmacy, Department of Biochemistry, İstanbul, Türkiye

## ABSTRACT

**Objectives:** The present study aimed to investigate the phytochemical constituents of *Cachrys cristata* roots, to evaluate the cholinesterase-inhibitory activity of the isolated compounds, and to assess their possible binding interactions with acetylcholinesterase and butyrylcholinesterase through molecular docking studies.

**Materials and Methods:** The roots were extracted with dichloromethane by Soxhlet extraction, and a coumarin-rich fraction was obtained by precipitation from the crude extract. Chromatographic purification of this fraction using Sephadex LH-20, reversed-phase $C_{18}$ column chromatography, and preparative thin-layer chromatography afforded ten known furanocoumarins: oxypeucedanin hydrate, oxypeucedanin, bergapten, xanthotoxin, 3'-hydroxyprantschimgin, oxypeucedanin ethanolate (oxypeucedanin hydrate-3"-ethyl ether), pabularinone, marmesin, pabulenol and saxalin. The structures of the isolated compounds were identified by (1)H NMR spectroscopy and comparison with literature data. Selected isolated compounds were evaluated for inhibitory activity against acetylcholinesterase and butyrylcholinesterase, and the results were further assessed by molecular docking.

**Results:** The tested furanocoumarins showed weak cholinesterase inhibitory activity. Bergapten was the most active compound against acetylcholinesterase, with an $IC_{50}$ value of 92.15 µM. For butyrylcholinesterase, bergapten, and pabulenol exhibited measurable inhibition, with $IC_{50}$ values of 150.25 µM and 157.28 µM, respectively.

**Conclusion:** This study contributes to the phytochemical characterization of *Cachrys cristata* roots and provides the first phytochemical evidence for the occurrence of furanocoumarin-type constituents in the roots of this species. The isolated compounds exhibited weak cholinesterase inhibitory activity, suggesting that the furanocoumarin scaffold may serve as a preliminary framework for further structural optimization rather than as a source of potent cholinesterase inhibitors.

**Keywords:** *Cachrys cristata*, coumarins, molecular docking, cholinesterase inhibition

## INTRODUCTION

The family Apiaceae (Umbelliferae) comprises 456 accepted genera and approximately 3,800 species and includes medicinal and aromatic plants widely used in traditional medicine.[1,2] Species in this family are rich in secondary metabolites, such as coumarins, terpenoids, flavonoids, steroids, and polyacetylenes. Owing to their diverse secondary metabolite profiles, these species exhibit various biological activities,

***Correspondence:** kaankuran@istanbul.edu.tr, **ORCID-ID:** orcid.org/0000-0003-2793-0577

**Received:** 22.09.2026 **Accepted:** 14.10.2026 **Publication Date:** 27.10.2026

**Cite this article as:** Kuran KF, Kuş C, Dolap ZE, Karavuş Kantemür ŞN, Öztürk KŞ, Altıparmak Ülbegi G, Miski M. Furanocoumarins from the roots of *Cachrys cristata* DC.: isolation, anticholinesterase activity, and molecular docking studies. Turk J Pharm Sci. 2026;23(3):165-173

Copyright© 2026 The Author(s). Published by Galenos Publishing House on behalf of Turkish Pharmacists' Association.
This is an open access article under the Creative Commons Attribution-NonCommercial-NoDerivatives 4.0 (CC BY-NC-ND) International License.

including antimicrobial, cytotoxic, anti-inflammatory, and analgesic effects, and are therefore regarded as potential sources of drug candidates.[3]

*Cachrys L.* is a genus in the family Apiaceae, comprising seven accepted species and is distributed in Europe, North Africa, Western Asia, and adjacent regions.[1] There are differing opinions in the literature regarding the taxonomic circumscription of the genus. According to Tutin (1968), *Cachrys* also includes *Prangos* Lindl. and *Hippomarathrum* Link; however, Boissier classified these taxa as three distinct genera in 1872.[4] In Türkiye, the genus is commonly known by vernacular names such as "Çaşır", "Tarhana Otu", "Çarşambaotu", and is represented by two species: *Cachrys* cristata and *Cachrys* crassiloba.[4,5] Although data on the traditional medicinal uses of *Cachrys* species remain limited, *Cachrys libanotis* L. has been reported for the treatment of rheumatism, whereas plant material historically reported *as Cachrys* alpina M. Bieb. has been used as an aphrodisiac.[6,7]

Various coumarin derivatives, especially furanocoumarins, have been reported from *Cachrys* species. Coumarins such as isoimperatorin, imperatorin, bergapten, xanthotoxin, isopimpinellin, prantschimgin, sprengelianin, ulopterol, and oxypeucedanin have been isolated from *Cachrys sicula*. Coumarin derivatives, including xanthotoxin, bergapten, isopimpinellin, psoralen, isooxypeucedanin, columbianetin, jatamansin, seselin, osthol, and suberosin, have also been detected in extracts and fractions obtained from *Cachrys sicula*, *Cachrys libanotis*, and *Cachrys pungens*.[8-10] In addition to these phytochemical studies, investigations of *Cachrys* species have generally focused on their essential oil compositions.[11-15]

Dementia is characterized by a decline in cognitive functions, including memory and thinking, which can interfere with everyday activities. Alzheimer's disease is the most common form of dementia.[16] Impaired cholinergic neurotransmission plays an important role in the pathophysiology of Alzheimer's disease. The inhibition of acetylcholinesterase (AChE) and butyrylcholinesterase (BChE), which helps maintain acetylcholine levels, is considered one of the main symptomatic approaches to support learning and memory functions.[17] To the best of our knowledge, no specific ethnobotanical record documents the use of *Cachrys cristata* for memory impairment, cognitive dysfunction, or neurodegenerative disorders. Therefore, the selection of cholinesterase inhibition as an endpoint in the present study was not based on a direct traditional claim for this species, but rather on the plant's phytochemical profile. Since the isolated constituents mainly belonged to the furanocoumarin class, and several coumarin/furanocoumarin derivatives, such as bergapten, xanthotoxin, and umbelliferone, have been reported to improve cognitive functions in experimental models through cholinergic, antioxidant, and anti-inflammatory mechanisms,[18,19] AChE and BChE inhibition assays were selected as a phytochemistry-driven bioactivity screening approach. These findings suggest that coumarins may be promising candidates for biological activity studies targeting neurodegenerative diseases.

Within this context, the present study evaluated the inhibitory effects of furanocoumarin-type compounds isolated from *Cachrys cristata* on AChE and BChE. The possible interactions of these compounds with the active sites of the enzymes were further investigated using molecular docking analyses.

## MATERIALS AND METHODS

### *Plant material*

The plant material was collected by Prof. Dr. Mahmut Miski and Ersan Pütün from the Alaşehir–Buldan road in Denizli Province, Türkiye, at an altitude of 1650 m on 9 June 1982. The plant was identified by Prof. Dr. Mine Koçyiğit Avcı as *Hippomarathrum cristatum* (DC.) Boiss. (syn. *Cachrys cristata* DC.). A voucher specimen prepared from the aerial parts of the plant was deposited in the Herbarium of the Faculty of Pharmacy, İstanbul University, under the accession number ISTE 48929.

### *General experimental procedures*

Hexane, dichloromethane, methanol (MeOH), ethyl acetate (EtOAc), acetonitrile (ACN), toluene, and sulfuric acid ($H_2SO_4$) were used for extraction, chromatographic separation, and thin-layer chromatographic analysis. DCM, EtOAc, and *p*-anisaldehyde were purchased from Sigma–Aldrich (St. Louis, MO, USA), while MeOH, ACN, toluene, and $H_2SO_4$ were purchased from Merck (Darmstadt, Germany). Sephadex LH-20 was purchased from GE Healthcare (Chicago, IL, USA). LiChroprep RP-18 (40–63 μm) was purchased from Merck and used for reversed-phase column chromatography. Silica gel 60 $F_{254}$ TLC plates (0.25 mm; Merck, Darmstadt, Germany) were used for analytical thin-layer chromatography, and Supelco silica gel 60 $F_{254}$ preparative TLC plates (0.5, 1, and 2 mm; Merck, Darmstadt, Germany) were used for preparative separations. TLC plates were visualized under UV light at 254 and 366 nm using a UV lamp (Camag, Muttenz, Switzerland). When necessary, the plates were sprayed with freshly prepared anisaldehyde–$H_2SO_4$ reagent, followed by heating. Chromatographic separations were carried out using Sephadex LH-20 column chromatography, reversed-phase $C_{18}$ column chromatography, and preparative thin-layer chromatography. Fractions showing similar TLC profiles were combined and further purified according to their chromatographic behavior. The structures of the isolated compounds were elucidated mainly by (1)H NMR spectroscopy. NMR spectra were recorded on a Bruker 500 MHz spectrometer using $CDCl_3$ as the solvent.

### *Extraction and isolation*

The roots used in the present study originated from the same collection as the voucher specimen. The root material was extracted shortly after collection in 1982, and the resulting extract was stored under deep-freeze conditions until the phytochemical investigation was performed.

The dried and coarsely powdered roots of *Cachrys cristata* DC. (280.0 g) were extracted with dichloromethane using a Soxhlet apparatus. The solvent was evaporated under reduced pressure to ca. 100 mL and kept refrigerated overnight. The resulting white crystalline precipitate was collected as a coumarin-rich fraction (4.0 g). This fraction (4.0 g) was initially

subjected to Sephadex LH-20 chromatography using a glass column measuring 50 cm in length and 5 cm in diameter. The column was eluted with a mixture of hexane–dichloromethane–MeOH (7:4:1, v/v/v) to obtain preliminary fractions. A total of 243 fractions were collected and monitored by TLC under UV light at 254 and 366 nm. Fractions showing similar TLC profiles were then combined and further purified according to their chromatographic behavior. Sephadex LH-20 fractions 223–242 directly afforded oxypeucedanin hydrate (58 mg). Sephadex LH-20 fractions 37–42 were further separated by reversed-phase $C_{18}$ column chromatography. Subfractions 21–22, obtained from this column, afforded oxypeucedanin (8.4 mg). Sephadex LH-20 fractions 43–50 were fractionated by reversed-phase $C_{18}$ column chromatography. Subfractions 27–32 afforded xanthotoxin (2.0 mg), while subfractions 34–43 yielded bergapten (3.8 mg). Subfractions 48–53 were further purified by preparative TLC using silica gel plates (0.5 mm thick) and toluene-dichloromethane-EtOAc-ACN (4:4:2:1, v/v/v/v) as the mobile phase, yielding oxypeucedanin ethanolate (2.2 mg) and pabularinone (0.8 mg). Sephadex LH-20 fractions 63-84 were further separated by reversed-phase $C_{18}$ column chromatography, and subfractions 39–45 afforded 3'-hydroxyprantschimgin (3.6 mg). Sephadex LH-20 fractions 85–105 were also separated by reversed-phase $C_{18}$ column chromatography. Subfractions 12–17 and 24–29 were purified by preparative TLC under the same conditions to yield marmesin (3.9 mg) and pabulenol (1.3 mg), respectively. Subfractions 30–38 were purified by preparative TLC using 1-mm silica gel plates and the same mobile phase to obtain saxalin (1.2 mg).

*Determination of cholinesterase inhibitory activities*

Compounds 1, 2, 3, 5, 7, and 9 were selected from the isolated compounds for cholinesterase inhibition assays based on the availability of sufficient material and acceptable purity following final purification, as assessed by TLC and (1)H NMR. The inhibitory activities against AChE (Sigma-Aldrich, Cat. No. C3389) and BChE (Sigma-Aldrich, Cat. No. C7512) were determined using the Ellman method,[20] with modifications based on Sevinçli et al. [21] The compounds and donepezil, used as the reference inhibitor, were dissolved in dimethyl sulfoxide (DMSO) and serially diluted to obtain final assay concentrations of 20, 40, 80, 120, and 160 μM for the isolated compounds; 1.2, 2.4, 4.8, and 9.6 μM for donepezil in the BChE assay; and 0.12, 0.24, 0.48, and 0.96 μM for donepezil in the AChE assay. Ten microliters of the isolated compound or donepezil solution was mixed with 220 μL of Ellman reagent (95.5 mM sodium phosphate buffer, pH 7.5, containing 955 μM ATChI or BTChI and 318 μM DTNB). For the control, an equal volume of DMSO was used in place of the inhibitor solution. Subsequently, 20 μL of AChE (0.4 U/mL) or BChE (0.3 U/mL) was added, and the absorbance was recorded at 412 nm at 1-min intervals for 10 min. The percentage inhibition was calculated using the following equation:

$$\text{Inhibition (\%)} = [1 - (\Delta A_\text{sample/min} / \Delta A_\text{control/min})] \times 100$$

where ΔA_sample/min and ΔA_control/min represent the rates of absorbance increase in the presence and absence of the inhibitor, respectively.

The cholinesterase inhibition assays were performed in three to four independent experiments, each with two to four technical replicates. $IC_{50}$ values were calculated by non-linear regression analysis using GraphPad Prism (version 11.0.2; San Diego, CA, USA). Inhibition percentages and $IC_{50}$ values are expressed as mean ± standard deviation.

*Molecular docking*

Molecular docking studies were performed using the Schrödinger software package (Schrödinger Release 2017-3, Schrödinger, LLC, New York, NY, USA). The crystal structures of human AChE in complex with donepezil (PDB ID: 4EY7)[22] and human BChE in complex with tacrine (PDB ID: 4BDS)[23] were retrieved from the Protein Data Bank and prepared using the Protein Preparation Wizard. Hydrogen atoms were added, bond orders were assigned, non-essential water molecules and heteroatoms were removed, and the structures were minimized using the OPLS3 force field.[24] The isolated furanocoumarins were prepared using LigPrep with default settings, including Epik-based ionization-state generation, and were minimized with the OPLS3 force field. Receptor grids were generated around the binding sites of the co-crystallized ligands: donepezil for AChE and tacrine for BChE. Docking calculations were performed using Glide SP with flexible ligand sampling.[25,26]

The docking protocols were validated by redocking the co-crystallized ligands into their respective active sites. Although electric eel AChE and equine serum BChE were used in *in vitro* enzyme inhibition assays, human cholinesterase crystal structures were selected for docking because they provide experimentally determined, ligand-bound models suitable for grid generation and redocking validation. In this context, the human BChE–tacrine complex 4BDS provides a ligand-bound model suitable for validating the docking protocol for BChE. A similar methodological approach was reported previously in a furanocoumarin-related cholinesterase study, in which electric eel AChE and horse serum BChE were used in enzymatic assays, and docking analyses were performed using a human BChE crystal structure.[27] Since the enzyme sources used in the *in vitro* assays and the docking models were not identical, the docking results were interpreted only as qualitative structural support for the possible binding poses and interaction patterns of the isolated furanocoumarins, rather than as species-specific quantitative predictions of inhibitory potency.

*Ethics approval and informed consent*

Ethics committee approval and informed consent were not required for this study, as it did not involve human participants or experimental animals.

## RESULTS

*Phytochemical results*

Ten furanocoumarin-type compounds were isolated from the coumarin-rich fraction of the dichloromethane extract obtained from the roots of *Cachrys cristata*. Their structures were identified by comparison of their (1)H NMR spectroscopic data with those reported in the literature as bergapten[28] (1) (3.8 mg),

xanthotoxin[28] (2) (2 mg), marmesin[29] (3) (3.9 mg), pabularinone[30] (4) (0.8 mg), pabulenol[31] (5) (1.3 mg), 3′-hydroxyprantschimgin[32] (6) (3.6 mg), oxypeucedanin[33] (7) (8.4 mg), oxypeucedanin ethanolate/oxypeucedanin hydrate-3″-ethyl ether[34] (8) (2.2 mg), oxypeucedanin hydrate[33] (9) (58 mg), and saxalin[34] (10) (1.2 mg). For compounds containing stereogenic centers, stereochemical assignments were made by comparison with reported data for the corresponding known compounds, and the measured optical rotation values were consistent with literature values. According to the available literature, furanocoumarins have not previously been reported from the roots of *Cachrys cristata*. The (1)H NMR spectra of the isolated compounds are provided in the Supplementary Figures S1-13. The molecular structures of the compounds are presented in Figure 1.

*Cholinesterase inhibitory activity*

The isolated compounds exhibited different inhibitory profiles against AChE and BChE (Table 1). Regarding AChE inhibition, bergapten (1) was the most active compound, with an $IC_{50}$ of 92.15 μM. Pabulenol (5) exhibited 31.71% inhibition at the highest tested concentration, 160 μM, whereas xanthotoxin (2) and marmesin (3) exhibited only limited activity. Oxypeucedanin (7) and oxypeucedanin hydrate (9) showed no significant AChE inhibitory activity at 160 μM.

For BChE, pabulenol (5) and bergapten (1) reached approximately 50% inhibition, displaying $IC_{50}$ values of 157.28 μM and 150.25 μM, respectively. The remaining compounds showed only weak BChE inhibitory activity and did not reach 50% inhibition within the tested concentration range. Although bergapten was the most active molecule against AChE and BChE, its inhibitory potency remained markedly lower than that of donepezil ($IC_{50}$ = 0.40 μM for AChE; 3.38 μM for BChE).

*Molecular docking results*

The AChE docking protocol was evaluated by redocking the co-crystallized ligand donepezil into the active site of the human AChE structure 4EY7. The redocked pose yielded an RMSD of 2.11 Å relative to the crystallographic pose, which is slightly above, but close to, the commonly used 2.0 Å threshold for docking validation. However, visual inspection of the superposed crystallographic and redocked poses showed that donepezil occupied the same active-site groove and largely preserved the overall orientation of the native ligand. The redocked pose also retained the principal interaction regions reported for the 4EY7 complex, particularly the aromatic region involving Trp86 and Trp286. Therefore, given the flexible and elongated structure of donepezil, the docking setup was acceptable for qualitative interpretation of the binding poses of the isolated furanocoumarins. The superposition of the crystallographic and redocked donepezil poses is provided in the Supplementary Figure S11. The 2D and 3D interaction diagrams of redocked donepezil are shown in Figure 2.

In the AChE docking analysis, the isolated furanocoumarins showed Glide SP scores ranging from -6.935 to -7.474 kcal/mol. Bergapten (1) exhibited the best docking score (-7.474 kcal/

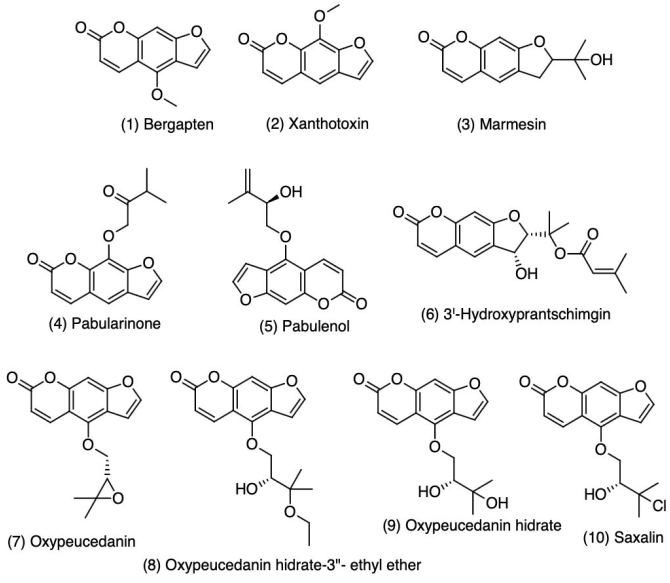



**Figure 1.** Structures of compounds isolated from *Cachrys cristata.*

**Table 1. AChE and BChE inhibitory activities of the isolated compounds.**

| | AChE | | BChE | |
|---|---|---|---|---|
| **Compound** | **Inhibition (%) at 160 μM** | **$IC_{50}$ (μM)** | **Inhibition (%) at 160 μM** | **$IC_{50}$ (μM)** |
| Oxypeucedanin | – | | 22.21 ± 2.47 | |
| Pabulenol | 31.71 ± 2.62 | | 50.61 ± 1.55 | 157.28 ± 9.68 |
| Bergapten | 65.87 ± 2.69 | 92.15 ± 1.73 | 53.28 ± 3.74 | 150.25 ± 6.63 |
| Xanthotoxin | 13.43 ± 7.94 | | 34.62 ± 8.07 | |
| Marmesin | 12.37 ± 7.98 | | 14.92 ± 6.74 | |
| Oxypeucedanin hydrate | – | | 20.65 ± 6.07 | |
| Donepezil | | 0.40 ± 0.03 | | 3.38 ± 0.45 |

Values are expressed as mean ± SD (n = 3). $IC_{50}$ values were not calculated for compounds showing less than 50% inhibition at 160 μM (the highest tested concentration). "–" indicates no significant inhibitory activity.
AChE, acetylcholinesterase; BChE, butyrylcholinesterase; SD, standard deviation.

mol), followed by marmesin (3), which had a score of -7.381 kcal/mol. The 2D and 3D docking poses of bergapten are shown in Figure 3.

The BChE docking protocol was evaluated by redocking the co-crystallized ligand tacrine into the active site of the human BChE structure 4BDS. The redocked pose showed an RMSD value of 1.44 Å compared with the crystallographic pose. The superposition of the crystallographic and redocked poses of tacrine is provided in the Supplementary Figure S12. The 2D and 3D interaction diagrams of redocked tacrine are shown in Figure 4.

In the BChE docking analysis, the isolated furanocoumarins showed Glide SP scores ranging from -6.165 to -7.471 kcal/mol. Pabulenol (5) exhibited the best docking score (-7.471 kcal/mol), followed by oxypeucedanin hydrate (9) (-7.387 kcal/mol), bergapten (1) (-6.869 kcal/mol), oxypeucedanin (7) (-6.728 kcal/mol), and xanthotoxin (2) (-6.630 kcal/mol). The 2D and 3D docking poses of pabulenol, the compound with the best BChE docking score, are shown in Figure 5.

The Glide SP docking scores of the investigated compounds and reference ligands are summarized in Table 2.

## DISCUSSION

The phytochemical investigation of the roots of *Cachrys cristata* led to the isolation of ten furanocoumarin-type compounds from the coumarin-rich fraction of the dichloromethane extract. The

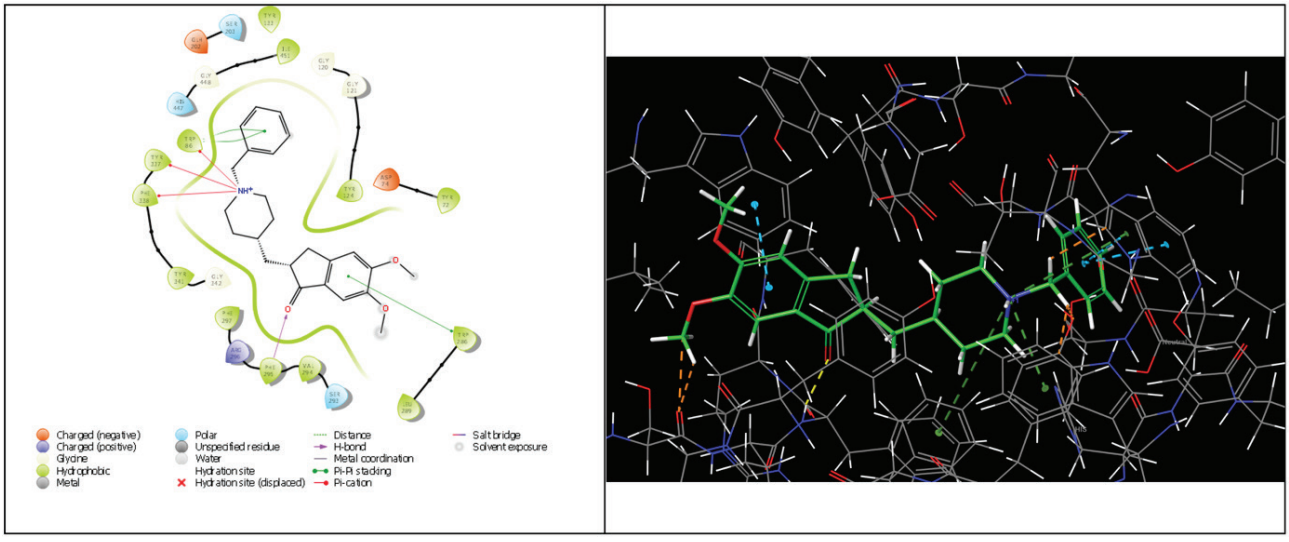



**Figure 2.** 2D and 3D redocked pose of donepezil in the active site of AChE (PDB ID: 4EY7).
AChE, acetylcholinesterase.

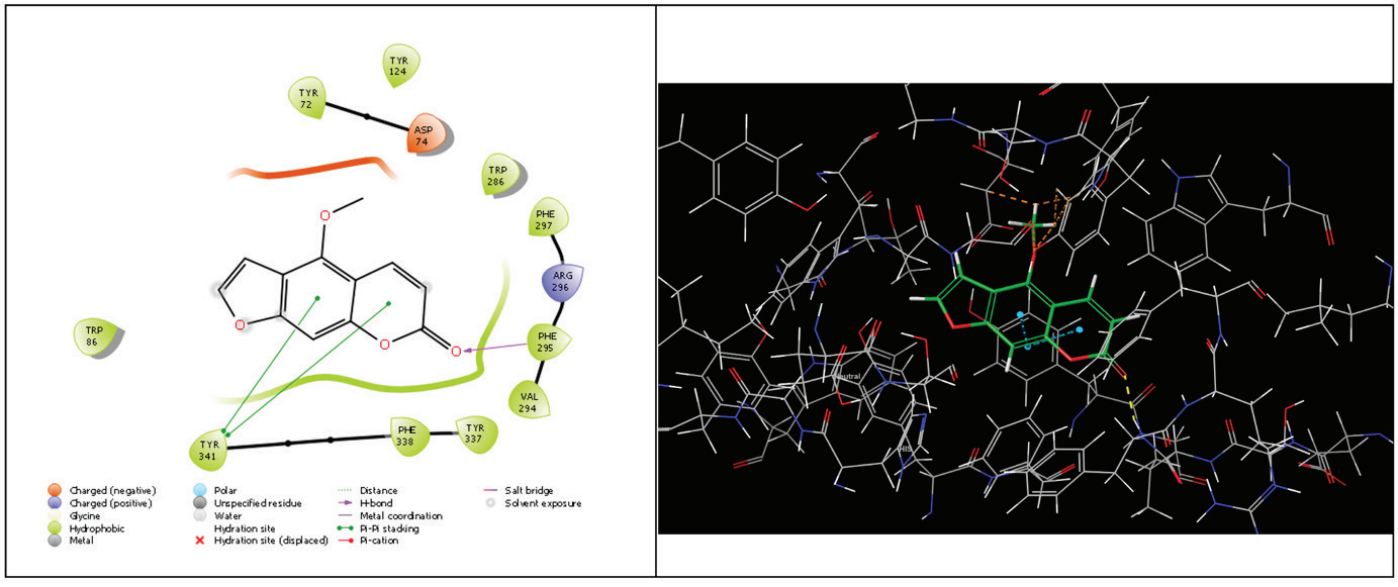



**Figure 3.** 2D and 3D docking pose of bergapten in the active site of AChE (PDB ID: 4EY7).
AChE, acetylcholinesterase.

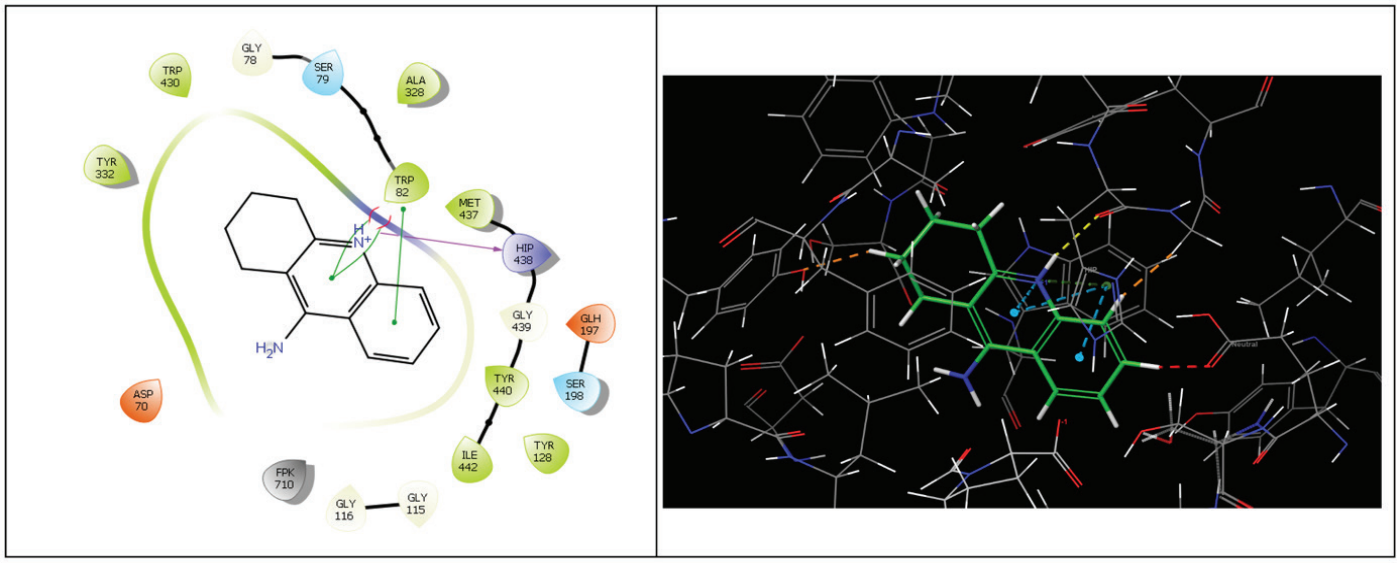



**Figure 4.** 2D and 3D redocked pose of tacrine in the active site of BChE (PDB ID: 4BDS).
BChE, butyrylcholinesterase.

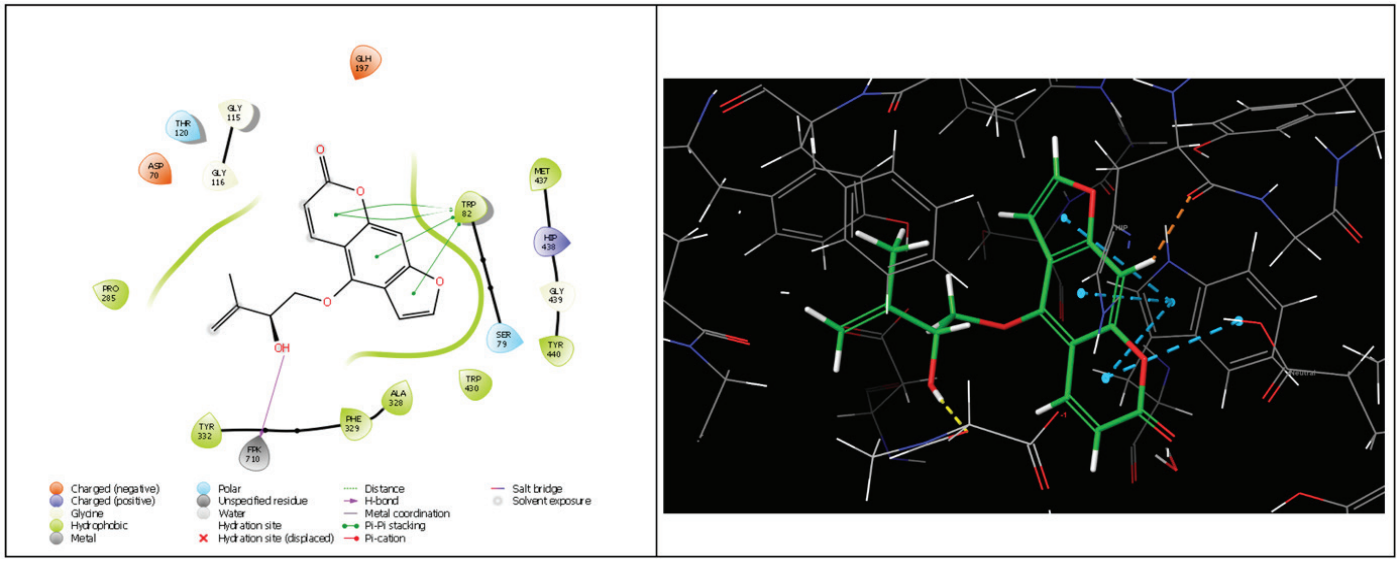



**Figure 5.** 2D and 3D docking pose of pabulenol in the active site of BChE (PDB ID: 4BDS)
BChE, butyrylcholinesterase.

**Table 2. Glide SP docking scores of the investigated furanocoumarins and reference ligands against AChE and BChE.**

| Compound | AChE Glide SP docking score | BChE Glide SP docking score |
|---|---|---|
| Bergapten (1) | -7.474 | -6.869 |
| Xanthotoxin (2) | -6.995 | -6.630 |
| Marmesin (3) | -7.381 | -6.165 |
| Pabulenol (5) | -7.183 | -7.471 |
| Oxypeucedanin (7) | -6.935 | -6.728 |
| Oxypeucedanin hydrate (9) | -7.166 | -7.387 |
| Donepezil | -12.798 | - |
| Tacrine | - | -7.793 |

Values are reported as Glide SP docking scores.
AChE, acetylcholinesterase; BChE, butyrylcholinesterase.

predominance of furanocoumarins in this fraction is consistent with the known chemical profile of Apiaceae taxa, particularly in genera that are rich in linear and angular furanocoumarin derivatives. This finding is noteworthy from a phytochemical perspective, since, according to the available literature, furanocoumarins have not previously been reported from the *roots of Cachrys cristata*.

In the cholinesterase inhibition assays, the isolated compounds generally showed weak inhibitory activity compared with donepezil. Among the tested compounds, bergapten (1) was the most notable AChE inhibitor, with an $IC_{50}$ value of 92.15 μM. In contrast, pabulenol (5) and bergapten (1) showed measurable but weak BChE inhibition, with $IC_{50}$ values of 157.28 μM and 150.25 μM, respectively. These findings suggest that the furanocoumarin scaffold alone is insufficient to confer strong cholinesterase inhibition, but may provide simple, natural framework for further structural optimization.

However, the estimated BChE $IC_{50}$ values for pabulenol and bergapten were close to the upper limit of the investigated concentration range (160 μM). Given that the inhibition percentages at the highest tested concentration were only slightly above 50%, these estimates should be interpreted with caution. The absence of measurements above 160 μM may introduce uncertainty into $IC_{50}$ estimates, and further evaluation over an extended concentration range would improve their precision.

Previous studies on Apiaceae furanocoumarins have reported variable cholinesterase inhibitory profiles depending on compound structure, enzyme source, and assay conditions. In *Angelica dahurica,* isoimperatorin, imperatorin, and oxypeucedanin were reported to be AChE-inhibitory constituents with $IC_{50}$ values of 74.6, 63.7, and 89.1 μM, respectively, whereas the reference inhibitor, berberine, showed an $IC_{50}$ value of 2.9 μM.[35] In another study on *Angelica dahurica* roots, oxypeucedanin and oxypeucedanin hydrate showed measurable but weaker cholinesterase inhibition than eserine, with $IC_{50}$ values of 69.3 and 136.4 μM against AChE and 65.6 and 71.2 μM against BChE, respectively.[36] Studies on *Angelica officinalis and Angelica archangelica* further indicated that some furanocoumarins may inhibit BChE more strongly than AChE; however, simple furanocoumarins such as bergapten, xanthotoxin, and isoimperatorin may be weak inhibitors or inactive depending on the assay system.[37,38] Therefore, the weak cholinesterase-inhibitory activity observed in the present study is generally consistent with previous reports and supports the view that the furanocoumarin scaffold alone is not sufficient for potent cholinesterase inhibition; rather, substitution patterns, side-chain features, and enzyme-specific interactions appear to be critical determinants of activity.

The AChE docking results partially supported the experimental activity profile. Bergapten (1) exhibited the most favorable docking score among the isolated compounds and was also the only compound with a measured AChE $IC_{50}$ value. Its docking pose indicated accommodation in the aromatic region of the AChE active-site groove, mainly via hydrophobic and π-type interactions with residues such as Tyr341 and Phe295 and other surrounding aromatic residues. However, the remaining compounds showed weak or negligible AChE inhibition despite comparable docking scores. This discrepancy indicates that the docking scores should be interpreted qualitatively rather than as direct predictors of inhibitory potency.

Comparison with donepezil further supports the observed weak AChE-inhibitory activity of the isolated furanocoumarins. Donepezil extends along the active-site groove and interacts with multiple binding regions, including aromatic contacts with Trp86 and Trp286. In contrast, the isolated furanocoumarins are smaller, mostly planar, and lack an extended linker or a cationic center. Although their fused coumarin–furan scaffold can be accommodated within the AChE active site, their limited interaction profile may preclude stronger binding and result in weaker inhibitory activity.

For BChE, pabulenol (5) showed the best docking score and displayed measurable inhibition. Its predicted pose suggested interactions with Trp82 and neighboring hydrophobic or aromatic residues such as Tyr332, Ala328, Met437, and Tyr440. The additional polar contact formed through its oxygenated side chain may contribute to its relatively favorable docking score. Bergapten (1), despite its lower docking score, also showed measurable BChE inhibition and was positioned near Trp82, where it maintained aromatic and hydrophobic contacts within the catalytic cavity.

Nevertheless, the BChE docking scores did not fully parallel the experimental results. Oxypeucedanin hydrate (9) showed a relatively favorable docking score but did not display comparable inhibitory activity. This suggests that factors such as ligand orientation, desolvation, conformational effects, and the absence of stronger catalytic-site interactions may influence the observed activity. Compared with tacrine, the tested furanocoumarins lacked a cationic center and did not reproduce the same strong interaction pattern with His438 and the active-site water network. This limited interaction profile may explain their weak inhibitory effects on BChE. Taken together, the AChE and BChE docking results should be interpreted cautiously, since the Glide SP docking scores of the isolated furanocoumarins were distributed within a relatively narrow range and did not fully parallel the experimental inhibition data. Therefore, the docking analysis was used only as qualitative structural support for possible binding orientations and interaction patterns, rather than as a quantitative predictor of cholinesterase inhibitory potency.

Overall, the biological and docking results indicate that the furanocoumarins isolated from *Cachrys cristata* exhibit only weak cholinesterase-inhibitory activity. However, the observed accommodation of these compounds within the AChE and BChE active-site cavities suggests that the furanocoumarin scaffold may serve as a starting point for designing semi-synthetic derivatives with enhanced binding interactions and stronger inhibitory activity.

*Study limitations*

The present study has some limitations. First, some isolated compounds could not be evaluated in the cholinesterase

inhibition assays because they were obtained in limited quantities. Therefore, biological evaluation was restricted to compounds available in sufficient quantities. Second, enzyme inhibition assays were performed as preliminary endpoint screening experiments; detailed kinetic studies were not conducted to determine the mechanism of inhibition. The molecular docking studies served only as qualitative structural support for possible binding orientations and interaction patterns; docking scores should not be interpreted as quantitative predictors of inhibitory potency.

## CONCLUSION

Furanocoumarins isolated from *Cachrys cristata* exhibited weak cholinesterase- inhibitory activity. Bergapten was the most active compound against AChE, while only bergapten and pabulenol reached sufficient BChE inhibition to allow $IC_{50}$ determination. Molecular docking studies supported the experimental findings qualitatively, indicating that these compounds can be accommodated within the active-site cavities mainly through hydrophobic and $\pi$-type interactions with key aromatic residues. However, their limited interaction profiles, lack of a cationic center, and absence of extended binding features likely account for their markedly weaker activity compared with donepezil. Overall, these results suggest that the furanocoumarin scaffold may serve as a simple natural framework for the design of more potent semi-synthetic cholinesterase inhibitors.

*Ethics*

**Ethics Committee Approval:** Ethics committee approval was not required for this study, as it did not involve human participants or experimental animals.

**Informed Consent:** Informed consent was not required for this study, as it did not involve human participants or experimental animals.

*Footnotes*

*Authorship Contributions*

Concept: F.K.K., M.M., Design: F.K.K., Data Collection or Processing: F.K.K., C.K., Z.E.D., Ş.N.K.K., K.Ş.Ö., G.A.Ü., Analysis or Interpretation: F.K.K., G.A.Ü., M.M., Literature Search: F.K.K., C.K., Z.E.D., Writing: F.K.K., Z.E.D., G.A.Ü.

**Conflict of Interest:** The authors declare no conflicts of interest.

**Financial Disclosure:** This study was funded by the Scientific Research Projects Coordination Unit of İstanbul University. Project number: TLO-2026-42628.

**Supplementary Figures S1-13:** https://d2v96fxpocvxx.cloudfront.net/bd1986e1-0bc1-4f4d-af66-3a184850a065/content-images/9b4a7fb8-bbb0-4dec-b556-84da3b5feff1.pdf

## REFERENCES

1. POWO. Plants of the World Online [Internet]. Royal Botanic Gardens, Kew; 2026. Available from: https://powo.science.kew.org/. Accessed 4 July 2026.
2. Wang XJ, Luo Q, Li T, Meng PH, Pu YT, Liu JX, Zhang J, Liu H, Tan GF, Xiong AS. Origin, evolution, breeding, and omics of Apiaceae: a family of vegetables and medicinal plants. Hortic Res. 2022;9:uhac076.
3. Sayed-Ahmad B, Talou T, Saad Z, Hijazi A, Merah O. The Apiaceae: Ethnomedicinal family as source for industrial uses. Ind Crops Prod. 2017;109:661-671.
4. Musolino V, Perri MR, Conforti F, Gliozzi M, Marrelli M, Mollace V. *Cachrys* L. Genus: a comprehensive review on botany, phytochemistry and biological properties. Plants (Basel). 2023;12:565.
5. Nezahat Gökyiğit Botanik Bahçesi. Türkiye Bitkileri Listesi [Internet]. Available from: https://www.bizimbitkiler.org.tr/list.html. Accessed 4 July 2026.
6. Aouachria S, Boumerfeg S, Benslama A, Boussoualim N, Trabsa H, Baghiani A. Phenolics contents, xanthine oxidoreductase inhibitory potential, antibacterial and antioxidant activities of *Cachrys libanotis* L. Root Extracts. J Drug Deliv Ther. 2020;10:71-79.
7. Baser KHC, Demirci B, Akalin E, Özhatay N. Composition of the essential oil of *Cachrys alpina* Bieb. J Essent Oil Res. 2004;16:167-168.
8. Grande M, Aguado MT, Mancheño B, Piera F. Coumarins and ferulol esters from *Cachrys sicula*. Phytochemistry. 1986;25:505-508.
9. Marrelli M, Perri MR, Amodeo V, Giordano F, Statti GA, Panno ML, Conforti F. Assessment of photo-induced cytotoxic activity of *Cachrys sicula* and *Cachrys libanotis* enriched-coumarin extracts against human melanoma cells. Plants (Basel). 2021;10:123.
10. Menichini G, Alfano C, Provenzano E, Marrelli M, Statti GA, Menichini F, Conforti F. *Cachrys pungens* Jan inhibits human melanoma cell proliferation through photo-induced cytotoxic activity. Cell Prolif. 2012;45:39-47.
11. Maresca V, Badalamenti N, Ilardi V, Bruno M, Basile A. The antioxidant properties and protective capacity of *Prangos trifida* and *Cachrys cristata* essential oils against Cd stress in *Lunularia cruciata* and *Brassica napus*. Antioxidants (Basel). 2023;12:793.
12. Sgadari F, Vaglica A, Porrello A, Crisafulli A, Schicchi R, Bruno M. *Cachrys pungens* Jan ex Guss.: the essential oil chemical composition of the accession growing wild in Sicily (Italy). Nat Prod Res. 2025;39:5996-6001.
13. Koutsaviti A, Georgiou C, Milenković M, Tzakou O. Composition and antimicrobial activity of the essential oils from different parts of *Cachrys cristata* DC. from Greece. Rec Nat Prod. 2015;9:436-440.
14. Smaili T, Bendif H, Flamini G, Öztürk M, Duru ME, Bruno M, Maggi F. Chemical composition, antioxidant and anticholinesterase activity of the essential oil of Algerian *Cachrys sicula* L. Nat Prod Res. 2022;36:4094-4102.
15. Matejić JS, Džamić AM, Ristić MS, Ranđelović VN, Marin PD. Essential oil composition of *Cachrys cristata* – a rare and endangered species in the flora of Serbia. Nat Prod Commun. 2012;7:235-236.
16. World Health Organization. Dementia [Internet]. Available from: https://www.who.int/news-room/fact-sheets/detail/dementia. Accessed 4 July 2026.
17. Hampel H, Mesulam MM, Cuello AC, Farlow MR, Giacobini E, Grossberg GT, Khachaturian AS, Vergallo A, Cavedo E, Snyder PJ, Khachaturian ZS. The cholinergic system in the pathophysiology and treatment of Alzheimer's disease. Brain. 2018;141:1917-1933.

18. Kowalczyk J, Kurach Ł, Boguszewska-Czubara A, Skalicka-Woźniak K, Kruk-Słomka M, Kurzepa J, Wydrzynska-Kuźma M, Biała G, Skiba A, Budzyńska B. Bergapten improves scopolamine-induced memory impairment in mice via cholinergic and antioxidative mechanisms. Front Neurosci. 2020;14:730.

19. Kurach Ł, Kulczycka-Mamona S, Kowalczyk J, Skalicka-Woźniak K, Boguszewska-Czubara A, El Sayed N, Osmani M, Iwaniak K, Budzyńska B. Mechanisms of the procognitive effects of xanthotoxin and umbelliferone on LPS-induced amnesia in mice. Int J Mol Sci. 2021;22:1779.

20. Ellman GL, Courtney KD, Andres V Jr, Featherstone RM. A new and rapid colorimetric determination of acetylcholinesterase activity. Biochem Pharmacol. 1961;7:88-95.

21. Sevinçli ZŞ, Soylu-Eter Ö, Hasbal Celikok G, Altiparmak Ulbegi G, Bayır E, Şendemir A, Aksoy Sagirli P, Karalı N. Novel 2-indolinone benzylpiperidine-thiosemicarbazone hybrids as cholinesterase inhibitors: design, synthesis and biological evaluation. Bioorg Chem. 2026;180:110150.

22. Cheung J, Rudolph MJ, Burshteyn F, Cassidy MS, Gary EN, Love J, Franklin MC, Height JJ. Structures of human acetylcholinesterase in complex with pharmacologically important ligands. J Med Chem. 2012;55:10282-10286.

23. Nachon F, Carletti E, Ronco C, Trovaslet M, Nicolet Y, Jean L, Renard PY. Crystal structures of human cholinesterases in complex with huprine W and tacrine: elements of specificity for anti-Alzheimer's drugs targeting acetyl- and butyryl-cholinesterase. Biochem J. 2013;453:393-399.

24. Sastry GM, Adzhigirey M, Day T, Annabhimoju R, Sherman W. Protein and ligand preparation: parameters, protocols, and influence on virtual screening enrichments. J Comput Aided Mol Des. 2013;27:221-234.

25. Friesner RA, Banks JL, Murphy RB, Halgren TA, Klicic JJ, Mainz DT, Repasky MP, Knoll EH, Shelley M, Perry JK, Shaw DE, Francis P, Shenkin PS. Glide: a new approach for rapid, accurate docking and scoring. 1. Method and assessment of docking accuracy. J Med Chem. 2004;47:1739-1749.

26. Halgren TA, Murphy RB, Friesner RA, Beard HS, Frye LL, Pollard WT, Banks JL. Glide: a new approach for rapid, accurate docking and scoring. 2. Enrichment factors in database screening. J Med Chem. 2004;47:1750-1759.

27. Senol FS, Orhan IE, Yilmaz G, Cicek M, Sener B. An in vitro and in silico approach to cholinesterase inhibitory and antioxidant effects of furanocoumarins from *Angelica officinalis* L. roots. Food and Chemical Toxicology. 2011;*49*:3350-3357.

28. Yassaa N, Hadjiaghaee R, Delnavazi MR, Mofasseri M, Ghafarzadegan R, Heydari F, Tavakoli S. Evaluation of antioxidant and antibacterial activities of the bioactive compounds from the leaves of *Ferulago trifida* Boiss. Iran J Chem Chem Eng. 2024;43:2855-2865.

29. Lee S, Shin DS, Kim JS, Oh KB, Kang SS. Antibacterial coumarins from *Angelica gigas* roots. Arch Pharm Res. 2003;26:449-452.

30. Chatterjee A, Banerji J, Basa SC. Lactonic constituents of *Prangos pabularia* Lindl. (Umbelliferae). Tetrahedron. 1972;28:5175-5182.

31. Lee YY, Lee S, Jin JL, Yun Choi HS. Platelet anti-aggregatory effects of coumarins from the roots of *Angelica genuflexa* and *A. gigas*. Arch Pharm Res. 2003;26:723-726.

32. Jiménez B, Grande MC, Anaya J, Torres P, Grande M. Coumarins from *Ferulago capillaris* and *F. brachyloba*. Phytochemistry. 2000;53:1025-1031.

33. Thanh PN, Jin WY, Song GY, Bae KH, Kang SS. Cytotoxic coumarins from the root of *Angelica dahurica*. Arch Pharm Res. 2004;27:1211-1215.

34. Harkar S, Razdan TK, Waight ES. Steroids, chromone and coumarins from *Angelica officinalis*. Phytochemistry. 1984;23:419-426.

35. Kim DK, Lim JP, Yang JH, Eom DO, Eun JS, Leem KH. Acetylcholinesterase inhibitors from the roots of *Angelica dahurica*. Arch Pharm Res. 2002;25:856-859.

36. Seo WD, Kim JY, Ryu HW, Kim JH, Han SI, Ra JE, Seo KH, Jang KC, Lee JH. Identification and characterisation of coumarins from the roots of *Angelica dahurica* and their inhibitory effects against cholinesterase. J Funct Foods. 2013;5:1421-1431.

37. Senol FS, Skalicka-Woźniak K, Khan MTH, Orhan IE, Sener B, Głowniak K. An *in vitro* and *in silico* approach to cholinesterase inhibitory and antioxidant effects of the methanol extract, furanocoumarin fraction, and major coumarins of *Angelica officinalis* L. fruits. Phytochem Lett. 2011;4:462-467.

38. Wszelaki N, Paradowska K, Jamróz MK, Granica S, Kiss AK. Bioactivity-guided fractionation for the butyrylcholinesterase inhibitory activity of furanocoumarins from *Angelica archangelica* L. roots and fruits. J Agric Food Chem. 2011;59:9186-9193.

Turk J Pharm Sci 2026;23(3):174-186
**DOI:** 10.4274/tjps.galenos.2026.78567

ORIGINAL ARTICLE

# Synthesis, Characterization, and *In Vitro* Anticancer Activity of $Fe_3O_4$-PEG-Quercetin Nanoparticles in a Non-Small Cell Lung Cancer (NSCLC) Model

**Yeşim SİS[1]*, Mükerrem Betül YERER[2]**

[1]Erciyes University, Ziya Eren Pharmaceutical Application and Research Center, Kayseri, Türkiye
[2]Erciyes University Faculty of Pharmacy, Department of Pharmacology, Kayseri, Türkiye

## ABSTRACT

**Objectives:** Lung cancer is one of the leading causes of cancer-related mortality worldwide, with non-small cell lung cancer (NSCLC) accounting for the vast majority of cases. Conventional chemotherapeutic approaches are frequently limited by systemic toxicity, poor bioavailability, and non-selective biodistribution. Nanoparticle-based drug delivery systems have emerged as a promising strategy to overcome these limitations. The present study aimed to synthesize a novel PEGylated magnetite nanoparticle system containing quercetin ($Fe_3O_4$-PEG-QUER) and evaluate its effects on the impedance-based cellular responses of the A549 NSCLC cell line compared with non-tumorigenic bronchial epithelial cells (BEAS-2B).

**Materials and Methods:** Nanoparticles were synthesized via the coprecipitation method. Quercetin was introduced during the preparation of the $Fe_3O_4$-PEG formulation, resulting in the $Fe_3O_4$-PEG-QUER formulation. All formulations $Fe_3O_4$, $Fe_3O_4$-QUER, $Fe_3O_4$-PEG, and $Fe_3O_4$-PEG-QUER were characterized using X-ray diffraction, fourier-transform infrared spectroscopy, Zeta-sizer, and nanoparticle tracking analysis. Impedance-based cellular responses were assessed in BEAS-2B and A549 cell lines using the xCELLigence real-time cell analysis system.

**Results:** $Fe_3O_4$-PEG-QUER showed apparent antiproliferative effects against A549 cells, with IC50 values of 289 µg/mL at 24 h and 160 µg/mL at 48 h. For BEAS-2B cells, the apparent IC50 values were above the highest tested concentration (> 400 µg/mL) at the evaluated time points. $Fe_3O_4$-PEG alone showed marked effects on the impedance-based cellular response of A549 cells, with apparent IC50 values of 27 and 19 µg/mL at 24 and 48 h, respectively. Because quercetin loading was not quantitatively determined, the nanoparticle concentrations represent total formulation mass and cannot be directly converted to quercetin-equivalent doses.

**Conclusion:** $Fe_3O_4$-PEG-QUER nanoparticles altered the impedance-based cellular response in the A549 NSCLC cell line, with smaller changes observed in BEAS-2B cells at lower concentrations. These findings provide preliminary *in vitro* evidence supporting further investigation of $Fe_3O_4$-PEG-QUER in lung cancer models.

**Keywords:** Nanoparticles, A549, XRD, NTA and xCELLigence

***Correspondence:** yesimsis@erciyes.edu.tr, **ORCID-ID:** orcid.org/0009-0009-3108-7122

**Received:** 03.03.2026 **Accepted:** 15.10.2026 **Publication Date:** 27.10.2026

**Cite this article as:** Sis Y, Yerer MB. Synthesis, characterization, and *in vitro* anticancer Activity of $Fe_3O_4$-PEG-quercetin nanoparticles in a non-small cell lung cancer (NSCLC) model. Turk J Pharm Sci. 2026;23(3):174-186

Copyright© 2026 The Author(s). Published by Galenos Publishing House on behalf of Turkish Pharmacists' Association.
This is an open access article under the Creative Commons Attribution-NonCommercial-NoDerivatives 4.0 (CC BY-NC-ND) International License.

## INTRODUCTION

Super-paramagnetism arises from the limited size of magnetic nanoparticles (MNP).[1] In biomedical applications, super-paramagnetic nanoparticles can be used, which become magnetic in the presence of a magnetic field but lose their magnetic properties when this field is removed.[2,3] Since MNP have a tendency to clump due to their high surface energy and magnetic interactions, the body perceives the nanoparticle as a foreign object and tries to get rid of it.[2] To prevent such problems, coatings such as polyethylene glycol (PEG), polyvinyl alcohol (PVA), dextran, carbohydrate and protein are used.[4-6] PEG is a hydrophilic, neutral, non-toxic, protein-resistant polymer with high surface fluidity.[7-12] Due to these properties, PEG was used as a surface coating agent in this study.

Inorganic nanoparticles, such as silica, gold, and iron-oxide, and organic nanoparticles, such as liposomes, polymeric nanoparticles, and micelles, are used as therapeutic nanoparticles. Since inorganic nanoparticles gave good results in preclinical studies, they are suitable for clinical use and have been approved for use in areas such as anemia treatment and thermal ablation of tumors.[13,14] In addition, while inorganic nanoparticles provide benefits in areas such as magnetic resonance imaging and individual drug use, organic nanoparticles can be used for hemostasis, gene therapy and cancer treatment.[15,16]

There are eight iron-oxide compounds known in nature, including the most well-known types such as magnetite, hematite, and maghemite; while magnetite has a face-centered cubic structure in blackish-brown color, hematite is red-brown in color, formed as a result of volcanic activity, and maghemite is formed as a result of the oxidation of magnetite.[17-19] Iron-oxide nanoparticle (IONP) can be synthesized by several methods including coprecipitation, hydrothermal synthesis, and microemulsion. IONP can be used for medical purposes such as replacement therapy for anemia,[20,21] and magnetic resonance imaging as a contrast agent.[22-24] In imaging cancer and pathological types, IONP can be detected based on their behavior in the magnetic field.[5]

Flavonoids are a diverse group of polyphenolic compounds whose names are derived from the Latin word flavus, meaning "yellow." They are widely distributed in fruits, vegetables, tea, and other plant-based foods and are involved in various biological processes in plants.[25,26] Flavonoids, which show effects such as anti-inflammatory, antimutagenic, antioxidant and anti-carcinogenic, are used in pharmaceutical and medical applications.[27-29] Some of the flavonoids, also known as secondary metabolites of plants, attract attention in medicine and agriculture because they contain bioactive compounds that can interfere with nucleic acids and proteins, show anti-microbial and pharmacological properties, and kill insects.[30] Flavonoids can also be used in areas such as butyrylcholinesterase, acetylcholinesterase, and BACE1 inhibition, prevention of atherosclerosis, insulin receptor activator, antithrombogenic, lipoxygenase inhibition, inhibition of H1N1 influenza disease and NDM-1 inhibition.[25]

Cancer is a disease that deeply affects the world, caused by an excessive proliferation in the number of cells as a result of uncontrolled division of cells.[31] While lung cancer is the most common type of cancer in men worldwide, it is the type of cancer that comes right after breast cancer in women.[32] Early diagnosis of cancer is of great importance in terms of treatment because the development of cancer can be limited by early diagnosis.[33] Growths and changes in organs can be detected with classical methods, but this process can take a long time because it must wait until thousands of cancer cells have formed, whereas, thanks to nanotechnology, it can be detected at much lower cell counts. Even if a cancer cell has formed, it is possible to diagnose it. Since nanoparticles have the ability to enter a single cancer cell, cancerous cells can be easily detected.[34] Furthermore, classical methods such as radiotherapy, surgery and chemotherapy used to treat cancer can also damage healthy cells and tissues and have toxic effects.[35] MNP provide health benefits owing to their many features, such as a stable structure, high compatibility with cells and tissues, and ease of synthesis. It has received considerable attention in studies within the field. These substances have been used for years, and some types have been approved by the European Medicines Agency and the Food and Drug Administration (FDA) and have been used to treat people.[36] Many clinically approved nanoparticles have been used for treatment purposes in various stages of some types of cancer; PEG-Doxil is the first medical nanomaterial approved by the FDA in 1995 and used in cancer treatment.[37]

In this study, the coprecipitation method was selected for the synthesis of the nanoparticle formulations. $Fe_3O_4$ was synthesized from $FeCl_2 \cdot 4H_2O$ and $FeCl_3 \cdot 6H_2O$ in air; quercetin and PEG were incorporated into the formulation, with PEG serving as a surface-modifying component. The intermediate and final formulations were characterized by X-ray diffraction (XRD), fourier-transform infrared spectroscopy (FT-IR), nanoparticle tracking analysis (NTA), Zeta-sizer, scanning electron microscopy (SEM), and energy-dispersive X-ray spectroscopy (EDX) to obtain complementary information on their physicochemical properties. The in *vitro* cellular responses to the formulations were subsequently evaluated in the A549 [non-small cell lung cancer (NSCLC)] and non-tumorigenic bronchial epithelial (BEAS-2B) cell lines using the xCELLigence real-time impedance-based monitoring system. The study therefore provides comparative physicochemical data and *in vitro* cellular-response data for $Fe_3O_4$, $Fe_3O_4$-PEG, $Fe_3O_4$-QUER, and $Fe_3O_4$-PEG-QUER- based formulations.

## MATERIALS AND METHODS

### *Chemicals and reagents*

All chemicals were used as received without further purification. The reagents employed in this study, along with their suppliers and purity grades, are summarized in Table 1.

### *Preparation of IONP*

$FeCl_2.4H_2O$:$FeCl_3.6H_2O$ was taken in the ratio of 1:2;[38-43] $FeCl_2.4H_2O$ and $FeCl_3.6H_2O$ were added to the reaction vessel,

**Table 1. Chemicals and reagents used in this study.**

| Chemical | Supplier | Purity/grade | CAS/notes |
|---|---|---|---|
| $FeCl_2 \cdot 4H_2O$ | Supelco | For analysis | 13478–10–9 |
| $FeCl_3 \cdot 6H_2O$ | Isolab | ≥ 97% | 10025–77–1 |
| Quercetin | Merck | ≥ 95% (HPLC) | 117–39–5 |
| PEG 1000 | BLDpharm | ⟩ 97% | 25322–68–3 |
| Ethanol | Isolab | ≥ 99.9% | 64–17–5 |
| Ammonia solution | Supelco | 25%, for analysis | 1336–21–6 |
| DMSO | PanReac | ≥ 99.5%, cell culture grade | 67–68–5 |
| PBS tablets | Sigma | pH 7.2–7.6 | – |
| DMEM (high glucose) | Sigma | Cell culture grade | A549 medium |
| RPMI-1640 | Sigma | Cell culture grade | BEAS-2B medium |

DMSO, dimethyl sulfoxide.

10 mL of pure water was added and placed in the oil bath on the magnetic stirrer set at 80 °C and 300 rpm. When 3 mL of 25% $NH_3$ was added to the reaction vessel after 15 minutes, the brown-toned reaction color turned into silvery black and it was observed that the substance condensed/precipitated at the bottom. After 15 minutes, the reaction was terminated and transferred to 50 mL falcon tubes, centrifuged at 3900 rpm-room temperature for 5 minutes, washed twice with pure water, and then left to dry in an oven set at 60 °C. The reaction pH was not measured or recorded during the original synthesis.

*IONP-PEG synthesis*

The IONP–PEG synthesis procedure was adapted from previously reported IONP–PEG formulations, particularly those described by Dorniani et al.[44] and Rosman et al.[45] In these studies, PEG was incorporated into magnetite-based formulations; Rosman et al.[45] reported one based on 0.2 g of dried IONP. The reported formulation conditions were scaled down and adapted for an *in situ* procedure in which PEG was introduced during the IONP synthesis rather than after isolation and drying of the nanoparticles. After 30 min of synthesis, 5 mL of a 10% (w/v) solution of PEG 1000, prepared by dissolving 0.5 g of PEG 1000 in 5 mL of ethanol, was added to the reaction mixture. The mixture was subsequently subjected to centrifugation, washing, and drying.

*IONP-QUER synthesis*

The IONP–quercetin synthesis procedure was adapted from previously reported magnetite–PEG–active compound formulations, particularly those described by Dorniani et al.[44] and Rosman et al.[45]; Dorniani et al.[44] reported a magnetite–PEG formulation containing 1% PEG and 2% gallic acid, whereas Rosman et al.[45] reported a related $Fe_3O_4$–PEG–gallic acid formulation based on 0.2 g of dried IONP. In the present study, the reported formulation conditions were scaled down and adapted for quercetin and for an *in situ* synthesis procedure. 0.0595 g $FeCl_2 \cdot 4H_2O$ and 0.140 g $FeCl_3 \cdot 6H_2O$ were added to 930 μL of purified water in a 30 mL glass vial. The vial was placed in a 100 mL conical flask and maintained at 80 °C and stirred at 300 rpm using a magnetic stirrer with an oil bath. After 15 min, 280 μL of 25% $NH_3$ solution was added. After an additional 15 min, 0.0625 g of quercetin was dissolved in 3125 μL of ethanol to prepare a 2% (w/v) quercetin solution, which was added directly to the reaction mixture. Stirring was continued for 1 h, after which the resulting reaction mixture was subjected to centrifugation, washing, and drying.

*IONP-PEG-QUER synthesis*

IONP was synthesized as described in the IONP-QUER synthesis, and 5 mL of a 1% (w/v) PEG 1000 solution (prepared by dissolving 0.05 g PEG 1000 in 5 mL of ethanol) was added after 30 minutes. After 1 hour, 0.0625 g of quercetin was dissolved in 3125 μL of ethanol to prepare a 2% (w/v) quercetin solution, which was then added to the reaction vessel. After 30 minutes, 350 μL of 25% $NH_3$ was added to the reaction vessel and the reaction was continued for another two and a half hours. At the end of this period, the reaction vessel was removed, centrifuged, washed, and dried (Figure 1).

*Physicochemical characterization*

All formulations were characterized by XRD for crystal structure and phase purity; FT-IR for verification of surface functionalization; dynamic light scattering (Zeta-sizer) for hydrodynamic size and zeta potential; NTA for size distribution and particle concentration; SEM for morphological evaluation; and EDX for elemental composition.

*Cell culture conditions*

A549 (ATCC CCL-185, NSCLC adenocarcinoma) and BEAS-2B (ATCC CRL-9609, non-tumorigenic bronchial epithelial cells) cell lines were used. A549 cells were maintained in DMEM (high glucose; Sigma) supplemented with 10% FBS and 1% penicillin-streptomycin. BEAS-2B cells were cultured in RPMI-1640 (Sigma) supplemented with 10% FBS and 1% penicillin-streptomycin. Both lines were maintained at 37 °C in a humidified 5% CO2 incubator. Cells were harvested by centrifugation at 1000 rpm for 5 minutes at 25 °C prior to the experiments.

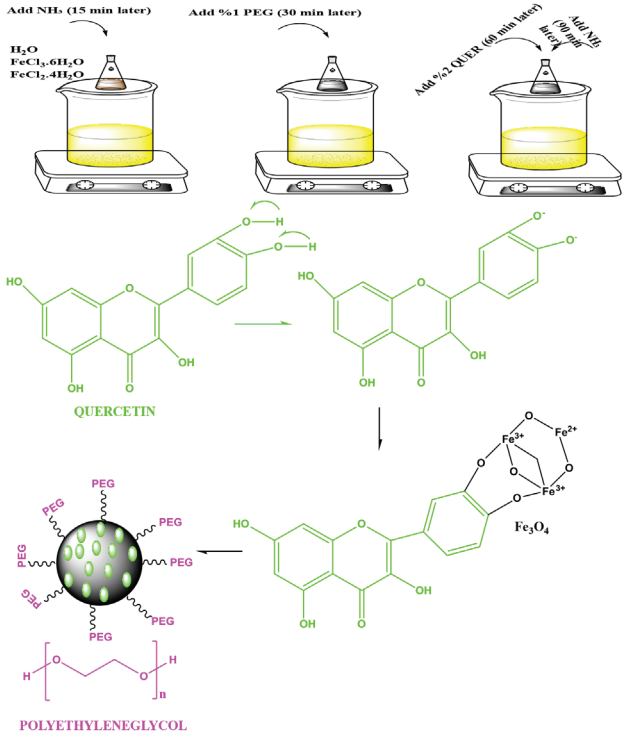



**Figure 1.** Experimental setup and schematic representation of IONP-PEG-QUER synthesis.

IONP, iron-oxide nanoparticle; QUER, quercetin.

*Preparation of drug solutions*

All formulations and free quercetin were prepared in dimethyl sulfoxide (DMSO) and in the appropriate culture medium (A549-DMEM/BEAS-2B-RPMI). Serial dilutions were performed in the appropriate culture medium to yield final concentrations of 12.5–400 µg/mL. After the prepared treatment solutions were added to the E-plate wells at a 1:1 volume ratio, the final DMSO concentration ranged from 0.5% at 400 µg/mL to 0.015625% at 12.5 µg/mL. A DMSO vehicle control was included in the experiments; however, concentration-matched vehicle controls were not included for each tested formulation concentration. Therefore, a possible contribution of the varying DMSO concentrations to the observed cellular responses cannot be fully excluded.

For experiments in which the cell index declined to approximately zero before 72 h, monitoring was terminated; therefore, a 72-h IC50 value was not determined and reported as N/D.

*Impedance-based cellular response assessment (xCELLigence)*

Cytotoxic effects were evaluated using the xCELLigence RTCA system (ACEA Biosciences/Agilent). A549 and BEAS-2B cells at the 5$^{th}$ passage were used for experiments. Cells were counted using a Bio-Rad cell counting device and seeded at a density of at least 10,000 cells per well in an xCELLigence E-plate (E-plate ID: 761460). Following cell seeding, impedance signals were monitored to establish the cellular baseline. The test formulations were applied at approximately 2 h and 22 h after cell seeding, according to the respective experimental setups. The treatment application times are also indicated in the corresponding xCELLigence graphs.

$Fe_3O_4$-PEG, $Fe_3O_4$-QUER, $Fe_3O_4$-PEG-QUER, and free quercetin were tested at concentrations of 12.5, 25, 50, 100, 200, and 400 µg/mL. Cellular responses were monitored for 48-72 h following treatment. At least three independent biological experiments were performed, each with two technical replicate wells for each tested concentration.

The xCELLigence RTCA system measures changes in electrical impedance associated with cellular attachment, spreading, proliferation, and other cellular responses; these changes are expressed as cell index values. Therefore, the cell index does not represent a direct measurement of cell viability. Apparent IC50 values were estimated separately at 24, 48, and 72 h using the corresponding cell index concentration–response data in the RTCA software. The concentration–response data were fitted to a sigmoidal dose–response model using DRC analysis (cell index at a time point vs. concentration). The curve settings were selected according to the concentration–response profile and goodness of fit. The resulting IC50 values were exported to GraphPad Prism 8.0.2 for statistical analysis. The corresponding culture medium was used as the control medium for each cell line: DMEM for A549 cells and RPMI-1640 for BEAS-2B cells. DMSO vehicle controls were also included in the experiments. These controls were included in the recorded RTCA data, and no separate manual normalization of cell index values was performed before IC50 analysis.

*Statistical analysis*

The xCELLigence results were calculated using RTCA software. For additional statistical evaluation, the data were analyzed using GraphPad Prism (version 8.0.2; GraphPad Software, San Diego, CA, USA). One-way analysis of variance, followed by Tukey's multiple comparisons test, was used for statistical comparisons. Each experimental condition was measured in technical duplicate wells. A $p$-value $< 0.05$ was considered statistically significant.

*Ethics*

There are no circumstances requiring ethics committee approval for this study.

Since only *in vitro* experiments were conducted within the scope of this study, patient consent was not required.

## RESULTS

*FT-IR*

The FT-IR spectra of $Fe_3O_4$, $Fe_3O_4$-PEG, $Fe_3O_4$-QUER, and $Fe_3O_4$-PEG-QUER nanoparticles are shown in Figure 2a. While the O-H bond peak was observed in the 3000-3232 range[39] the Fe-O bond in the iron-oxide structure gave a peak in the 540-555 $cm^{-1}$ range.[40] The C = O bond from quercetin in the 1651 $cm^{-1}$ range,[38] while the $CH_2$ peak at 1344-1375 $cm^{-1}$ and the C-C-O/C-O-H peak at 987-1056 $cm^{-1}$ were observed. The C-H peak gave a peak of 833-871 $cm^{-1}$ and the C = C aromatic ring peak of 1589-1612 $cm^{-1}$.[40,43]

*XRD analysis*

In the $Fe_3O_4$ structure, 30, 35, 43, 53, 57 and 62 2Θ values are respectively (HighScore Plus-ICPDS No: 88–0315); Bragg reflections were determined as 220, 311, 400, 422, 511, 440 and it was observed that the cubic crystal structure of IONP was formed.[44] The addition of PEG and quercetin during the preparation process did not result in an apparent loss of the characteristic cubic crystal structure of $Fe_3O_4$ (Figure 2b).

*NTA*

One mg of $Fe_3O_4$, $Fe_3O_4$-PEG, $Fe_3O_4$-QUER and $Fe_3O_4$-PEG-QUER was weighed and dissolved in 2000 µL ethanol and size analyses were performed on the NTA device (ethanol was chosen because it is a good solvent for quercetin). Measurements were made in three repetitions and the average was taken as basis. According to NTA analysis, the average size of IONPs is 99.1 nm. Since the number of particles with a size of 54.6 nm was high, iron-oxide gave the strongest peak at this point. The size distribution is not homogeneous (Figure 3a). When coated with iron-oxide PEG, an increase in size was observed and the average size increased to 170.5 nm as the polymer was attached to the structure (Figure 3b). For the formulation containing quercetin, the particle size decreased (average size: 66.6 nm) (Figure 3c). When PEG was present in the iron-oxide–quercetin formulation, the particle size increased compared to the structure of iron-oxide-quercetin. However, its size remained between 1–100 nm where nanoparticles are found (Figure 3d).

*Zeta potential analysis*

While 1 mg of $Fe_3O_4$, $Fe_3O_4$-PEG and $Fe_3O_4$-PEG-QUER was weighed and dissolved in 1000 µL of ethanol and given to the device, 1 mg of $Fe_3O_4$-QUER was also weighed and dissolved in 2000 µL of ethanol and given to the device. Zeta potential measurements were performed in triplicate under room-temperature conditions using a Malvern Zeta-sizer. The reported zeta potential values represent the mean of the three repeated measurements. The "Zeta Deviation" values represent the standard deviation of the zeta potential distribution reported by the instrument software and do not represent the variability between repeated measurements (Figure 4a-d).

Zeta potential measurements are summarized in Table 2. Bare $Fe_3O_4$ carried a negative surface charge (-9.74 mV). PEGylation shifted the surface charge to near-neutrality (+0.183 mV), consistent with the electrically neutral nature of PEG and its established charge-shielding effect. The formulation containing quercetin exhibited a more negative surface charge (-14.0 mV for $Fe_3O_4$-QUER), attributable to the phenolic hydroxyl groups of quercetin. The $Fe_3O_4$-PEG-QUER formulation exhibited an intermediate charge of -8.18 mV.

*SEM images*

The morphology of the synthesized $Fe_3O_4$-PEG-quercetin nanoparticles was analyzed using SEM. Figures 5a-d present SEM images and particle-size distributions of functionalized magnetite nanoparticles, both with and without quercetin. The particles exhibited sizes predominantly in the 100–200 nm range. A predominantly spherical morphology was observed; however, some degree of particle agglomeration was also evident in the SEM images.

*EDX analysis*

Elemental analysis was performed to determine the presence of expected elements in the synthesized formulations and to evaluate their elemental percentages. Elemental analysis was performed to determine the presence of expected elements in the synthesized formulation and to evaluate their elemental percentages. The Fe peak confirmed the presence of $Fe_3O_4$ in the formulation (Figure 6a). In formulations containing PEG and quercetin, relative iron percentages decreased, which may be attributable to these components (Figure 6b-d).

*Impedance-based cellular response (xCELLigence)*

The cellular responses to all formulations were evaluated at concentrations ranging from 12.5 to 400 µg/mL using the xCELLigence system (Figure 7). Cellular responses were

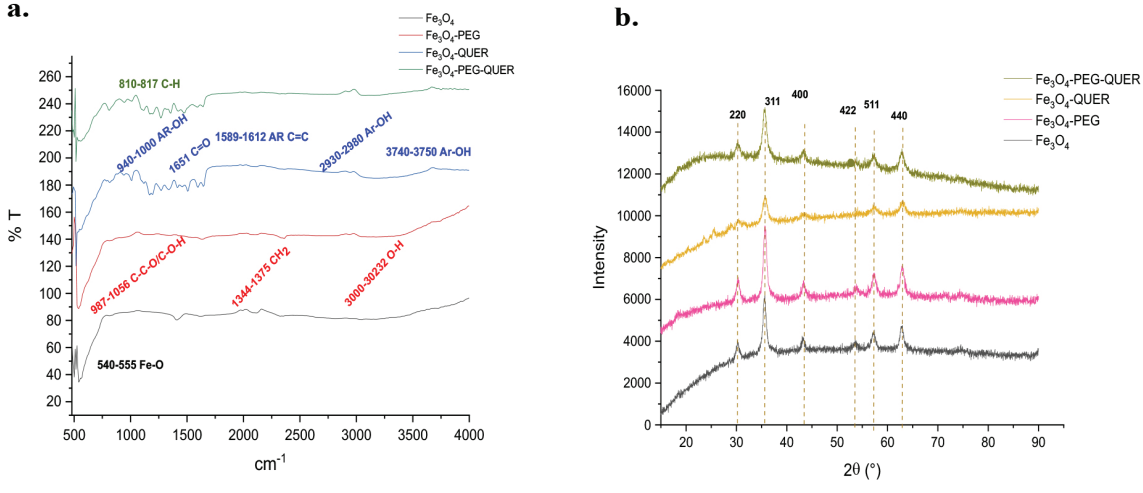



**Figure 2. a.** FT-IR spectra- 400–4000 $cm^{-1}$; **b.** XRD graph.

FT-IR, fourier-transform infrared spectroscopy; XRD, X-ray diffraction; QUER, quercetin.

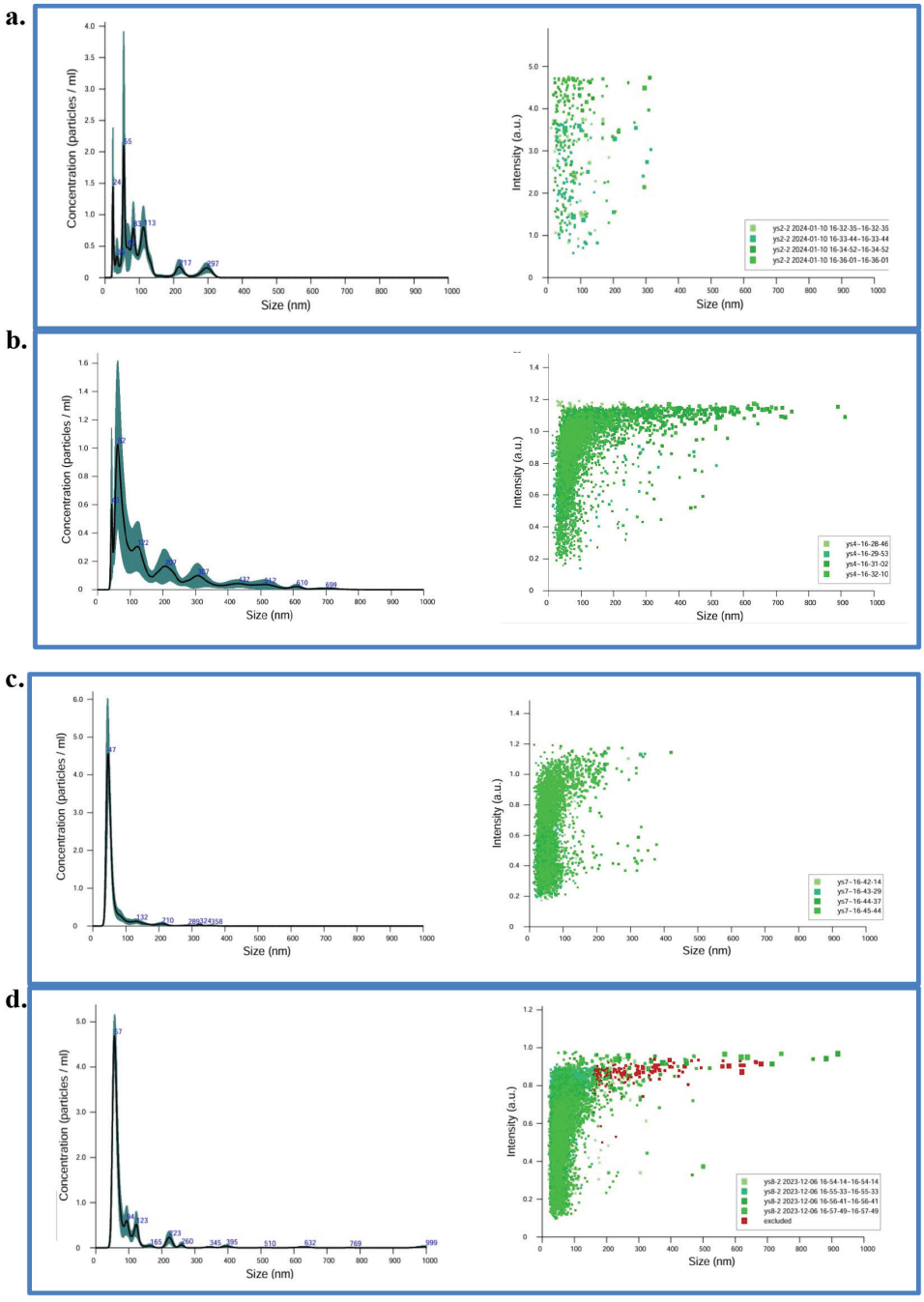



**Figure 3. a**. NTA result for $Fe_3O_4$ (mean particle size: 99.1 nm; strongest peak: 54.6 nm); **b.** NTA result for $Fe_3O_4$-PEG (mean particle size: 170.5 nm; strongest peak: 61.1 nm); **c.** NTA result for $Fe_3O_4$-QUER (mean particle size: 66.6 nm; strongest peak: 46.2 nm); **d.** NTA result for $Fe_3O_4$-PEG-QUER (mean particle size: 96.8 nm; strongest peak: 56.6 nm).

NTA, nanoparticle tracking analysis; QUER, quercetin.

monitored for 48–72 h, depending on the response profile. IC50 values determined at 24, 48, and 72 h are summarized in Table 3. Statistical comparisons between the tested conditions and untreated controls were significant ($p < 0.0001$).

Free quercetin exhibited significant cytotoxic activity at low concentrations (approximately 25 µg/mL) in both BEAS-2B and A549 (NSCLC) cell lines. $Fe_3O_4$-PEG exhibited cytotoxic activity in A549 cells (IC50 values: 27 and 19 µg/mL at 24 and 48 h, respectively), whereas higher concentrations were required to elicit a comparable response in BEAS-2B cells (IC50 values: 394, 394, and 360 µg/mL at 24, 48, and 72 h, respectively). These findings indicate that $Fe_3O_4$-PEG has greater cytotoxic activity in A549 cells than in non-tumorigenic BEAS-2B cells under the tested conditions.

In contrast, $Fe_3O_4$-PEG-QUER showed IC50 values above the highest tested concentration (› 400 µg/mL) in BEAS-2B cells at 24, 48, and 72 h. In A549 cells, $Fe_3O_4$-PEG-QUER exhibited cytotoxic activity at relatively low concentrations, with IC50 values of 289 and 160 µg/mL at 24 and 48 h, respectively. Thus, compared with free quercetin, $Fe_3O_4$-PEG-QUER showed lower cytotoxic activity in BEAS-2B cells while retaining measurable cytotoxic activity in A549 cells under the tested conditions.

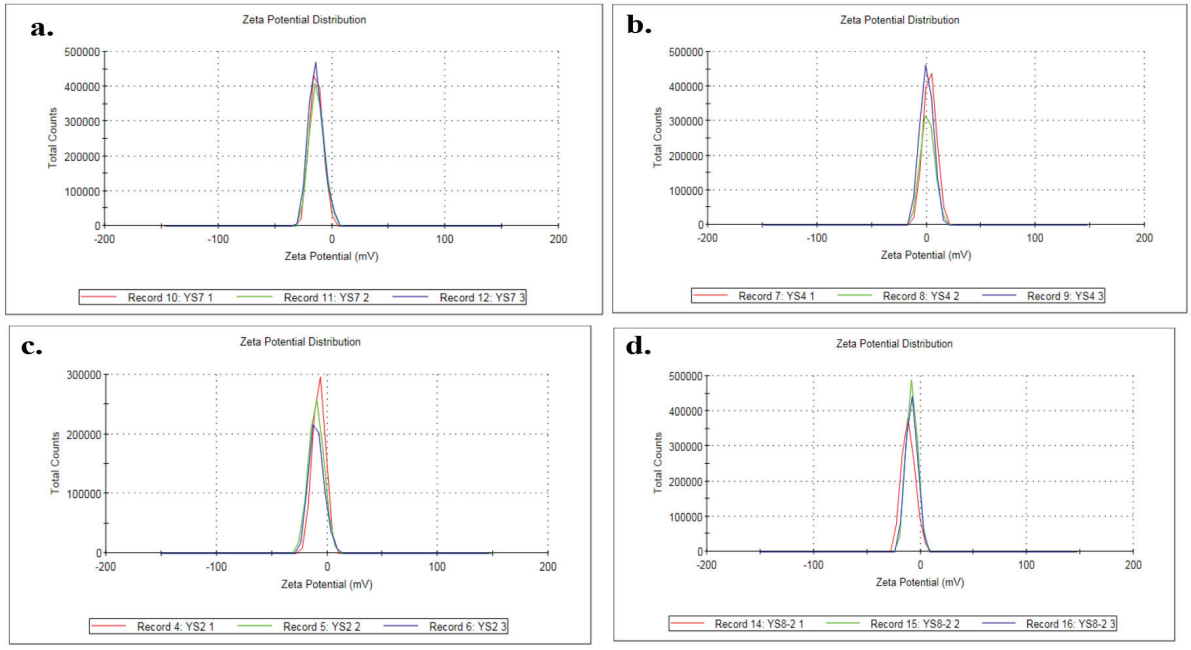



**Figure 4. a.** $Fe_3O_4$; **b.** $Fe_3O_4$-PEG; **c.** $Fe_3O_4$-QUER; **d.** $Fe_3O_4$-PEG-QUER zeta potential graph.
QUER, quercetin.

**Table 2. Zeta potential results of the synthesized nanoparticle formulations based on three repeated measurements.**

| Formulation | Zeta potential (mV) | Zeta deviation (mV) | Charge |
|---|---|---|---|
| $Fe_3O_4$ (IONP) | -9.74 | 6.66 | Negative |
| $Fe_3O_4$-PEG | +0.183 | 5.97 | Near-neutral |
| $Fe_3O_4$-QUER | -14.0 | 6.52 | Negative |
| $Fe_3O_4$-PEG-QUER | -8.18 | 5.35 | Negative |

QUER, quercetin.

**Table 3. Apparent IC50 values (µg/mL) derived from xCELLigence cell index concentration-response data for all formulations in BEAS-2B and A549 cells at 24, 48, and 72 h.**

| Formulation | BEAS-2B | | | | A549 (NSCLC) | | | |
|---|---|---|---|---|---|---|---|---|
| | IC50 24h | IC50 48h | IC50 72h | *p*-value | IC50 24h | IC50 48h | IC50 72h | *p*-value |
| $Fe_3O_4$-PEG | 394 µg/mL | 394 µg/mL | 360 µg/mL | $p < 0.0001$ | 27 µg/mL | 19 µg/mL | N/D* | $p < 0.0001$ |
| $Fe_3O_4$-QUER | › 400 | 170 µg/mL | 363 µg/mL | $p < 0.0001$ | 161 µg/mL | 182 µg/mL | N/D* | $p < 0.0001$ |
| $Fe_3O_4$-PEG-QUER | › 400 | › 400 | › 400 | $p < 0.0001$ | 289 µg/mL | 160 µg/mL | N/D* | $p < 0.0001$ |
| QUER | 25 µg/mL | 25 µg/mL | 24 µg/mL | $p < 0.0001$ | 25 µg/mL | 25 µg/mL | 134 µg/mL | $p < 0.0001$ |

*N/D: Not determined. IC50 values were determined from the corresponding cell index concentration-response data at 24, 48, and 72 h after treatment. Values › 400 µg/mL indicate that the IC50 was not reached within the tested concentration range. N/D indicates that the cell index values decreased to zero before 72 h, resulting in termination of the experiment before the corresponding time point could be evaluated reliably. The reported p-values represent the overall one-way ANOVA results.
BEAS-2B, non-tumorigenic bronchial epithelial cells; QUER, quercetin; ANOVA, analysis of variance; NSCLC, non-small cell lung cancer.

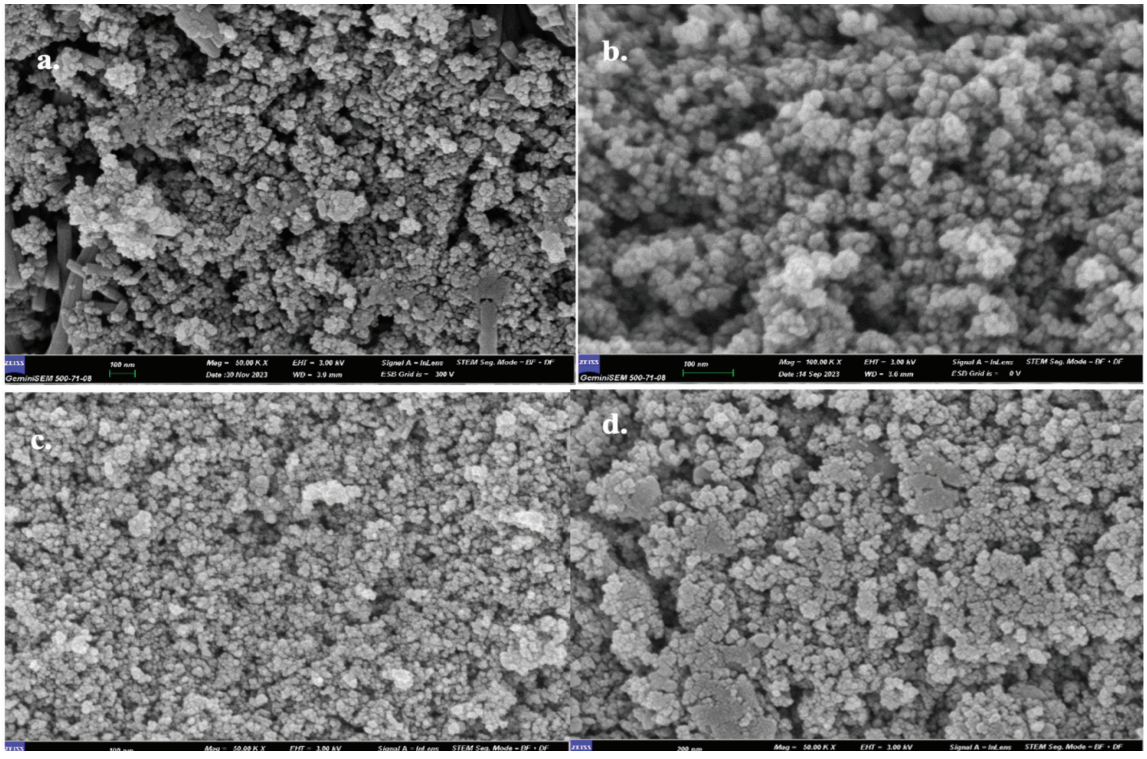



**Figure 5.** SEM images of the nanoparticle formulations: **a.** $Fe_3O_4$ (scale bar: 100 nm); **b.** $Fe_3O_4$ PEG (scale bar: 200 nm and 100 nm); **c.** $Fe_3O_4$ QUER (scale bar: 100 nm); and **d.** $Fe_3O_4$ -PEG-QUER (scale bar: 200 nm).

SEM, scanning electron microscopy; QUER, quercetin.

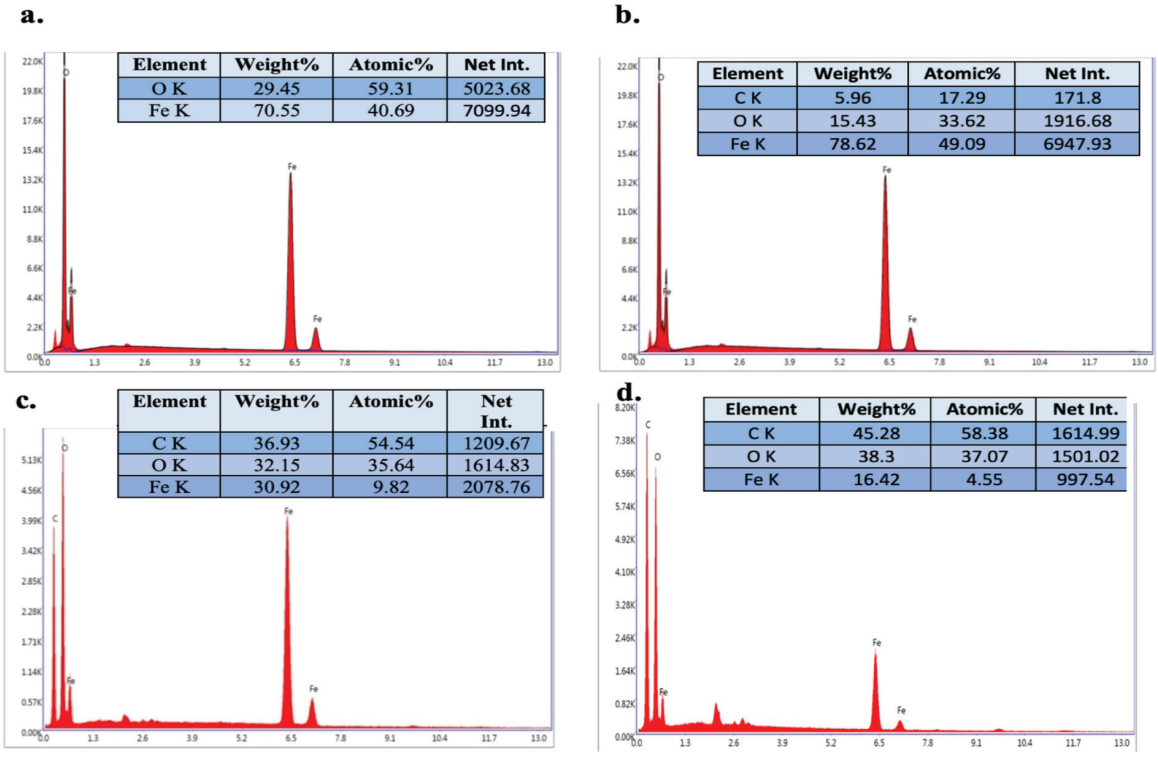



**Figure 6.** EDX spectra of the nanoparticle formulations: **a.** $Fe_3O_4$; **b.** $Fe_3O_4$-PEG; **c.** $Fe_3O_4$-QUER; and **d.** $Fe_3O_4$-PEG-QUER.

EDX, energy-dispersive X-ray spectroscopy; QUER, quercetin.

Overall, $Fe_3O_4$-PEG and $Fe_3O_4$-PEG-QUER produced measurable cytotoxic responses in A549 cells, whereas responses in BEAS-2B cells generally occurred at higher concentrations. Statistical comparisons with untreated controls were significant for the tested conditions ($p < 0.0001$).

Synthesized formulations were applied to cells in the concentration range of 12.5–400 µg/mL, and their effects were monitored for 48–72 hours using a time-dependent real-time xCELLigence system. As shown in the xCELLigence results tables, the cytotoxicity profiles differed between A549 and BEAS-2B cell lines. Because this is a real-time analysis, the graphs allow the toxicity profiles to be compared over time (Figure 7).

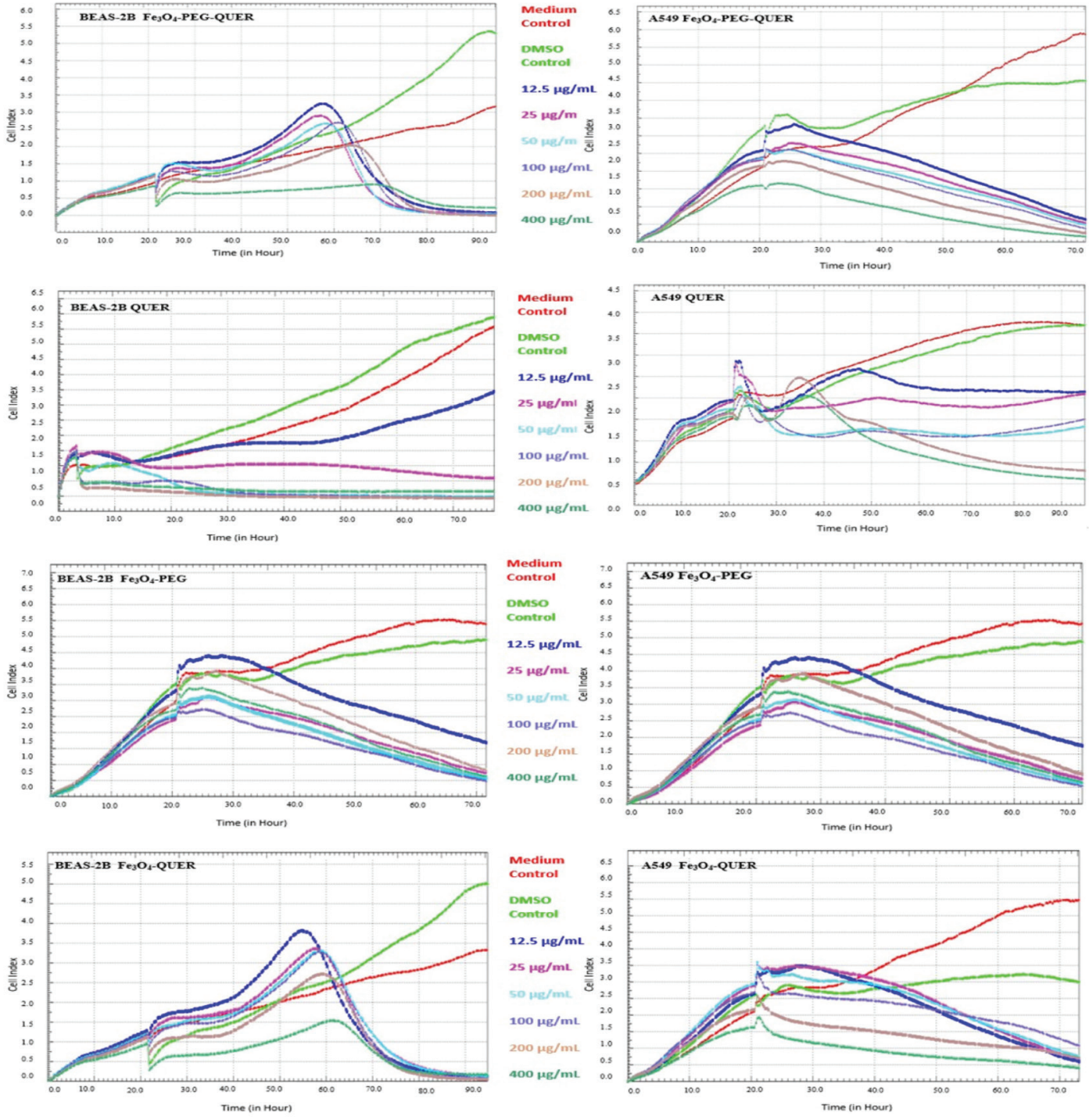



**Figure 7.** Real-time monitoring of the effects of $Fe_3O_4$-PEG, $Fe_3O_4$-QUER, $Fe_3O_4$-PEG-QUER, and free quercetin (QUER) on BEAS-2B and A549 cells using the xCELLigence system at 48 and 72 h.

BEAS-2B, non-tumorigenic bronchial epithelial cells.

The selectivity index (SI), calculated as the ratio of the IC50 value in BEAS-2B cells to that in A549 cells, was used to describe the relative difference in response between the two cell lines. SI values greater than 1 indicate a higher relative IC50 in BEAS-2B cells than in A549 cells, whereas values below 1 indicate a lower relative IC50 in BEAS-2B cells than in A549 cells. The SI values calculated for the tested formulations at 24, 48, and 72 h are presented in Table 4.

## DISCUSSION

Magnetic IONP are particularly important in diseases due to oxidative damage.[46,47] However, there are several factors that strongly affect the antioxidant activity of nanomaterials, such as chemical composition, surface charge, particle size, and coating of the surface.[48-50] The surface coating can be biocompatible, non-toxic, and allow targeted drug delivery.[51,52]

In biomedical applications where MNP are used, stable, biocompatible nanoparticles are obtained by coating metals and metal oxides with a polymer. Fe in iron-oxide nanoparticles is reversibly used by cells.[53,54]

PEG, PVA and polyvinylpyrrolidone; superparamagnetic $Fe_3O_4$ material coated with coatings such as peptide, carbohydrate or protein facilitates drug loading and controlled release.[55]

Cancer is one of the leading causes of death, and the number of cancer-related deaths is increasing over time. Whether nanostructures can have an anticancer effect on the targeted area is a difficult research; many researchers have integrated commercial anticancer drugs into magnetite.[56,57] Drug systems integrated into this magnetite face challenges such as poor solubility, poor circulation in the bloodstream, and reduced drug clearance. Therefore, an effective drug delivery mechanism must be formulated to overcome such problems.[58] Quercetin is a widely known flavonoid found in fruits and vegetables.[59,60] Quercetin can be used in many fields as anticancer, anti-inflammatory, and antioxidant.[61] In addition to these areas of use, it has anticancer properties; It has high effectiveness on colon, breast and lung cancer.[62] More recently, quercetin-containing PEG-coated magnetic iron-oxide nanoparticles have also been investigated for their potential anti-tumor effects in cancer cells.[63] The present study was designed to examine a quercetin-containing $Fe_3O_4$ formulation *in vitro*. Similarly, the physicochemical properties of quercetin-containing $Fe_3O_4$ nanoparticles are suitable for use as an anticancer agent.[64] This provided the rationale for investigating an $Fe_3O_4$-based formulation containing PEG and quercetin, and for evaluating its *in vitro* effects on A549 and BEAS-2B cells.

The sizes and shapes of MNP vary depending on the method of synthesis. If MNP are synthesized in non-aqueous environments such as solvothermal, microwave and thermal decomposition methods, they are not suitable for use in the field of bio-application because they are hydrophobic.[57] Hydrophilic, cost-effective and environmentally friendly MNP can be synthesized by the precipitation method, which is easy to synthesize.[65] However, MNP obtained with this method has limitations such as not having a homogeneous size distribution and low stability.[66]

In their IONP ($Fe_3O_4$) synthesis, Jarzebski et al.[67] found an average peak of 208 nm and the most intense peak of 154 nm in the NTA results. (They used a laser beam with a wavelength of 405 nm). In this study, the mean particle size was determined to be 99.1 nm, while the most intense peak was observed at 54.6 nm. Thus, the particle size falls within the 1–100 nm range generally defined for nanoparticles. If we could control the size of our formulation, we could achieve an average size of approximately 54.6 nm, which corresponds to the strongest peak. Using the Microfluidics M110P device, we were able to further reduce particle sizes under high pressure.

Nurbas et al.[68] synthesized IONP from $FeCl_2.4H_2O$:$FeCl_3.6H_2O$ (2:1) and added NaOH to the medium instead of $NH_3$. They found the Zeta potential of NP, which they obtained with a size of approximately 35 nm, to be -24.80 mV. The value found is more negative than that of the IONP synthesized in this study, although the IONP has a smaller particle size. If they had applied the NP they synthesized to the cell, they would likely have obtained better results, since the particle size was smaller than that of the NP we obtained. Since the zeta potential of the IONP synthesized in this study is -9.74 mV, this may have contributed to the observed cellular response through interactions with the cellular environment.

Verma et al.[49] synthesized IONP from $FeCl_2$ and $FeCl_3$ using 0.4 M HCl and 0.5 M NaOH, and attached Quercetin and PLGA to IONP. They administered PLGA-MNP and MNP at dosages of 10–250 µg/mL to the A549 cell line and analyzed the cells with xCELLigence (Roche). They observed that the MNP they applied reduced the cell index slightly, whereas MNP coated with PLGA did not cause a significant change. According to TEM, they found

**Table 4. Selectivity index (SI) values of $Fe_3O_4$-based formulations and free quercetin in A549 and BEAS-2B cells at 24,48 and 72 h.**

| Formulation | SI 24 h* | SI 48 h* | SI 72 h* |
|---|---|---|---|
| $Fe_3O_4$-PEG | 14.59 | 20.74 | N/D |
| $Fe_3O_4$-QUER | > 2.48 | 0.93 | N/D |
| $Fe_3O_4$-PEG-QUER | > 1.38 | > 2.50 | N/D |
| Free quercetin | 1.00 | 1.00 | 0.18 |

*SI. SI was calculated as the ratio of the IC50 value in BEAS-2B cells to that in A549 cells at the corresponding time point (SI = IC50, BEAS-2B / IC50, A549). Values preceded by ">" indicate that the IC50 value in BEAS-2B cells was not reached within the tested concentration range and therefore represent a lower limit of the SI. N/D indicates that the corresponding IC50 value was not determined; see the $IC_{50}$ table footnote for the experimental reason.
BEAS-2B, non-tumorigenic bronchial epithelial cells; QUER, quercetin.

the MNP particle size they produced to be approximately 9 nm, and the MNP-PLGA size to be approximately 54 nm.[49] Although the size of the PLGA-coated particles they produced and the methods used to measure size differed from those of our MNP-PEG formulation, we can say that the observed response at a lower concentration under the tested conditions, relative to our formulation, may be associated with it being smaller in size. Since PLGA is a negatively charged polymer, it may have increased the negative charge of the magnetite, making cellular entry difficult. In our study, when neutral PEG was used, the magnetite shifted to the neutral area and therefore the 24-hour IC50 and 48-hour IC50 values for the A549 cell line were approximately 27-19 µg/mL, respectively. It was effective at very small doses.

*Study limitations*

Several limitations should be considered when interpreting the findings of this study. The amount of quercetin associated with the $Fe_3O_4$-PEG-QUER formulation was not quantitatively determined; consequently, quercetin loading efficiency, encapsulation efficiency, recovery yield, and release kinetics could not be established. The available physicochemical characterization techniques did not allow a definitive determination of the molecular nature of the interaction between $Fe_3O_4$, PEG, and quercetin; therefore, covalent conjugation should not be inferred from the present data.

Cytotoxicity experiments were performed using total formulation concentrations, which precluded direct comparisons of quercetin-equivalent doses. The maximum concentration tested was 400 µg/mL, and IC50 values above this concentration were therefore considered > 400 µg/mL. The original experimental design did not include a bare $Fe_3O_4$ treatment group, nanoparticle-only impedance controls, or an orthogonal viability assay. The absence of nanoparticle-only impedance controls limited the assessment of potential particle-related interference with the impedance-based measurements, while the lack of an orthogonal viability assay prevented independent confirmation of the observed cellular responses. In addition, the final DMSO concentration varied across the tested formulation concentrations, and concentration-matched vehicle controls were not included at each dose. Therefore, a potential contribution of DMSO to the observed cellular responses cannot be excluded.

Collectively, these findings provide preliminary *in vitro* evidence of the physicochemical characteristics and cellular responses of $Fe_3O_4$-PEG-QUER and warrant further investigation in appropriate experimental models. The observed cellular responses should not be interpreted as evidence of established safety, targeted delivery, enhanced cellular uptake, or therapeutic efficacy. The current study is limited to in vitro experiments; further studies incorporating complementary cellular assays, appropriate nanoparticle controls, quantitative quercetin analysis, and characterization under biologically relevant conditions are needed to address these limitations. Further *in vivo* and, subsequently, clinical investigations would be required to establish the therapeutic potential of these formulations.

## CONCLUSION

In the present study, a ternary $Fe_3O_4$-PEG-QUER nanoparticle formulation was synthesized via the coprecipitation method. A nanoscale formulation was designed to combine $Fe_3O_4$, PEG, and quercetin. Comprehensive characterization using XRD, FT-IR, NTA, Zeta-sizer, SEM, and EDX provided complementary information on the physicochemical properties of the four formulations.

XRD confirmed the presence of the inverse spinel cubic crystal structure in the $Fe_3O_4$-containing formulations. FT-IR provided information on the characteristic functional groups associated with PEG and quercetin. NTA showed that $Fe_3O_4$-PEG-QUER had a mean particle diameter in the sub-100 nm range under the measurement conditions. Zeta potential analysis showed that the PEG-containing formulation exhibited a near-neutral surface charge, which may influence cellular interactions. SEM showed predominantly spherical particle morphology, while EDX provided information on the elemental composition of the formulations.

*In vitro* assessment of impedance-based cellular responses using the xCELLigence system demonstrated differential impedance profiles between A549 NSCLC and BEAS-2B cells under the tested conditions. The apparent IC50 values for $Fe_3O_4$-PEG-QUER in A549 cells were 289 µg/mL at 24 h and 160 µg/mL at 48 h, whereas those exceeded 400 µg/mL. Notably, $Fe_3O_4$-PEG alone exhibited lower apparent IC50 values in A549 cells than $Fe_3O_4$-PEG-QUER did, indicating that the addition of quercetin did not enhance the observed antiproliferative response under the present experimental conditions. Because the concentrations were expressed as total formulation mass and the quercetin content of $Fe_3O_4$-PEG-QUER was not quantitatively determined, the observed responses could not be directly compared at equivalent quercetin doses. These findings represent preliminary *in vitro* observations and do not establish the safety, targeted delivery, enhanced cellular uptake, or therapeutic efficacy of the formulations. Further studies using complementary cellular assays and appropriate experimental models are needed to clarify the contribution of quercetin to the observed effects and to investigate the potential of these formulations.

*Ethics*

**Ethics Committee Approval:** There are no circumstances requiring ethics committee approval for this study.

**Informed Consent:** Since only *in vitro* experiments were conducted within the scope of this study, patient consent was not required.

*Footnotes*

*Authorship Contributions*

Concept: Y.S., M.B.Y., Design: Y.S., M.B.Y., Data Collection or Processing: Y.S., M.B.Y., Analysis or Interpretation: Y.S., M.B.Y., Literature Search: Y.S., M.B.Y., Writing: Y.S., M.B.Y.

**Conflict of Interest:** The authors declare no conflicts of interest.

**Financial Disclosure:** The authors declared that this study received no financial support.

## REFERENCES


1. Gubbala S, Nathani H, Koizol K, Misra RDK. Magnetic properties of nanocrystalline Ni–Zn, zn–mn, and ni–mn ferrites synthesized by reverse micelle technique. Physica B: Condensed Matter. 2004;348:317-328.
2. Arruebo M, Fernández-Pacheco R, Ibarra MR, Santamaría J. Magnetic nanoparticles for drug delivery. Nano Today. 2007;2:22-32.
3. Rana S, Philip J, Raj B. Micelle based synthesis of cobalt ferrite nanoparticles and its characterization using Fourier transform infrared transmission spectrometry and thermogravimetry. Materials Chemistry and Physics. 2010;124:264-269.
4. McBain SC, Griesenbach U, Xenariou S, Keramane A, Batich CD, Alton EW, Dobson J. Magnetic nanoparticles as gene delivery agents: enhanced transfection in the presence of oscillating magnet arrays. Nanotechnology. 2008;19:405102.
5. Laurent S, Forge D, Port M, Roch A, Robic C, Vander Elst L, Muller RN. Magnetic iron oxide nanoparticles: synthesis, stabilization, vectorization, physicochemical characterizations, and biological applications. Chem Rev. 2008;108:2064-2110.
6. Dobson J. Magnetic nanoparticles for drug delivery. Drug Development Research. 2006;67:55-60.
7. Veiseh O, Gunn JW, Zhang M. Design and fabrication of magnetic nanoparticles for targeted drug delivery and imaging. Adv Drug Deliv Rev. 2010;62:284-304.
8. Karakoti AS, Das S, Thevuthasan S, Seal S. PEGylated inorganic nanoparticles. Angew Chem Int Ed Engl. 2011;50:1980-1994.
9. Mukhopadhyay A, Joshi N, Chattopadhyay K, De G. A facile synthesis of PEG-coated magnetite (Fe3O4) nanoparticles and their prevention of the reduction of cytochrome c. ACS Appl Mater Interfaces. 2012;4:142-149.
10. Ahmed MA, Okasha N, Mansour SF, El-dek SI. Bi-modal improvement of the physico-chemical characteristics of peg and Mfe2o4 subnanoferrite. Journal of Alloys and Compounds. 2010;496:345-350.
11. Feng B, Hong RY, Wang LS, Guo L, Li HZ, Ding J, Zheng Y, Wei DG. Synthesis of $Fe_3O_4$/APTES/Peg diacid functionalized magnetic nanoparticles for MR imaging. Colloids and Surfaces A: Physicochemical and Engineering Aspects. 2008;328:52-59.
12. Zhang Y, Kohler N, Zhang M. Surface modification of superparamagnetic magnetite nanoparticles and their intracellular uptake. Biomaterials. 2002;23:1553-1561.
13. Sainz V, Conniot J, Matos AI, Peres C, Zupancic E, Moura L, Silva LC, Florindo HF, Gaspar RS. Regulatory aspects on nanomedicines. Biochem Biophys Res Commun. 2015;468:504-510.
14. McCarthy JR, Weissleder R. Multifunctional magnetic nanoparticles for targeted imaging and therapy. Adv Drug Deliv Rev. 2008;60:1241-1251.
15. Petros RA, DeSimone JM. Strategies in the design of nanoparticles for therapeutic applications. Nat Rev Drug Discov. 2010;9:615-627.
16. Peer D, Karp JM, Hong S, Farokhzad OC, Margalit R, Langer R. Nanocarriers as an emerging platform for cancer therapy. Nat Nanotechnol. 2007;2:751-760.
17. Cornell RM, Schwertmann U. The iron oxides. 2003.
18. Gossuin Y, Gillis P, Hocq A, Vuong QL, Roch A. Magnetic resonance relaxation properties of superparamagnetic particles. Wiley Interdiscip Rev Nanomed Nanobiotechnol. 2009;1:299-310.
19. Schwertmann U. Solubility and dissolution of iron oxides. Plant and Soil. 1991;130;1-25.
20. Macdougall IC. Evolution of iv iron compounds over the last century. J Ren Care. 2009;35(Suppl 2):8-13.
21. Danielson BG. Structure, chemistry, and pharmacokinetics of intravenous iron agents. J Am Soc Nephrol. 2004;15(Suppl 2):S93-S98.
22. Gupta AK, Gupta M. Synthesis and surface engineering of iron oxide nanoparticles for biomedical applications. Biomaterials. 2005;26:3995-4021.
23. Wang YX, Hussain SM, Krestin GP. Superparamagnetic iron oxide contrast agents: physicochemical characteristics and applications in MR imaging. Eur Radiol. 2001;11:2319-2331.
24. Na HB, Song IC, Hyeon T. Inorganic nanoparticles for MRI contrast agents. Advanced Materials, 2009;21:2133-2148.
25. Panche AN, Diwan AD, Chandra SR. Flavonoids: an overview. J Nutr Sci. 2016;5:e47.
26. Zheng X, Zhang X, Zeng F. Biological functions and health benefits of flavonoids in fruits and vegetables: a contemporary review. Foods. 2025;14:155.
27. Lee YK, Yuk DY, Lee JW, Lee SY, Ha TY, Oh KW, Yun YP, Hong JT. (-)-Epigallocatechin-3-gallate prevents lipopolysaccharide-induced elevation of beta-amyloid generation and memory deficiency. Brain Res. 2009;1250:164-174.
28. Metodiewa D, Kochman A, Karolczak S. Evidence for antiradical and antioxidant properties of four biologically active N,N-diethylaminoethyl ethers of flavanone oximes: a comparison with natural polyphenolic flavonoid (rutin) action. Biochem Mol Biol Int. 1997;41:1067-1075.
29. Walker EH, Pacold ME, Perisic O, Stephens L, Hawkins PT, Wymann MP, Williams RL. Structural determinants of phosphoinositide 3-kinase inhibition by wortmannin, LY294002, quercetin, myricetin, and staurosporine. Mol Cell. 2000;6:909-919.
30. Wink M. Phytochemical diversity of secondary metabolites. Encyclopedia of Plant and Crop Science. 2004;915-919.
31. Pal D, Nayak KA. Nanotechnology for targeted delivery in cancer therapeutics. Int J Pharm Sci Rev Res. 2010;1:1-10.
32. Ferlay J, Soerjomataram I, Dikshit R, Eser S, Mathers C, Rebelo M, Parkin DM, Forman D, Bray F. Cancer incidence and mortality worldwide: sources, methods and major patterns in GLOBOCAN 2012. Int J Cancer. 2015;136:E359-E386.
33. Auyang YS. Cancer causes and cancer research on many levels of complexity. Creat Technol. 2006:1-15.
34. Singh KK. Nanotechnology in cancer detection and treatment. Technology in Cancer Research and Treatment. 2005;4:583-583.
35. Singh PO, Nehru MR. Nanotechnology and cancer treatment. Asian J Exp Sci. 2008;22:6.
36. Anselmo AC, Mitragotri S. Nanoparticles in the clinic. Bioeng Transl Med. 2016;1:10-29.
37. Barenholz Y. Doxil®--the first FDA-approved nano-drug: lessons learned. J Control Release. 2012;160:117-134.
38. Yoo E, Cheng HA, Nardacci LE, Beaman DJ, Drinnan CT, Lee C, Fishbein KW, Spencer RG, Fisher OZ, Doiron AL. Activatable interpolymer complex-superparamagnetic iron oxide nanoparticles as magnetic resonance contrast agents sensitive to oxidative stress. Colloids and Surfaces B: Biointerfaces. 2017;158:578-588.
39. Shah ST, Yehye WA, Chowdhury ZZ, Simarani K. Magnetically directed antioxidant and antimicrobial agent: synthesis and surface functionalization of magnetite with quercetin. PeerJ. 2019;7:e7651.

40. Shah ST, A Yehya W, Saad O, Simarani K, Chowdhury Z, A Alhadi A, Al-Ani LA. Surface functionalization of ıron oxide nanoparticles with gallic acid as potential antioxidant and antimicrobial agents. Nanomaterials (Basel). 2017;7:306.

41. Bukhari SB, Memon S, Mahroof-Tahir M, Bhanger MI. Synthesis, characterization and antioxidant activity copper-quercetin complex. Spectrochim Acta A Mol Biomol Spectrosc. 2009;71:1901-1906.

42. Kumar SR, Priyatharshni S, Babu VN, Mangalaraj D, Viswanathan C, Kannan S, Ponpandian N. Quercetin conjugated superparamagnetic magnetite nanoparticles for in-vitro analysis of breast cancer cell lines for chemotherapy applications. J Colloid Interface Sci. 2014;436:234-242.

43. Cheng HA, Drinnan CT, Pleshko N, Fisher OZ. Pseudotannins self-assembled into antioxidant complexes. Soft Matter. 2015;11:7783-7791.

44. Dorniani D, Kura AU, Hussein-Al-Ali SH, Bin Hussein MZ, Fakurazi S, Shaari AH, Ahmad Z. In vitro sustained release study of gallic acid coated with magnetite-PEG and magnetite-PVA for drug delivery system. ScientificWorldJournal. 2014;2014:416354.

45. Rosman R, Saifullah B, Maniam S, Dorniani D, Hussein MZ, Fakurazi S. Improved anticancer effect of magnetite nanocomposite formulation of GALLIC acid ($Fe_3O_4$-PEG-GA) against lung, breast and colon cancer cells. Nanomaterials (Basel). 2018;8:83.

46. Zhu J, Wang J, Wang X, Zhu J, Yang Y, Tian J, Cui W, Ge C, Li Y, Pan Y, Gu H. Facile synthesis of magnetic core–shell nanocomposites for MRI and CT bimodal imaging. Journal of Materials Chemistry B. 2015;3:6905-6910.

47. Chorny M, Hood E, Levy RJ, Muzykantov VR. Endothelial delivery of antioxidant enzymes loaded into non-polymeric magnetic nanoparticles. J Control Release. 2010;146:144-151.

48. Song G, Zhao M, Chen H, Lenahan C, Zhou X, Ou Y, He Y. The role of nanomaterials in stroke treatment: targeting oxidative stress. Oxid Med Cell Longev. 2021;2021:8857486.

49. Verma NK, Crosbie-Staunton K, Satti A, Gallagher S, Ryan KB, Doody T, McAtamney C, MacLoughlin R, Galvin P, Burke CS, Volkov Y, Gun'ko YK. Magnetic core-shell nanoparticles for drug delivery by nebulization. J Nanobiotechnology. 2013;11:1.

50. Cîrcu M, Nan A, Borodi G, Liebscher J, Turcu R. Refinement of magnetite nanoparticles by coating with organic stabilizers. Nanomaterials (Basel). 2016;6:228.

51. Santiago-Rodríguez L, Lafontaine MM, Castro C, Méndez-Vega J, Latorre-Esteves M, Juan EJ, Mora E, Torres-Lugo M, Rinaldi C. Synthesis, stability, cellular uptake, and blood circulation time of carboxymethyl-inulin coated magnetic nanoparticles. J Mater Chem B. 2013;1:2807-2817.

52. Lam T, Avti PK, Pouliot P, Maafi F, Tardif JC, Rhéaume É, Lesage F, Kakkar A. Fabricating water dispersible superparamagnetic iron oxide nanoparticles for biomedical applications through ligand exchange and direct conjugation. Nanomaterials (Basel). 2016;6:100.

53. Bulte JW, Kraitchman DL. Iron oxide MR contrast agents for molecular and cellular imaging. NMR Biomed. 2004;17:484-499.

54. Chomoucka J, Drbohlavova J, Huska D, Adam V, Kizek R, Hubalek J. Magnetic nanoparticles and targeted drug delivering. Pharmacol Res. 2010;62:144-149.

55. Reddy LH, Arias JL, Nicolas J, Couvreur P. Magnetic nanoparticles: design and characterization, toxicity and biocompatibility, pharmaceutical and biomedical applications. Chem Rev. 2012;112:5818-5878.

56. Yang XL, Ju XJ, Mu XT, Wang W, Xie R, Liu Z, Chu LY. Core-shell chitosan microcapsules for programmed sequential drug release. ACS Appl Mater Interfaces. 2016;8:10524-10534.

57. Ding G, Guo Y, Lv Y, Liu X, Xu L, Zhang X. A double-targeted magnetic nanocarrier with potential application in hydrophobic drug delivery. Colloids Surf B Biointerfaces. 2012;91:68-76.

58. Schladt TD, Schneider K, Schild H, Tremel W. Synthesis and bio-functionalization of magnetic nanoparticles for medical diagnosis and treatment. Dalton Trans. 2011;40:6315-6343.

59. Kumari A, Yadav SK, Pakade YB, Singh B, Yadav SC. Development of biodegradable nanoparticles for delivery of quercetin. Colloids Surf B Biointerfaces. 2010;80:184-192.

60. Wu TH, Yen FL, Lin LT, Tsai TR, Lin CC, Cham TM. Preparation, physicochemical characterization, and antioxidant effects of quercetin nanoparticles. Int J Pharm. 2008;346:160-168.

61. Chakraborty S, Stalin S, Das N, Choudhury ST, Ghosh S, Swarnakar S. The use of nano-quercetin to arrest mitochondrial damage and MMP-9 upregulation during prevention of gastric inflammation induced by ethanol in rat. Biomaterials. 2012;33:2991-3001.

62. Kakran M, Sahoo NG, Li L. Dissolution enhancement of quercetin through nanofabrication, complexation, and solid dispersion. Colloids Surf B Biointerfaces. 2011;88:121-130.

63. Tiburzi S, Lezcano V, Principe G, Montiel Schneider MG, Miravalles AB, Lassalle V, Bruzzone A, González-Pardo V. Quercetin-loaded magnetic nanoparticles: a promising tool for antitumor treatment in human breast cancer cells. J Drug Target. 2025;33:1227-1242.

64. Barreto ACH, Santiago VR, Mazzetto SE, Denardin JC, Lavín R, Mele G, Ribeiro ME, Vieira IG, Gonçalves T, Ricardo NM, Fechine PB. Magnetic nanoparticles for a new drug delivery system to control quercetin releasing for cancer chemotherapy. J Nanopart Res. 2011;13:6545-6553.

65. Pereira C, Pereira AM, Fernandes C, Rocha M, Mendes R, Fernández-García MP, Guedes A, Tavares PB, Grenèche J.-M, Araújo JP, Freire C. Superparamagnetic $MFE_2O_4$ (M = fe, co, MN) nanoparticles: tuning the particle size and magnetic properties through a novel one-step coprecipitation route. Chemistry of Materials. 2012;24:1496-1504.

66. Qu H, Ma H, Riviere A, Zhoub W, O'Connor JC. One-pot synthesis in polyamines for preparation of water-soluble magnetite nanoparticles with amine surface reactivity. J Mater Chem. 2012;22:3311-3319.

67. Jarzebski M, Kościński M, Bialopiotrowıcz T. Determining the size of nanoparticles in the example of magnetic iron oxide core-shell systems. Journal of Physics Conference Series. 2017;885:012007.

68. Nurbas M, Ghorbanpoor H, Avcı H. An eco-friendly approach to synthesis and characterization of magnetite ($Fe_3O_4$) nanoparticles using platanus orientalis l. Leaf extract. Digest Journal of Nanomaterials and Biostructures. 2017;12:993-1000.